

**SYNTHESIS, CHARACTERISATION AND APPLICATION OF SILVER-DOPED
CARBON NANOTUBES AND NANOPOROUS POLYMERS FOR PURIFICATION
OF WATER SAMPLES**

by

LUTENDO EVELYN RANANGA

DISSERTATION

Submitted in fulfilment of the requirements for the degree of

MASTER OF SCIENCE

in

CHEMISTRY

in the

FACULTY OF SCIENCE AND AGRICULTURE

(School of Physical and Mineral Sciences)

at the

UNIVERSITY OF LIMPOPO

SUPERVISOR: Dr T Magadzu

2013

DECLARATION

I declare that the dissertation hereby submitted to the University of Limpopo, for the degree of Master of Science in Chemistry has not previously been submitted by me for a degree at this or any other university; that it is my own work in design and in execution, and that all material contained herein has been duly acknowledged.

Surname, Initials (Ms)

Date

DEDICATIONS

To my Creator, for his unconditional love and support.

PUBLICATIONS AND ORAL PRESENTATIONS

Publication

L.E. Rananga and T. Magadzu. Interaction of 1% silver doped carbon nanotubes-cyclodextrin nanocomposites with *Escherichia coli* bacteria during water purification, submitted.

Oral presentations

L.E. Rananga and T. Magadzu. Enhanced activity of Ag-MWCNTs/ β -CD nanocomposites for the removal of *E. coli* bacteria from contaminated water samples. Presented at the 50th annual conference of the Microscopy Society of Southern Africa, University of Cape Town, December, 2012.

L.E. Rananga and T. Magadzu. Synthesis and application of metal nanoparticles, carbon nanotubes and nanoporous polymers for purification of water samples, presented at the University of Limpopo research day, at Bolivia lodge, South Africa, September, 2011.

Poster presentation

L.E. Rananga and T. Magadzu. Interaction of 1% silver doped carbon nanotubes-cyclodextrin nanocomposites with *Escherichia coli* bacteria during water purification. Presented at the 3rd Biennial Young water professional conference at Stellenbosch University, Cape Town, July, 2013.

ACKNOWLEDGEMENTS

Primarily I would like to thank in a very special way the Creator of the Universe my God, who created me and has done marvellous things for me, indeed, 'In all my ways I will acknowledge Him, and he shall direct thy paths, Proverbs 3:16.'

Thanks to my supervisor, Dr Takalani Magadzu for his enthusiasm and guidance with inordinate support and interest to my studies.

I would like to thank the Department of Chemistry and the Head of Department, Dr Mary S Thomas for her encouraging words of support. Thanks to Wilhemina Sebati for her great assistance in bacterial studies.

My appreciation goes to Dr Chantelle Baker and the Electron Microscope Unit at University of Limpopo Medunsa Campus, for their assistance in carrying out the TEM and FE-SEM work spending most of their time in assisting me. I would like to show gratitude to Dr Baker for editing my dissertation.

Many thanks to the University of Witwatersrand for their assistance in my sample analysis using XRD and BET. I would like to send my vote of appreciation to Dr Sabelo Mhlanga and Prof Dave Billing, together with my special MSc friends, Michelle Nyoni and Natsai Chiwaye for their support and assistance.

I appreciate and thank Prof Masoko from the Department of Microbiology at the University of Limpopo. Assistance from Marumo Lekganyane with bacterial studies is gratefully acknowledged.

Special thanks go to the National Research Foundation (NRF) for funding my research.

I would like to acknowledge my Father Dr Ntshengedzeni Collins Rananga for his encouragement, love, financial support and his leadership role in my studies and in my life. I love you.

I also want to acknowledge my mother Namadzavho Esther Rananga, for her love encouragement, and financial support in my studies. I love you.

I want to thank my sisters Seani and Apfaho, as well as my younger brother Unarine for their unfathomable love and encouragement in my studies and in my life. I love you all.

I would like to thank the love of my life, Paul Mehleketo Macevele for his never ending support both in my personal life and studies. I love you.

I also acknowledge my late grandmother Vho-Martha Ravhengani and the late, Vho-Frank Rananga who in their life time gave me constructive advice and support.

I want to thank my Uncle Mashudu Ravhengani, for his love, support and involvement in my life.

I also thank Mr Bernard Rananga, 'Makhadzi', Vho-Tshinakaho Tshifularo, Vho-Sophia Rananga, Vho-Elisa Sikhapha, including all my brothers, sisters, aunts, and cousins who are too many to mention by name for all their support.

ABSTRACT

Drinkable water is water that is safe enough to be consumed by humans or used with low risk of immediate or long term harm. World-wide, insufficient access to portable water and use of sources contaminated with disease vectors, pathogens, and unacceptable levels of toxins is a huge problem. The use of such water for drinking and food preparation leads to the widespread of acute and chronic illnesses. This is a major cause of death and misery in many undeveloped countries. Reduction of waterborne diseases is a major public health goal in developing countries. Nanotechnology offers the possibility of an efficient removal of pollutants and microorganisms from water.

Essentially, three classes of nanoscale materials were investigated as functional materials for water purification in this study. Silver nanoparticles, carbon nanotubes and beta (β)-cyclodextrin polymers were synthesised and characterised specifically for purification of water samples.

β -cyclodextrin is soluble in both water and other aqueous media. In order to render cyclodextrins insoluble, they were converted into highly cross-linked polymers, by polymerisation with a bifunctional linker, hexamethylene diisocyanate. Cyclodextrins were functionalised and synthesised with either the allyl or the benzoyl group. Characterisation with fourier transform infrared (FTIR) spectrophotometer confirmed the functionalisation process. Thereafter the scanning electron microscopy (SEM) analysis confirmed the polymers' morphology to be spongy, and capable of absorbing contaminants.

Multi-walled carbon nanotubes (MWCNTs) were treated with a mixture of sulphuric and nitric acid in order to introduce the carboxyl and hydroxyl groups. These were characterised by SEM, transmission electron microscopy (TEM), X-ray diffraction (XRD) and FTIR spectroscopy to confirm the functionalisation process.

Silver nanoparticles were synthesised from sodium citrate and silver nitrate, using sodium dodecyl sulphate as a surfactant. Their characterisation was done by SEM, energy dispersive X ray (EDX) spectroscopy, TEM, UV/Vis spectroscopy and XRD to

confirm a face centred cubic structure with an estimated crystallite size ranging from 50 to 100 nm.

β -cyclodextrin polymers, functionalised multi-walled carbon nanotubes and silver nanoparticle-doped MWCNTs/cyclodextrin composites were characterised by SEM, TEM, XRD, Brunauer-Emmet-Teller (BET) and EDX. Analysis of the phenolic compound, 4-hydroxynitrobenzene in water, using these nanocomposites, demonstrated good capabilities of removing organic contaminants from water samples as indicated by their high absorption efficiencies of the contaminants.

The synthesised metal-organic composites were tested for their effectiveness in removing organic contaminants as well as for eliminating *Escherichia coli* bacteria from water. The synthesised composites presented up to 97% absorption efficiency of organic contaminants and up to 100% inactivation of the bacteria. There was complete destruction of bacteria from the water analysed at various times and varying concentrations. After a long exposure of the nanocomposites to *E. coli*, pits were noticeable on the external morphology of the bacteria, thus suggesting that the nanocomposites are bactericidal. The bacterial activity increased with temperature, when studied between 10 °C and 30 °C.

TABLE OF CONTENTS

DECLARATION	ii
DEDICATIONS.....	iii
PUBLICATIONS AND ORAL PRESENTATIONS	iv
ACKNOWLEDGEMENTS	v
ABSTRACT	vii
TABLE OF CONTENTS	ix
LIST OF TABLES.....	xvii
LIST OF FIGURES.....	xix
LIST OF SCHEMES.....	xxiii
LIST OF ABBREVIATIONS.....	xxiv
LIST OF SYMBOLS	xxvi
CHAPTER 1	1
1.1 RESEARCH PROBLEM.....	1
1.1.1 Source and background of the problem.....	1
1.1.2 Statement of the research problem.....	2
1.2 LITERATURE REVIEW	3
1.2.1 Metal nanoparticles.....	3
1.2.2 Carbon nanotubes	3
1.2.3 Nanoporous polymers.....	4
1.3 PURPOSE OF THE STUDY	4
1.3.1 Aim of the study	4

1.3.2 Objectives of the study	4
1.4 SIGNIFICANCE OF THE PROPOSED RESEARCH.....	5
1.5 OUTLINE OF THE STUDY	5
1. 6 REFERENCES.....	7
CHAPTER 2	10
LITERATURE REVIEW.....	10
2.1 INTRODUCTION.....	10
2.2 CONTAMINANTS IN WATER	10
2.2.1 Organic contaminants.....	10
2.2.1.1 Detergents.....	10
2.2.1.2 Dis-infection by-products.....	11
2.2.1.3 Dioxins	11
2.2.1.4 Natural organic matter.....	12
2.2.1.5 Polycyclic aromatic hydrocarbons	12
2.2.1.6 Polychlorinated biphenyls.....	12
2.2.2 Inorganic contaminants.....	13
2.2.2.1 Arsenic	13
2.2.2.2 Asbestos	14
2.2.2.3 Lead	14
2.2.2.4 Mercury	15
2.2.3 Bacterial contamination	15
2.2.3.1 Escherichia coli	16
2.2.3.2 Cryptosporidium	17
2.2.3.3 Shigella	17
2.2.3.4 <i>Vibrio cholera</i>	18

2.2.3.5 Faecal coliform	18
2.2.4 Viral contamination	19
2.2.4.1 Hepatitis A.....	19
2.2.4.2 Rotavirus	19
2.2.4.3 Norovirus.....	20
2.3 CURRENT PURIFICATION TECHNIQUES	21
2.3.1 Chlorination.....	21
2.3.2 Ultraviolet light/lamps.....	21
2.3.3 Reverse osmosis	22
2.3.4 Filtration membranes	23
2.4 NANOTECHNOLOGY IN WATER TREATMENT.....	24
2.4.1 Metal nanoparticles.....	24
2.4.2 Carbon nanotubes	26
2.4.3 Nanoporous polymers.....	27
2.4.4 Application of nanocomposite materials and filtration membranes to contaminated water	30
2.5 CHARACTERISATION TECHNIQUES	32
2.5.1 Transmission electron microscopy (TEM).....	32
2.5.2 Scanning electron microscope (SEM).....	32
2.5.3 Ultraviolet/Visible spectrophotometer (UV/Vis)	33
2.5.4 Fourier transform Infrared spectroscopy (FTIR).....	34
2.5.5 Brunauer-Emmett -Teller (BET)	35
2.5.6 Powder X-ray diffraction (PXRD)	35
2.6 REFERENCES.....	37
CHAPTER 3	45
RESEARCH METHODOLOGY	45

3.1 INTRODUCTION.....	45
3.2 REAGENTS AND CHEMICALS	45
3.3 CHARACTERISATION TECHNIQUES	46
3.3.1 Field Emission Scanning Electron Microscopy (FE-SEM)	46
3.3.2 Transmission electron microscopy.....	47
3.3.3 X-Ray diffraction	48
3.3.4 Fourier transform Infrared spectroscopy	49
3.3.5 Brunauer-Emmett-Teller analysis	49
3.4 EXPERIMENTAL.....	49
3.4.1 Synthesis of functionalised β -cyclodextrin nanocomposites	49
3.4.1.1 Synthesis of the insoluble β -cyclodextrin nanocomposites	49
3.4.1.2 Mono-2-substituted benzoyl β -cyclodextrin polymer	50
3.4.1.3 Mono-2-substituted allyl β -cyclodextrin polymer.....	51
3.4.2 Functionalisation of carbon nanotubes	52
3.4.3 Synthesis of β -CD/MWCNT nanocomposites	52
3.4.4 Synthesis of silver nanoparticles.....	52
3.4.5 Synthesis of silver nanoparticles on functionalised MWCNTs (Ag-MWCNTs)	53
3.4.6 Polymerisation of Ag-MWCNTs onto β -cyclodextrin polymers.....	53
3.4.7 Investigation of 4-hydroxynitrobenzene (PNP) using UV-Vis spectrophotometry	53
3.4.8 Antibacterial Application	56
3.4.8.1 Preparation of nutrient agar plates	56
3.4.8.2 Preparation of nutrient broth and growth of biomass.....	56
3.4.8.3 Preparation of water samples by micro-dilution.....	57
3.4.8.4 Dis-infection of water.....	57

3.4.8.5 Kinetics of bacterial growth rate in the presence of Ag-MWCNTs/ β -CD nanocomposites	59
3.5. REFERENCES.....	60
CHAPTER 4	61
RESULTS AND DISCUSSION.....	61
4.1 INTRODUCTION.....	61
4.2 CHARACTERISATION OF SYNTHESISED NANOCOMPOSITE MATERIALS	61
4.2.1 FTIR results	61
4.2.1.1 The FTIR spectra of raw and functionalised MWCNTs	61
4.2.1.2 The FTIR spectra of mono-2-substituted benzoyl β -cyclodextrin polymer	62
4.2.1.3 The FTIR spectra of mono-2-substituted allyl β -cyclodextrin polymer... 64	
4.2.2 Characterisation of the synthesised nanocomposite materials and cyclodextrin polymers by FE-SEM and TEM	66
4.2.2.1 FE-SEM and TEM of multi-walled carbon nanotubes (MWCNTs).....	66
4.2.2.2 FE-SEM and TEM of cyclodextrin polymer (β -CD HMDI).....	68
4.2.2.3 FE-SEM and TEM micrographs of cyclodextrin polymers incorporated with 1 wt. % multi-walled carbon nanotubes	68
4.2.2.4 FE-SEM and TEM micrographs of silver nanoparticles.....	69
4.2.2.5 FE-SEM and TEM micrographs of 32 wt. % Ag-MWCNTs nanocomposite material	71
4.2.2.6 FE-SEM and TEM micrographs of 10 wt. % Ag/ β -cyclodextrin nanocomposites	72
4.2.2.7 FE-SEM and TEM micrographs of 1 wt. % Ag-MWCNTs/ β -CD nanocomposites.....	73
4.2.2.8 FE-SEM micrographs of mono-2-substituted benzoyl β -cyclodextrin polymer and mono-2-substituted allyl β -cyclodextrin polymer.....	75

4.2.3	Characterisation of the synthesised nanocomposite materials by XRD.....	76
4.2.3.1	XRD profile of carbon nanotubes	76
4.2.3.2	XRD profile of Ag nanoparticles, MWCNTs and 32 wt. % Ag-MWCNTs nanocomposite materials	78
4.2.3.3	XRD profile of 10 wt. % Ag/ β -CD nanocomposite material in comparison with the profile of Ag nanoparticles.	80
4.2.3.4	XRD profile of 1 wt. % Ag-MWCNTs/ β -CD in comparison with the 10 wt. % Ag/ β CD and 32 wt. % Ag-MWCNTs nanocomposite material.....	82
4.2.4	Characterisation of Ag nanoparticles using UV-Vis spectrophotometer.....	85
4.2.5	BET results of the nanocomposite materials.....	86
4.3	PURIFICATION OF WATER SAMPLES CONTAMINATED WITH 4-HYDROXYNITROBENZENE	88
4.3.1	Determination of the absorbance wavelength of 4-hydroxynitrobenzene	88
4.3.2	Calibration curve of 4-hydroxynitrophenol at 318 nm.....	89
4.3.3	Effect of mono-2-substituted benzoyl β -cyclodextrin polymer and mono-2-substituted allyl β -cyclodextrin polymer on the removal of organic contaminants from water.....	90
4.3.4	Effect of MWCNTs loadings on the β -cyclodextrin polymers for removal of organic contaminants from water.....	91
4.3.5	Comparative studies of β -CD, MWCNTs, 10 wt. % Ag/ β -CD and 1 wt. % Ag-MWCNTs/ β -CD for removal of organic contaminants from water	93
4.4	PURIFICATION OF WATER SAMPLES CONTAMINATED WITH ESCHERICHIA COLI BACTERIA USING DIFFERENT NANOMATERIALS	94
4.4.1	Determination of the initial colony forming unit	94
4.4.2	Effect of Ag nanoparticles on removal of bacteria from water.....	96
4.4.2.1	Treatment of water using 300 mg of Ag nanoparticles	96
4.4.2.2	Treatment of water using 150 mg of Ag nanoparticles	97

4.4.3 Comparative studies of cyclodextrin polymers and MWCNTs on removal of <i>E. coli</i> bacteria from water samples	100
4.4.4 Comparative studies of different nanocomposite materials on removal of <i>E. coli</i> bacteria from water samples	103
4.5 INVESTIGATION OF THE GROWTH CURVE OF <i>E. COLI</i> BACTERIA BY MEASURING THE OPTICAL DENSITY IN THE PRESENCE OF 1 wt. % Ag-MWCNTs/ β -CD NANOCOMPOSITE MATERIAL.....	108
4.5.1 Introduction	108
4.5.2 Effect of 1 wt. % Ag-MWCNTs/ β -CD nanocomposite material on the optical density measurement of <i>E. coli</i> in contaminated water.....	108
4.5.3 Investigation of the interaction between 1 wt. % Ag-MWCNTs/ β -CD nanocomposite material and <i>E. coli</i> bacteria in broth medium after 90 minutes .	111
4.6 INVESTIGATION OF THE ROLE PLAYED BY 1 wt. % Ag-MWCNTS/ β -CD NANOCOMPOSITE MATERIALS ON THE DESTRUCTION OF <i>E. coli</i> BACTERIA IN WATER BY MEANS OF SCANNING ELECTRON MICROSCOPY.....	112
4.6.1 Introduction	112
4.6.2 The structure of <i>E. coli</i> bacteria	112
4.6.3 Interaction of <i>E. coli</i> bacteria with 1 wt. % Ag-MWCNTs/ β -CD nanocomposite material over a period of 60 minutes.....	114
4.6.4 Interaction of <i>E. coli</i> bacteria with 1 wt. % Ag-MWCNTs/ β -CD nanocomposite material after 150 and 210 minutes	116
4.7 EFFECT OF TEMPERATURE ON INTERACTION OF Ag-MWCNTS NANOCOMPOSITE MATERIAL WITH <i>E. coli</i> BACTERIA.....	118
4.7.1 Determination of the colony forming unit and percentage reduction of <i>E. coli</i> bacteria in the presence of 32 wt. % Ag-MWCNTs nanocomposite material at different incubation temperatures	118
4.7.2 Determination of the kinetic parameters: Interaction of 32 wt. % Ag-MWCNTs with <i>E. coli</i> bacteria at different temperatures.....	120

4.7.2.1 First order analysis of the antibacterial activity of 32 wt. % Ag-MWCNTs nanocomposite material at 10 °C.....	120
4.7.2.2 First order analysis of the antibacterial activity of 32 wt. % Ag-MWCNTs nanocomposite material at 15 °C.....	121
4.7.2.3 First order analysis of the antibacterial activity of 32 wt. % Ag-MWCNTs nanocomposite material at 20 °C.....	122
4.7.2.4 First order analysis of the antibacterial activity of 32 wt. % Ag-MWCNTs nanocomposite material at 25 °C.....	123
4.7.2.5 First order analysis of the antibacterial activity of Ag-MWCNTs nanocomposite material at 30 °C.....	124
4.7.2.6 Summary of the results obtained after determination of the kinetic order using first order analysis	125
4.8 REFERENCES.....	129
CHAPTER 5.....	132
Conclusions and Recommendations.....	132
5.1 CONCLUSIONS.....	132
5.2 RECOMMENDATIONS.....	134
APPENDICES.....	135

LIST OF TABLES

Table 4.1: Estimation of crystallite size from XRD patterns for raw and functionalised MWCNTs.....	77
Table 4.2: Estimation of crystallite size from XRD patterns for Ag nanoparticles and 32 wt. % Ag/MWCNTs nanocomposite material.	79
Table 4.3: Estimation of crystallite size from XRD patterns of 10 wt. % Ag/ β -CD nanocomposite material.....	82
Table 4.4: Estimation of crystallite size from XRD patterns for 1 wt. % Ag-MWCNTs/ β -CD nanocomposite material.	84
Table 4.5: BET surface area and pore volume analysis of nanocomposite materials.....	86
Table 4.6: Results showing the percentage of 4-hydroxynitrobenzene absorbed by the polymers and their final concentrations.	90
Table 4.7: Results showing the percentage of 4-hydroxynitrobenzene absorbed by MWCNTs nanocomposites and their final concentrations.	91
Table 4.8: Results showing the percentage of 4-hydroxynitrobenzene absorbed by β -CD, MWCNTs, 10 wt. % Ag/ β -CD and 1 wt. % Ag/MWCNTs/ β -CD nanocomposites and their final concentrations.	93
Table 4.9: Number of colonies obtained after micro-dilutions.....	95
Table 4.10: Water purification results after introducing 300 mg silver nanoparticles to contaminated water with <i>E. coli</i> bacteria. Initial cfu = 117×10^5	96
Table 4.11: Water purification results after introducing 150 mg of silver nanoparticles for the removal of <i>E. coli</i> bacteria. Initial cfu = 62000.	97

Table 4.12: Colony forming units obtained after introduction of cyclodextrin polymers and MWCNTs on removal of <i>E. coli</i> bacteria from water samples. Initial cfu = 62000.....	100
Table 4.13: Percentage inactivity of <i>E. coli</i> bacteria obtained after introduction of cyclodextrin polymers and MWCNTs.....	100
Table 4.14: The colony forming unit of nanocomposite materials obtained during the removal of <i>E. coli</i> bacteria from water samples. Initial cfu = 15400.	103
Table 4.15: The percentage inactivity of <i>E. coli</i> bacteria by different nanocomposite materials during water purification.	106
Table 4.16: Optical density measurements of <i>E. coli</i> at 600 nm.....	108
Table 4.17: The colony forming unit and the percentage reduction calculated from number of colonies. Initial cfu = 15400.....	118
Table 4.18: First order rate constants for antibacterial effect of Ag-MWCNTs nanocomposites at different temperatures applied.....	126

LIST OF FIGURES

Figure 2.1: The structure of a rod-shaped bacterium [24].....	16
Figure 2.2: Examples of carbon based nano-materials (CNMs). (a) Fullerene C ₆₀ , (b) A single walled carbon nanotube, (c) Multi walled carbon nanotubes [72].	26
Figure 2.3: Schematic illustration of nanoporous structures (d represent the diameter of a cylindrical pore and t represent the thickness of the inner surface). Inset: arbitrary cylindrical nanopore in nanoporous structures [78]..	28
Figure 2.4: The structures of β -cyclodextrin [79].	29
Figure 2.5: The three different types of hydroxyl groups of a CD [80].	30
Figure 3.1: Sputter coater.....	46
Figure 3.2: Field Emission Scanning electron microscope.	47
Figure 3.3: Transmission electron microscope.	48
Figure 3.4: UV/Vis spectrophotometer used to analyse 4-hydroxynitrobenzene samples.	55
Figure 3.5: Nutrient agar plate.....	56
Figure 3.6: Preparation of nutrient broth.....	57
Figure 3.7: The process of water dis-infection from bacteria at controlled temperature.	58
Figure 4.1: FTIR spectra of (a) raw MWCNTs and (b) functionalised MWCNTs.	62
Figure 4.2: FTIR of the synthesised benzoyl substituted β -CD polymer.....	64
Figure 4.3: FTIR spectrum of the synthesised Allyl substituted β -CD polymer.	65

Figure 4.4: (a) FE-SEM images for unfunctionalised MWCNTs, (b) TEM images for unfunctionalised MWCNTs (c) FE-SEM of functionalised MWCNTs, and (d) TEM of functionalised MWCNTs.	67
Figure 4.5: (a) FE-SEM micrograph of β -CD polymer and (b) TEM micrograph of β -CD polymer.	68
Figure 4.6: (a) FE-SEM of 1 wt. % MWCNTs/ β -CD nanocomposites and (b) TEM of 1 wt. % MWCNTs/ β -CD nanocomposites. The arrows indicate the CNTs.	69
Figure 4.7: (a) FE-SEM micrograph of silver micro-particles and (b) TEM micrograph of silver nanoparticles.	70
Figure 4.8: EDX spectrum of silver nanoparticles.	70
Figure 4.9: (a) FE-SEM micrograph of 32 wt. % Ag-MWCNTs nanocomposite and (b) TEM micrograph of 32 wt. % Ag-MWCNTs nanocomposites.	71
Figure 4.10: EDX of Ag-MWCNTs nanocomposites.	72
Figure 4.11: (a) FE-SEM micrograph of 10 wt. % Ag/ β -CD nanocomposites and (b) TEM micrograph of 10 wt. % Ag/ β -CD nanocomposites.	73
Figure 4.12: (a) FE-SEM micrograph of 1 wt. % Ag-MWCNTs/ β -CD nanocomposites and (b) TEM micrograph of 1 wt. % Ag-MWCNTs/ β -CD nanocomposites.	74
Figure 4.13 EDX of 1 wt. % Ag-MWCNTs/ β -CD nanocomposites.	74
Figure 4.14: (a) FE-SEM micrograph of benzoyl substituted β -CD polymer and (b) FE-SEM micrograph of allyl substituted β -CD polymer.	75
Figure 4.15: XRD patterns of (a) raw MWCNTs and (b) functionalised MWCNTs.	76
Figure 4.16: XRD patterns of synthesised Ag nanoparticles and MWCNTs, in comparison with 32 wt. % Ag-MWCNTs nanocomposite material.	78

Figure 4.17: XRD patterns of synthesised silver nanoparticles and 10 wt. % Ag/ β -CD nanocomposite materials.....	81
Figure 4.18: The XRD pattern of Ag-MWCNTs/ β -CD nanocomposite material.	83
Figure 4.19: UV-visible absorption spectra of AgNO ₃ solution and silver nanoparticles.....	85
Figure 4.20: A plot showing absorbance against wavelength of 4-hydroxynitrobenzene.	88
Figure 4.21: The standard curve of 4-hydroxynitrobenzene at 318 nm.	89
Figure 4.22: Comparison of different masses of MWCNTs/ β -CD nanocomposites during water treatment at 318 nm wavelength.....	92
Figure 4.23: Results obtained after 24 h incubation of (a) 10 ⁻¹ dilution, (b) 10 ⁻² dilution, (c) 10 ⁻³ dilution and (d) 10 ⁻⁴ <i>E. coli</i> dilution standards.	94
Figure 4.24: Antibacterial performance of silver on <i>E. coli</i> over 30 minutes. ...	97
Figure 4.25: Antibacterial performance of silver nanoparticles on <i>E. coli</i> over 20 minutes.....	99
Figure 4.26: Comparison of colony forming units versus time of different nanocomposite materials used for water purification.....	102
Figure 4.27: Comparison of colony forming unit versus time of different nanocomposites used for water purification.	105
Figure 4.28: Optical density as a function of time for <i>E. coli</i> supplemented with Ag-MWCNT/ β -CD nanocomposites in nutrient broth medium.	109
Figure 4.29: Nutrient agar plates showing (a) bacterial growth before introduction of 1 wt. % Ag-MWCNTs/ β -CD nanocomposite material, and plates supplemented with (b) 5 mg, (b) 10 mg and (c) 100 mg 1 wt. % Ag-MWCNTs/ β -CD nanocomposite material after 90 minutes of the bacterial interaction with these nanocomposites.....	111

Figure 4.30: FE-SEM micrograph of <i>E. coli</i> bacteria.	113
Figure 4.31: FE-SEM micrograph of <i>E. coli</i> treated with 1 wt. % Ag-MWCNTs/ β -CD nanocomposite materials (a) after 2 minutes, (b) after 4 minutes, (c) after 6 minutes and (d) after 60 minutes interaction. Arrows indicate MWCNTs.	114
Figure 4.32: FE-SEM of <i>E. coli</i> 'pit' formation after (a) 150 minutes and (b) after 210 minutes interaction treatment with 1 wt. % Ag-MWCNTs/ β -CD nanocomposite material. The arrows illustrate the pits formed.....	116
Figure 4.33: Antibacterial effect of Ag-MWCNTs at different temperatures. .	119
Figure 4.34: A first order analysis of showing antibacterial effect of 32 wt. % Ag-MWCNTs at 10 °C.	121
Figure 4.35: A first order analysis showing antibacterial effect of 32 wt. % Ag-MWCNTs at 15 °C.	122
Figure 4.36: A first order analysis showing antibacterial effect of 32 wt. % Ag-MWCNTs at 20 °C.	123
Figure 4.37: A first order analysis showing antibacterial effect of 32 wt. % Ag-MWCNTs at 25 °C.	124
Figure 4.38: A first order analysis showing antibacterial effect of 32 wt. % Ag/MWCNTs at 30 °C.	125
Figure 4.39: A plot of $\ln k$ vs. $1/T$ for determining the activation energy of the reaction.....	127

LIST OF SCHEMES

Scheme 3.1: Conversion of cyclodextrin soluble polymer to an insoluble polymer using HMDI.	50
Scheme 3.2: Preparation of the benzoyl substituted β -cyclodextrin.	50
Scheme 3.3: Preparation of the allyl substituted β -cyclodextrin.	51
Scheme 3.4: Mechanism of absorption of 4-hydroxynitrobenzene.	54

LIST OF ABBREVIATIONS

Ag	Silver
C=O	Carbonyl group
CDs	Cyclodextrins
CFU	Colony forming unit
CNTs	Carbon nanotubes
COOH	Carboxylic acid group
DMF	Dimethylformamide
<i>E. coli</i>	Escherichia coli
EDX	Energy dispersive X-ray analysis
EPA	Environmental protection agency's
fMWCNTs	Functionalised multi-walled carbon nanotubes
FWHM	Full width at half maximum
HMDI	Hexamethylene diisocyanate
IR	Infrared spectroscopy
MCL	maximum contaminant level
MWCNTs	Multi-walled carbon nanotubes
NDMA	N-nitrosodimethylamine
OH	Hydroxyl group
PAHs	Polycyclic aromatic hydrocarbons
PCBs	Polychlorinated biphenyls

PVC	Polyvinyl chloride
PXRD	Powder X-ray diffraction
RO	Reverse osmosis
SEM	Scanning electron microscope
TEM	Transmission electron microscopy
UV-Vis	Ultraviolet-visible
VOCs	Volatile organic chemicals
XRD	X-ray Diffraction
fMWCNTs	functionalised multi-walled carbon nanotubes
Ag/ β -CD	Silver β -cyclodextrin
Ag-MWCNTs	Silver multi-walled carbon nanotubes
Ag-MWCNTs/ β -CD	Silver multi-walled carbon nanotubes β -cyclodextrin
MWCNTs/ β -CD	Multi-walled carbon nanotubes β -cyclodextrin

LIST OF SYMBOLS

A	Absorbance
Å	Angstrom
B	Width at half maximum height
BET	Brunauer-Emmet-Teller
c	Concentration
cm	Centimetre
dm	Decimetre
e	Molar absorbance
g	Gram
I	Incident light's intensity
J	Joule
k	Constant
K	Kelvin
l	Path length
mL	Millilitre
mM	Millimolar
mol	Moles
nm	Nanometres
Θ	Theta
°C	Degree Celsius

P	Relative pressure
t	Crystallite size
W	Weight
α	Alpha
β	Beta
γ	Gamma
λ	Wavelength
μm	Micrometre

CHAPTER 1

1.1 RESEARCH PROBLEM

1.1.1 Source and background of the problem

Presently most countries are facing problems with drinking water. The problems are very severe especially in developing countries [1]. Over 75% of the earth's surface is covered with water, and approximately 97.5% of this percentage made up by salt water, which leaves only 2.5% available as fresh water. Nearly 70% of the fresh water is frozen in the icecaps of Antarctica and Greenland; with most of the remaining present as soil moisture, or lying in deep underground aquifers as ground water which is not accessible for human use. Less than 1 wt. % of the world's fresh water is therefore, accessible for direct human use. The accessible water is found in lakes, rivers and the underground reservoirs shallow enough to be tapped at an affordable cost [2, 3].

Scarcity of safe drinking water remains a global problem and is expected to rise with increasing population growth and environmental change [4]. Drinking polluted or contaminated water can cause serious health problems, e.g. cholera and other diarrhoeal diseases which cause many deaths, especially amongst children in developing countries. Water that does not meet accepted drinking water standards should be treated to ensure that the health of the consumer or community is not compromised through exposure to toxic pollutants [4]. The World Health Organization (WHO) recommended that any water intended for drinking should contain faecal and total coliform counts of 0.00 in any 100 mL sample [5]. When bacteria are encountered in water samples, immediate investigative action should be taken [5].

Organic matter in water is the source of many water quality challenges. Even though not specifically toxic, they often produce aesthetically undesirable problems such as colour, odour and bad taste [6]. Natural organic matter can lead to formation of potentially harmful disinfection by-products such as trihalomethanes, halo-aromatic compounds, and other chlorinated organic compounds [7]. Most of these organic compounds are toxic and pose a serious threat to human health, even at very low levels [8].

Given the importance of clean water to people in developed and developing countries, numerous organisations are considering the potential application of nanoscience to solve technical challenges associated with the removal of water contaminants [9, 10].

1.1.2 Statement of the research problem

Safe drinking water is one of the most basic needs in society, but the main problem is lack of availability of fresh water for human consumption. Countless people in the world are experiencing many diseases; some are dreaded, due to consumption of contaminated water [11]. Most often the source of water is raw water from rivers and lakes in which inadequately treated industrial and urban effluents are disposed and in this way, contaminants such as organics, inorganic and micro-organisms are introduced into the water systems [12]. According to the South African constitution, access to safe drinking water is a basic human right and hence the study and research based on organic contaminants removal in water is crucial [11].

Various methods of water treatment have historically been used, such as sedimentation, flocculation, dis-infection and filtration [13]. Conventional dis-infection methods, such as ozonation, and UV (ultraviolet) light have been employed, as good disinfectants. Unfortunately their running and maintenance costs are too high to be sustainable [14]. Chlorination is an effective and affordable disinfectant; but regrettably it degrades some of the organic contaminants into more harmful by-products such as trihalomethanes, polychlorinated biphenyls and trihaloacetic acids. These by-products are known to be either endocrine disruptors or carcinogenic [11]. Previous investigations have shown that carbon nanotubes, silver nanoparticles and cyclodextrin have demonstrated abilities to remove organic contaminants to parts per billion levels [15].

This study focuses upon the preparation, characterisation and investigation of various combinations of these nanocomposite materials for water purification. The relevance of the nanocomposites to enhance removal of organic contaminants and bacteria from polluted water was tested using an *in vitro* model.

1.2 LITERATURE REVIEW

1.2.1 Metal nanoparticles

The major focus in this study is on the use of metal nanoparticles for the removal and detection of severely toxic contaminants such as pesticides, halogenated organics, heavy metals, and micro-organisms, found in drinking water. Metal nanoparticles have two key properties that make them particularly attractive as sorbents: (i) they have larger surface areas than bulk particles and (ii) they can also be functionalised with various chemical groups to increase their affinity towards target compounds [16].

Silver nanoparticles, nanodots or nano-powders are spherical in shape. They are high surface area metal particles with extraordinary antibacterial activity [17]. Zinc oxide nanoparticles and nanoscale zero-valent iron have successfully been used to remove arsenic from ground water, even though bulk zinc oxide cannot absorb arsenic [18]. Some people who drink water containing arsenic in excess of acceptable levels accumulating over many years could experience skin damage or problems with their circulatory system, and may have an increased risk for cancer [19, 20].

1.2.2 Carbon nanotubes

Carbon nanotubes (CNTs) were first rediscovered by Iijima in 1991 [20]. They are hollow nanosized tubes that resemble graphene sheets into a tube. There are two main types of CNTs namely single-walled carbon nanotubes (SWCNTs) and multi-walled carbon nanotubes (MWCNTs) [21].

Researchers are using carbon nanotubes to manufacture substances that have controlled shapes, density, and dimensions for specific filtration applications. Carbon nanotube filters offer a level of precision, suitable for different applications as they can remove a range of particles from 25 nm polio viruses from water to larger pathogens such as *E. coli* and *Staphylococcus aureus* bacteria [22]. Similarly, Park (1998) also found that nanotube based water filters could filter bacteria and smaller

viruses, which were be resilient and reusable. They could be cleaned for reuse by heating the nanotube filter or purging [22].

1.2.3 Nanoporous polymers

Nanoporous polymers are a class of porous materials with diameters between 1 and 100 nm. The nanoporous polymer of choice to be studied in the current investigation is cyclodextrin. Cyclodextrins (CDs) are biosynthetic cyclic oligomers consisting of anhydrous glucopyranosyl units linked together through α -1, 4-glycosidic linkages [23]. They are fundamentally starch derivatives obtained through the enzymatic degradation of starch by glycosyl transferase of *Bacillus macerans*. The three most common CDs are α -, β - and γ -CDs [24]. However, the high solubility of cyclodextrins limits their application in the removal of organic pollutants from water. β -CD was chosen because it's the least soluble in water compared with α - and γ - CDs. It was also reported to be the most restricted in solution, in terms of its solubility; this property renders the β -CD the first priority for water purification, since the first step required making the cyclodextrin insoluble [25].

An elaborate review of all these functional materials is given in chapter 2.

1.3 PURPOSE OF THE STUDY

1.3.1 Aim of the study

The aim of this research is to investigate purification of water samples by using silver doped carbon nanotubes and nanoporous polymers.

1.3.2 Objectives of the study

- (i) To synthesise silver nanoparticles, silver doped carbon nanotubes and cyclodextrin polymers using different preparation procedures and parameters.
- (ii) To characterise silver nanoparticles, carbon nanotubes and cyclodextrin polymers using FE-SEM, EDX, TEM, FTIR and BET.
- (iii) To purify contaminated water samples using the synthesised metal nanoparticles, silver doped carbon nanotubes and cyclodextrin polymers.
- (iv) To perform *in vitro* microbial tests using silver nanoparticles.

- (v) To investigate the combined effect of silver nanoparticles, carbon nanotubes and cyclodextrin polymers for purification of water samples.

1.4 SIGNIFICANCE OF THE PROPOSED RESEARCH

Water is an important resource for domestic, industrial, agricultural and recreational purposes. It is a finite and vulnerable resource that is essential for sustaining life [26]. The quality of water is however, significantly deteriorating due to the accumulation of organic pollutants in aqueous systems [27]. The most significant finding, given the importance of clean water, is to establish convenient, cheap and reliable ways to purify water for everyday use, especially for people in developing countries [28]. The outcome of this project may contribute towards assisting industries such as mining industries, recycling waste water industries, pharmaceutical industries as well as municipalities in their quest to solve the problem of water contamination. This may furthermore complement other methods to improve the health of numerous developing nations.

1.5 OUTLINE OF THE STUDY

In this dissertation, the activity of silver nanoparticles, carbon nanotubes and cyclodextrin polymers for water purification have been investigated. A review of the literature on the synthesis, structure and properties of nanomaterials is discussed in Chapter 2.

A literature review was carried out with respect to the following topics: (a) contaminants in water; with emphasis on organic, inorganic, bacterial and viral contamination, (b) current purification techniques, (c) nanotechnology in water treatment, (d) application of nanocomposite materials to contaminated water, and (e) characterisation techniques. The above topics were reviewed with relevance to the work completed in this investigation.

The experimental methods used to prepare silver nanoparticles, carbon nanotubes, cyclodextrin polymers and nanocomposite materials are also presented in chapter 3.

Characterisation results of the prepared nanocomposite materials are presented in Chapter 4. Results and discussion of purification of water samples contaminated with both organic contaminants and *E. coli* bacteria are also reported in Chapter 4. Investigations of the effects of temperature and catalysis during the water purification process are also discussed in Chapter 4.

Conclusions and recommendations of the study undertaken on water purification are presented in Chapter 5. In this dissertation, Figures, schemes and tables are integrated within the text followed by a detailed listing of the references at the end of each chapter.

The appendices cover calculations of crystallite sizes, colony forming unit calculations, percentage inactivation of the bacteria and calculations on activation energy.

1. 6 REFERENCES

1. Daily, G.C., Ehrlich P.R. and Postel, S.L. 1996. Human appropriation of renewable fresh water. *Journal of Science*, 271. 785 - 788.
2. Gleick, P. 2000. Water insecurity and emotional distress. Island Press. 379 - 382.
3. Ehrlich, P.R., Ehrlich, A.H., Matson, P.A. and Vitousek, P.M. 1986. Human appropriation of the products of photosynthesis. *Journal of biosciences*, 36. 368 - 373.
4. Reddy, C.D. and Voortman, W.J. 2005. Package Water Treatment Plant Selection. *Water research commission report*, 450. 3 - 7.
5. Havelaar, A. and Bartram, J. 1996. World Health Organization: Guidelines for drinking water quality. *World health organisation*, 2. 29 - 31.
6. Thurman, E.M. 1985. Organic geochemistry of natural waters. Maritinus Nijhoff, Dr W. Junk Publishers, Dordrecht. 2119 - 2125.
7. Murray, C.A. and Parsons, S.A. 2004. Removal of NOM from drinking water: Fenton's and photo-Fenton's process. *Journal of chemosphere*, 54. 1017 - 1023.
8. Gallard, H. and von Gunten, U. 2002. Chlorination of natural organic matter: kinetics of chlorination and of THM formation. *Journal of water research*, 36. 65 - 74.
9. Korom, S., Bekker K. and Helweg, O.J. 2000. Water for Life: Making it happen. *World health organisation, United Nations international children's emergency fund*. 21 - 28.
10. Maynard, A. 2007. Nanotechnology in context - Size matter. *Journal of nature*, 444. 267 - 269.
11. Momba, M.N.B. and Broukavert, B.M. 2005. Water problems. *Water research commission report*, 5. 249 - 251.
12. Schutte, C.F. and Folcke, W. 2007. Water problems. *Water research commission report*, 8. 195 - 198.
13. Parsons, S.A. and Jefferson, B. 2006. Introduction of portable water treatment processes. Blackwell publishing Ltd, Oxford, UK. 311 - 317.

14. Solsona, F. and Pearson, I. 1995. Water problems. *Water research commission report*, 9. 449 - 455
15. Mhanga, D.S. 2008. *Quantitative analysis for the removal of natural organic matter and degradation by-products from water using cyclodextrin nanoporous polymers*. Johannesburg. SA. 29, 31 - 36.
16. Boutayeb, A. and Boutayeb, S. 2005. The burden of non-communicable diseases in developing countries. *International journal for equity in health*, 4. 13 - 17.
17. Furno, F., Morley, K.S. Bong, B., Sharp, B.L., Arnold, P.L., Howdle, S.M., Bayston, R., Brown P., Winship, P.D. and Reid, H.J. 2004. Silver nanoparticles and polymeric medical device: A new approach to prevention of infection. *Journal of antimicrobial chemotherapy*, 54. 1019 - 1024.
18. Chibi, C. and Vinnicombe, D.A. 1999. Promising Approaches in the removal of fluoride and nitrate in rural drinking water supplies. *Water research commission workshop*, Pretoria, South Africa. 33 - 35.
19. Brittany, L., Carino, V., Kuo J., Leong L. and Ganesh, R. 2006. Adsorption of organic compounds to metal oxide nanoparticles. *World applied science journal*, 3. 20 - 35.
20. Iijima, S. 1991. Atoms in carbon cages: The structure and properties of endohedral fullerenes. *Journal of nature*, 354. 56 - 60.
21. Kuzmany, H., Kukovecz, A., Simon, F., Holzweber, M., Kramber, C. and Pilcher, T. 2004. Functionalization of carbon nanotubes. *Journal of synthetic metals*, 141. 113 - 118.
22. Park, K.D. 1998. Bacterial adhesion on PEG modified polyurethane surfaces. *Journal of biomaterials*, 19. 851 - 859.
23. Roco, M.C. 1999. Nanoporous polymers for water purification. *Journal of nanoscience and nanotechnology*, 1. 143 - 153.
24. Bender, M.L. and Komiyama, M. 1978. Cyclodextrin chemistry. Springer Verlag, New York. 786 - 787.

25. Croft, A.P, Bartsch, R.A. 1983. Synthesis of chemically modified cyclodextrins. *Tetrahedron Letters*, 39. 1417 - 1474.
26. Margiloff, I.B. 1997. Carbon nanotubes and cyclodextrin for removing organic contaminants. *Journal of chemical engineering*, 93. 10 - 13.
27. Suffet, H.I. and MacCathy P. 1989. Aquatic Humic Substances: Influence on fate and treatment of pollutants. *Journal of American chemical society*, 7. 333 - 362.
28. Conroy, R.M., Meegan, M.E., Joyce, T.M., McGuigan K.G. and Barnes J. 2001. Use of solar dis-infection protects children less than 6 years from cholera. *Journal of archives of disease in childhood*, 85. 293 - 295.

CHAPTER 2

LITERATURE REVIEW

2.1 INTRODUCTION

This chapter serves to explore the literature, terminologies and information that establish the main thrust of this research. Different nanotechnology methods for purification of water samples will be outlined and discussed in detail. Organic contaminants and other major water contaminants will be extensively deliberated.

2.2 CONTAMINANTS IN WATER

2.2.1 Organic contaminants

The term 'organic' in this research pertains to compounds that have the element carbon as a principal constituent. Organic compounds are of many types and have various origins.

2.2.1.1 Detergents

Constituents commonly found in shampoo, detergents and fabric softener are precursors of a suspected cancer-causing chemical in treated wastewater i.e. nitrosamines. In a study by Hawley *et al.* (2005) it was reported that harmful nitrosamines from quaternary amines, are found in many consumer products. Pre-treatment with ozone or chlorine does not lessen the amount of nitrosamines that accumulate, and as a result; many of these nitrosamines end up in drinking water, wastewater and recreational water [1].

Nitrosamine or N-nitrosodimethylamine (NDMA) is of specific interest because it is a toxic organic chemical which is also carcinogenic to humans. Nitrosamines, such as NDMA, are formed during dis-infection processes of drinking water, wastewater, and recreational water, but particularly during dis-infection of the chloramines. Their formation has caused considerable concern, because the United States

Environmental Protection Agency (EPA) has classified several nitrosamines as human carcinogens [2].

2.2.1.2 Dis-infection by-products

Dis-infection by-products are formed when disinfectants used in water treatment plants such as chlorine react with bromide and/or natural organic matter (decaying vegetation) present in the source water. Dis-infection by-products which have been identified in drinking water, includes trihalomethanes, haloacetic acids, bromate, and chlorite [3]. Since the discovery of chlorinating by-products in drinking water in 1974, numerous toxicological studies conducted confirmed that dis-infection by-products are carcinogenic in laboratory animals (e.g., including bromate, certain trihalomethanes and haloacetic acids) [4]. Some dis-infection by-products have also been shown to cause adverse reproductive or developmental effects in laboratory animals [5].

2.2.1.3 Dioxins

Dioxins are organic polyhalogenated compounds of white crystalline needles that are vital in nature because they act as environmental pollutants [6]. Dioxin is not produced or used commercially, but it's a contaminant formed in the production of some chlorinated organic compounds. Dioxins occur as by-products in the manufacture of organochlorides, in the burning of chlorine-containing substances such as polyvinyl chloride (PVC) plastics, in the bleaching of paper, and from natural sources such as volcanoes and forest fires [6].

Humans are primarily exposed to dioxins by eating food contaminated by these chemicals. Dioxin accumulates in the fatty tissues, where they may persist for months or years. People who have been exposed to high levels of dioxin have developed conditions such as chloracne, a skin disease marked by severe acne-like pimples. Dioxin also causes health problems if present in public or private water supplies in amounts greater than the drinking water standard set by EPA [6].

2.2.1.4 Natural organic matter

Natural organics in drinking water are caused by the decay of naturally occurring vegetation and animals i.e., lignins or tannins. They are mainly found in lakes, rivers and man-made water reservoirs [7]. Other examples include organic acids, amino acids and humic substances. The presence of these compounds, dissolved in water, would be part of the natural environmental condition of that water resource. Natural organics cause bad odour, taste and also give colour to drinking water; but most importantly, they regulate the formation of dis-infection by-products during the chlorine purification process [8].

2.2.1.5 Polycyclic aromatic hydrocarbons

Polycyclic aromatic hydrocarbons (PAHs) are a group comprising more than 100 different chemicals that are formed during the incomplete burning of coal, oil, gas, garbage, or other organic substances like tobacco or charred meat [9]. PAHs enter water through discharges from industrial and wastewater treatment plants. Since most PAHs do not dissolve easily in water, they stick to solid particles which then sediment at the bottom of lakes or rivers. Microorganisms can break down PAHs in soil or water after a period of weeks or months [10]. In soils, PAHs are most likely to stick tightly to particles; but certain PAHs move through the soil to contaminate underground water. As a pollutant, they are of concern because they have also been identified as carcinogenic, mutagenic and teratogenic [11].

2.2.1.6 Polychlorinated biphenyls

Polychlorinated biphenyls (PCBs) are a class of organic compounds which can be odourless, tasteless and clear to pale-yellow, viscous liquids and highly chlorinated mixtures. They are formed by electrophilic chlorination of biphenyls with chlorine gas. Presently the major sources of polychlorinated biphenyls in drinking water are mainly runoffs from landfills; and discharge of waste chemicals [12].

Some people who drink water containing polychlorinated biphenyls well in excess of the maximum contaminant level for many years, could experience changes in their skin, thymus gland, immune deficiencies, or reproductive or nervous system difficulties, and may have an increased risk of developing cancer. PCBs have been demonstrated in literature to cause cancer as well as a variety of other adverse health effects on the immune system, reproductive system, nervous system, and endocrine system [13].

2.2.2 Inorganic contaminants

The second category of water contaminants includes inorganic chemicals and heavy metals. These are usually substances of mineral origin, salt, metals, and minerals. Heavy metal toxicity or poisoning arises when the body accumulates an excessive amount of a heavy metal, such as mercury, lead, arsenic, cadmium, aluminium or nickel which places the individual at risk of serious illness. These heavy metals play no known biological role in the human body, unlike with some other elements such as selenium (which is an effective antioxidant), iron (required by blood cells), and copper (which is an integral part of many enzymes). Since they are not useful to the body, these heavy metals are accumulated and stored in tissues; over time they eventually cause serious health problems [14].

2.2.2.1 Arsenic

Arsenic is an odourless and tasteless metalloid element that enters drinking water supplies from natural deposits in the ground or from adjacent agricultural and industrial practices. Arsenic as well as arsenic containing compounds are human carcinogens, and can cause cancer. Exposure to arsenic may occur through several anthropogenic sources including mining, pesticides, pharmaceuticals, glass and microelectronics, but the most dominant sources of exposure today has been through natural sources [15].

General health effects that are associated with arsenic exposure include cardiovascular and peripheral vascular disease, developmental anomalies,

neurologic and neurobehavioral disorders, diabetes, hearing loss, portal fibrosis, hematologic disorders (anaemia, leukopenia and eosinophilia) and multiple cancers. It has consistently been shown by various studies, that there are significantly higher mortality rates and increasing mortality rates for cancers of the skin, lung, liver, urinary bladder, kidney, and colon in many areas of known arsenic pollution [16].

2.2.2.2 Asbestos

Asbestos is a term that represents a group of minerals that have numerous common properties which are heat resistant and chemically inert. In the 1980s it was recognized that inhalation exposure to asbestos fibres can cause severe health problems such as mesothelioma, lung cancer, and asbestosis. Due to these effects, many mines producing commercial asbestos during the time were closed down and a concerted effort was made to eradicate asbestos from schools, work places, and public buildings [17].

Presently, however, the major sources of asbestos in drinking water are from asbestos cement water mains and erosion of natural deposits. People who drink water containing asbestos well in excess of the maximum contaminant level (MCL) for many years have been shown to have an increased risk of developing benign intestinal polyps and lung abnormalities such as pleural thickening or scarring this was observed in about 18% of the adults tested [17].

2.2.2.3 Lead

Lead, a metal found in natural deposits is usually used in household plumbing materials and water service lines. The greatest exposure to lead is swallowing or inhaling lead paint chips and dust. Lead in drinking water can cause a variety of adverse health effects [18]. In children, exposure to lead in drinking water above normal levels can result in delays in physical and mental development, along with slight deficits in attention span and learning abilities. In adults, it can cause increased blood pressure and could possibly also develop related kidney conditions [19].

Lead is rarely found in source water, but enters tap water through corrosion of plumbing materials, and therefore homes built before 1986 are more likely to have lead pipes, fixtures and solders. However, new homes are also at risk, as even legally “lead-free” plumbing may still contain up to 8% lead. The most common persistent problem is with brass or chrome-plated brass faucets and fixtures which can leach significant amounts of lead into the water, especially hot water [20].

2.2.2.4 Mercury

Mercury is a liquid metal found in natural deposits as ore material containing other elements. Elemental mercury is released from industrial processes, agricultural processes, household, commercial and medical products containing mercury, sewage discharge and sediment. Mercury is unique amongst metals in that it can evaporate when released into water or soil. Microbes can convert inorganic forms of mercury to organic forms which can be bio-accumulated by aquatic life [21].

Toxicity caused by excessive mercury exposure is now becoming recognized as a widespread environmental problem and is continuing to attract a great deal of public attention. This toxicity is caused by either drinking contaminated water, eating fish contaminated with mercury, leaching of mercury from badly placed dental fillings as well as from vaccinations containing thimerosal, an organomercury compound. Elemental mercury vapour may cause nervous system damage when exposed to high concentrations [14].

2.2.3 Bacterial contamination

Bacteria are responsible for many diseases caused by drinking contaminated water. Organisms such as *Escherichia coli*, *Salmonella* spp, *Vibrio* spp, and *Cryptosporidium* are known to be transmitted by water and cause ill health in communities consuming such waters [22]. It becomes very expensive for health institutions to manage and treat such diseases and in most cases, such epidemics result in human mortality [23]. A few examples of common bacteria that contaminate water are discussed below:

2.2.3.1 Escherichia coli

Escherichia coli (*E. coli*) named after Theodor Escherichia, is a Gram-negative, rod-shaped bacterium (Figure 2.1) commonly found in the lower intestine of warm-blooded organisms. Most *E. coli* strains are harmless, but some serotypes can cause serious food poisoning in humans, and are occasionally responsible for product recalls [24].

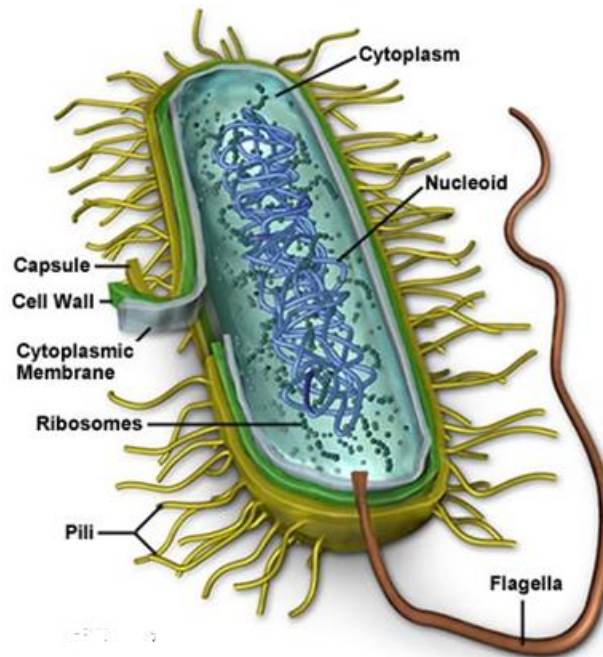


Figure 2.1: The structure of a rod-shaped bacterium [24].

The presence of *E. coli* in water is a strong indication of recent sewage or animal waste contamination. Sewages may contain many types of disease-causing organisms such as *E. coli* due to the presence of human and animal waste. During rainfalls, snow melts, or other types of precipitation, *E. coli* may be washed into creeks, rivers, streams, lakes, or groundwater. When these waters are used as sources of drinking water and the water is either not treated or inadequately treated, *E. coli* may be present. Virulent strains of *E. coli* can cause gastroenteritis, urinary tract infections, and neonatal meningitis. In rare cases, virulent strains are also responsible for haemolytic-uremic syndrome, peritonitis, mastitis, septicaemia and Gram-negative pneumonia [25].

2.2.3.2 Cryptosporidium

Cryptosporidium parvum is a protozoan parasite that causes cryptosporidiosis. There has been a greater force to remove *Cryptosporidium* from municipal water supplies since its outbreak [26]. *Cryptosporidium* infected faecal material enters the water supply either by cross contamination of sewage lines with water lines, or alternatively by surface water infected with contaminated animal waste. Having infected its host, the oocysts erupt, thus releasing four flagellated spores that attach to the walls of the gastrointestinal tract, and eventually form oocysts which will undergo the same life cycle [27].

Symptoms occur 2 to 10 days after infection which amongst others include diarrhoea, headache, abdominal cramps, nausea, vomiting, and a fever. There is no treatment regime against the protozoa, although it is possible to treat the symptoms. After about 1-2 weeks, the symptoms subside as the immune system fights the infection. However, in persons with a compromised immune system such as infants, aged or frail, or those already with AIDS, cryptosporidiosis may become life threatening. Water treatment processes that utilise coagulation, sedimentation, filtration and chlorination may possibly remove these organisms. However, due to its small size and its resistance to chlorination, these treatments may not always be successful [27].

2.2.3.3 Shigella

Shigella is a family of bacteria that can cause sudden and severe diarrhoea (gastroenteritis) in humans. Shigellosis, the illness caused by the ingestion of *Shigella* bacteria, is also known as bacillary dysentery. *Shigella* bacteria can cause food poisoning, making *Shigella* one of the most communicable and severe forms of the bacterial-induced diarrheal infections [28].

Shigella thrives in the human intestine and is commonly spread through water, food and person-to-person contact. *Shigella* is the third most common pathogen transmitted through food. *Shigella* infections can then be acquired by drinking, swimming in or playing in the contaminated water [29].

2.2.3.4 *Vibrio cholera*

Vibrio cholera (also *Kommabacillus*) is a Gram-negative comma-shaped bacterium with a polar flagellum that causes Cholera in humans. *Vibrio cholera* together with other species of the same genus belongs to the Proteobacteria [30].

This species, was first isolated as the cause of cholera by Italian anatomist Filippo Pacini in 1854, but his discovery was not widely known until Robert Koch, working independently thirty years later, publicised the knowledge and the means to fight the disease. Transmission is primarily due to faecal contamination of food and water due to poor sanitation, but this bacterium can, however, live naturally in any environment [31].

2.2.3.5 Faecal coliform

Faecal coliform is a facultative-anaerobic, rod-shaped, Gram-negative, non-sporulating bacterium. Faecal coliforms are bacteria that are associated with human or animal waste. They usually inhabit human or animal intestinal tracts, and their presence in drinking water is a strong indication of recent sewage or animal waste contamination. Coliform bacteria include genera that originate in faeces (e.g. *Escherichia*) as well as other general bacteria which are not of faecal origin (e.g. *Enterobacter*, *Klebsiella*, *Citrobacter*) [32].

Water pollution caused by faecal contamination is a serious problem due to the potential of contracting diseases from pathogens. Concentrations of pathogens from faecal contamination are usually small, and therefore it is not practical to test for pathogens in every water sample that is collected. Instead, the presence of pathogens is determined with indirect evidence by testing for an indicator organism such as coliform bacteria. Coliforms come from similar sources as those of pathogenic organisms. Coliforms are quite easy to identify, they usually exist in larger numbers than more dangerous pathogens, and respond to treatment similar to many other pathogens. As a result, testing for coliform bacteria can be a good indication of whether other pathogenic bacteria are present or not [33].

2.2.4 Viral contamination

2.2.4.1 Hepatitis A

Hepatitis A is an enteric virus that is extremely small and can be spread by contaminated water, eventually causing severe outbreaks [34]. The virus is excreted by a person carrying it, and if the sewage contaminates the water supply, then the virus is carried in the water until it is ingested by a possible host. Common symptoms include inflamed liver, accompanied by lassitude, anorexia, weakness, nausea, fever and jaundice. A mild case may only require a week or two of rest, while a severe case, can result in severe liver damage and possible death of the infected patient [27].

2.2.4.2 Rotavirus

Rotavirus is the most common cause of severe diarrhoea among infants and young children. It causes infections such as stomach flu, despite having no viral link to influenza. The genus is double-stranded RNA viruses from the family *Reoviridae*. By the age of five, nearly every child in the world would have been infected with rotavirus at least once in their lifetime [35]. However, with each infection acquired, immunity develops, and subsequent infections are less severe. Adults are less severely affected by this virus [36].

The virus is transmitted by the faecal-oral route. The presence of rotavirus in water and sewage displays contamination of the virus in the environment. It infects and damages the cells that line the small intestine and thus causes severe gastroenteritis. Although the rotavirus was discovered in 1973 and accounts for up to 50% of hospitalisations for severe diarrhoea in infants and children, [37] its importance is still not widely publicised within the public health community, particularly in developing countries. In addition to its impact on human health, rotavirus also infects animals, and is a pathogen of livestock [38].

2.2.4.3 Norovirus

The norovirus is an RNA virus that causes approximately 90% of epidemic non-bacterial outbreaks of gastroenteritis around the world. The norovirus may be responsible for 50% of all foodborne outbreaks of gastroenteritis in the United States [39]. Norovirus affects people of all ages, and is transmitted by faecally contaminated food or water, by person-to-person contact, through air-borne mechanisms of the virus and subsequent contamination of surfaces [40].

After infection, immunity to norovirus is usually incomplete and temporary. There is an inherited predisposition to infection and therefore individuals with blood type O are more prone to infection, [41] whereas blood types B and AB can confer partial immunity against symptomatic infection. Outbreaks of the norovirus infection often occur in closed or semi-closed communities, such as long-term care facilities, overnight camps, hospitals and prisons where the infection spreads very quickly either by person-to-person transmission or through contaminated food. Many Norovirus outbreaks have been traced to food that was handled by one infected person [42].

2.3 CURRENT PURIFICATION TECHNIQUES

The methods described below are not exhaustive, but covers significantly used current water purification techniques.

2.3.1 Chlorination

Chlorine is used to destroy disease-causing organisms in water, an essential step in delivering safe drinking water and protecting public health. Chlorine is by far the most commonly used disinfectant in all regions of the world, and has helped to virtually eliminate waterborne diseases such as cholera, typhoid and dysentery. Chlorination is effective against many pathogenic bacteria, but at normal dosage rates it does not destroy all viruses, cysts, or worms [43]. As with many chemical innovations, what was once thought to be completely harmless has turned out to be poisonous. Over the past 30 years, scientists have discovered that while chlorine kills microbes, it also reacts with organic matter already in the water to form toxic chemicals, the organochlorines. The organochlorine commonly found at the highest concentration is chloroform, which is carcinogenic [44].

The problem with chlorine is that it converts the organochlorides into deadly trihalomethanes and unidentified mutagen cancer cocktails. To date, several hundred known organochlorines have been found in drinking water but most of them are still chemically unidentified. Chloroform is toxic and it illustrates the most important feature of chlorination or chlorine reactions with organic matter. Natural organochlorines generally serve as chemical deterrents to predators and parasites [45].

2.3.2 Ultraviolet light/lamps

Ultraviolet radiation has commonly been used to eradicate microorganisms in water. Mercury low pressure lamps generating 254 nm UV light are an effective means of disinfecting water. The adsorption of UV light by the DNA and proteins in the microbial cell inactivates the microorganism. Most ultraviolet purification systems are combined with various forms of filtration. UV light is only capable of destroying microorganisms such as bacteria, viruses, fungi, algae, yeast, and oocytes like

Cryptosporidium and *Giardia*. UV light generally has no impact on chlorine, volatile organic chemicals (VOCs), heavy metals, and other chemical contaminants [46].

A major disadvantage of UV filtration is that it does not leave disinfection residuals that are needed to persist in maintaining clean water. UV-disinfected water may become re-contaminated if exposed to further bacterial contamination. A UV water filter may not be effective if water is highly turbid or contaminated with sedimentary and organic materials. A pre-filter would be necessary to remove any materials that may mask the viruses and bacteria from UV light [47].

2.3.3 Reverse osmosis

Reverse osmosis (RO) is a filtration method that removes many types of large molecules and ions from solutions by applying pressure to the solution when it is on one side of a selective membrane. The result is that the solute is retained on the pressurized side of the membrane and the pure solvent is allowed to pass to the other side. The membrane does not allow large molecules or ions through the pores, but allows smaller components of the solution to pass freely [48]. Reverse osmosis, however, involves a diffusive mechanism so that separation efficiency is dependent on solute concentration, pressure, and water flux-rate. Reverse osmosis is most commonly known for its use in purification of sea water, by removing salt and other substances [48].

One of the disadvantages of reverse osmosis from a health perspective is that it de-mineralizes water. Trace minerals are important to human health since research has shown that drinking de-mineralized water on a regular basis caused digestive problems and nutritional deficiencies. While reverse osmosis is effective for removing a variety of contaminants in water, it does not remove volatile organic chemicals, chlorine and chloramines, pharmaceuticals, and a host of other synthetic chemicals found in municipal water [49].

Water entering the reverse osmosis system should also be free of bacteria. While reverse osmosis systems do remove nearly all microorganisms, the risk of contamination through tiny leaks or deteriorating parts, prevents reverse osmosis systems from being used to actively remove bacteria. Chemical contamination is one of the biggest problems that we face, as over a thousand cancer causing chemicals

have already been identified from tap water. From a health perspective, this is therefore one of the biggest disadvantages of reverse osmosis [50].

2.3.4 Filtration membranes

Membrane filtration describes a family of separation methods. The basic principle is to use semi-permeable membranes to separate fluids, gases, particles and/or solutes [51]. Membranes are usually shaped as a thin film, which allows transport of some materials. Semi-permeable membranes have pores ranging from 0.5 nm to 5 μm . Microfiltration (MF) and Ultrafiltration (UF) are filtration processes that operate on a physical sieving separation process [52]. They are best used for the removal of suspended solids, the reduction of turbidity, and as a pre-treatment to desalination technologies such as nano-filtration and reverse osmosis. Microfiltration utilises only physical filtration to remove particles in the 0.1 to 10 micron range. For complete removal of viruses, ultra filtration is required. The pores of ultrafiltration membranes can remove particles ranging from 0.001-0.1 μm from fluids [52].

Nano-filtration is a relatively recent membrane process used most often with low total dissolved solids water such as surface water and fresh groundwater, with the purpose of softening (polyvalent cation removal) and removal of disinfection by-product precursors such as natural organic matter and synthetic organic matter [53]. This means nutrients should be added back to bring the water back to the standards levels for drinking water. Nano-filtration methods remove fewer solutes, so may avoid the need to re-mineralize the water [53].

2.4 NANOTECHNOLOGY IN WATER TREATMENT

The term 'nanotechnology' describes materials, systems and processes that exist or operate at the extremely small scale of a few hundred nanometres (nm) or less. Nanotechnology has the potential to profoundly change our economy and to improve our standard of living, just as the impact that information technology has had throughout the world just in the past two decades [54]. The high surface area to mass ratios of nanoparticles can greatly enhance the adsorption capacities of sorbent materials. Using nanoparticles could chemically degrade pollutants instead of simply moving them somewhere else, including pollutants for which existing technologies are inefficient or cost prohibitive. Behari *et al.* (2008) suggested that nanotechnology offers more effective, efficient, durable, and affordable approaches to removing specific types of pollutants from water [55].

2.4.1 Metal nanoparticles

The production of metal nanoparticles is becoming a very important field in chemistry, biology, and materials science. Metal nanoparticles have been investigated extensively in recent years because of their size-dependent electronic and optical properties and the possibility of arranging them in micro- and nano-assemblies [56]. Much effort has been devoted to the synthesis and characterisation of stable dispersions of nanoparticles made of silver, gold, and other noble metals [57]. Exciting prospects for the development of novel electronic devices, electro-optical applications, and catalysis have been established [58].

The major focus will be to review the use of metal nanoparticles for the removal and detection of severely toxic contaminants such as pesticides, halogenated organics, heavy metals, and micro-organisms, found in drinking water. Metal nanoparticles have two key properties that make them particularly attractive as sorbents, they have much larger surface areas than bulk particles and they can also be functionalised with various chemical groups to increase their affinity towards target compounds [55]. Silver (Ag) is a transition metal element having atomic number 47 and atomic mass 107.87 g/mol. Silver nanoparticles are spherical or flake-like high surface area metal particles having high antibacterial activity. The medicinal uses of silver have

been documented since 1000 B.C. Currently the investigation of this phenomenon has regained importance due to the increase of bacterial resistance to antibiotics, caused by their overuse [59].

Silver nanoparticles possess an effective anti-bacterial activity and they are widely recognised as being effective because of their enormous high surface area. For a long time silver has been known to have a disinfecting effect and has found applications in many traditional medicines and culinary items [60]. Recently silver nanoparticles, as well as various silver-based compounds containing ionic silver (Ag^+) or metallic silver (Ag^0) exhibiting antimicrobial activity have been synthesised [61]. Antibacterial activity of the silver-containing materials can be used, for example, in medical applications in order to reduce infections, in burn treatments and arthroplasty. They may be used to prevent bacterial colonisation and biofilm formation on prostheses, catheters, vascular grafts, dental materials, stainless steel materials, and human skin [62].

Silver ions have been demonstrated to be useful and effective in bactericidal applications, but due to the unique properties of nanoparticles, nanotechnology now presents a reasonable alternative for the development of new bactericides. Metal particles in the nanometre size range exhibit physical properties that are different from both the ionic and the bulk materials. This makes them exhibit remarkable properties such as increased catalytic activity due to morphologies with highly active facets [63]. Silver-containing materials can be employed to eliminate microorganisms on textile fabrics or they can be used for water treatment. Silver nanoparticles also exhibit a potent cyto-protective activity toward HIV-infected cells and because of such incredibly wide ranges of applications, numerous synthetic methods have been developed [64]. Contrary to bactericidal effects of ionic silver, the antimicrobial activity of colloid silver particles is influenced by the dimensions of the particles - hence the smaller the nanoparticles, the greater the antimicrobial effect [65]. Studies also show that Ag nanoparticles shows enhanced antibacterial effects against *E. coli* used with amoxicillin, a β -lactam antibiotics [66].

Zinc oxide nanoparticles and nanoscale zero-valent iron have successfully been used to remove arsenic from ground water, even though bulk zinc oxide cannot absorb arsenic [67]. Some people who drink water containing arsenic in excess of

EPA standards over many years could experience skin damage or problems with their circulatory system, and may therefore have an increased risk of developing cancer [68].

2.4.2 Carbon nanotubes

Carbon nanotubes are allotropes of carbon with hollow nano-sized tubes that resemble graphene sheets into a tube [69]. Carbon nanotubes were rediscovered when synthesised by Iijima in 1991 [70]. There are two main types of carbon nanotubes (Figure 2), namely single-walled carbon nanotubes (SWCNTs) and multi-walled carbon nanotubes (MWCNTs) [71].

Single walled carbon nanotubes consist of only one layer and can be fabricated in a variety of ways on a modified version of arc-discharge generators used for fullerene synthesis. Multi-walled carbon nanotubes are made of more than one layer that form concentric tubes separated by 0.35 nm, similar to the basal plane separation in graphite. Structurally a SWCNT is a rolled-up, single-layer graphene sheet (Figure 2.2b) with a diameter of c.a. 1 nm and a length of several micrometres or longer, whereas a MWCNTs contains two or more concentric layers with various diameters and lengths (Figure 2.2c) [72].

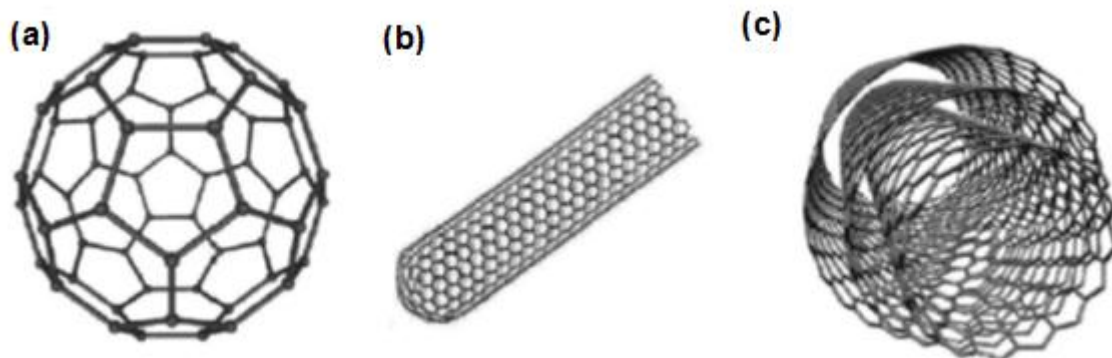


Figure 2.2: Examples of carbon based nano-materials (CNMs). (a) Fullerene C_{60} , (b) A single walled carbon nanotube, (c) Multi walled carbon nanotubes [72].

Carbon nanotubes have attracted much attention from researchers because of their thermal, mechanical, electrical and adsorption properties [73]. They have a length-to-

diameter ratio significantly larger than any other nanostructured materials. These novel properties make them potentially useful in many diverse applications extending across nanotechnology, electronics, optics and any other field of material science, as well as potential uses in architectural fields [69].

Carbon nanotubes and their derivatives are used in plastics, catalysts, battery and fuel-cell electrodes, super-capacitors, water purification systems, orthopaedic implants, conductive coatings, adhesives and composites, sensors, and components in the electronics, aircraft, aerospace, and automotive industries [72, 74]. Carbon nanomaterials have shown high adsorption capacity for polycyclic aromatic hydrocarbon pesticides, endocrine disrupting chemicals, pharmaceuticals and other contaminants. Properties of carbon nanotubes such as large surface area and affinity for hydrophobic organic compounds make them an efficient adsorbent, thus creating potential applications both for wastewater treatment and water decontamination [75]. Adsorption by carbon nanomaterials is characterised by higher capacity. Lu *et al.* (2005) reported a higher adsorption and shorter equilibrium time needed for trihalomethanes attached to carbon nanotubes [76].

The accessible sorption sites of CNT bundles include the surface area, the interstitial and groove areas formed between the CNTs, as well as the inner pores of the tubes. Carbon nanotubes can contain functional groups such as -OH, -C=O, and -COOH. Functionalisation of CNTs is aimed at facilitating easy processing, but similarly, their adsorption properties with organic chemicals can be greatly altered. Functional groups may also increase diffusional resistance and reduce the accessibility and affinity of CNT surfaces for organic chemicals [75].

2.4.3 Nanoporous polymers

Nanoporous polymers (Figure 2.3) are a class of porous materials with diameters between 1 and 100 nm which are starch derivatives obtained through the enzymatic degradation of starch by glycosyl transferase of *Bacillus macerans*. The type of nanoporous polymer to be studied here is cyclodextrins. Cyclodextrins (CDs) are biosynthetic cyclic oligomers consisting of anhydrous glucopyranosyl units linked together through α -1, 4-glycosidic linkages [77].

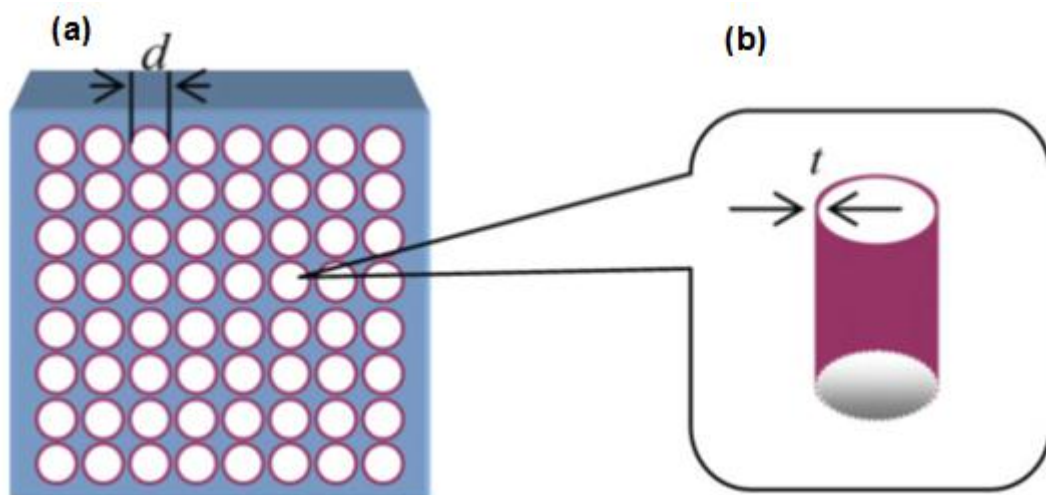


Figure 2.3: Schematic illustration of nanoporous structures (d represent the diameter of a cylindrical pore and t represent the thickness of the inner surface). Inset: arbitrary cylindrical nanopore in nanoporous structures [78].

Cyclodextrins have hydrophilic exteriors and hydrophobic interiors (Figure 2.4 and Figure 2.5). The CD rings are about 8 Å deep and 5-10 Å in diameter, depending on the number of glucose units. Cyclodextrins are also capable of interacting with a range of guest molecules within their cylindrical hydrophobic cavities which form the basis for the inclusion of various organic species. The structures of the formed complexes are largely dependent on the sizes of the cavities of the CDs [78].

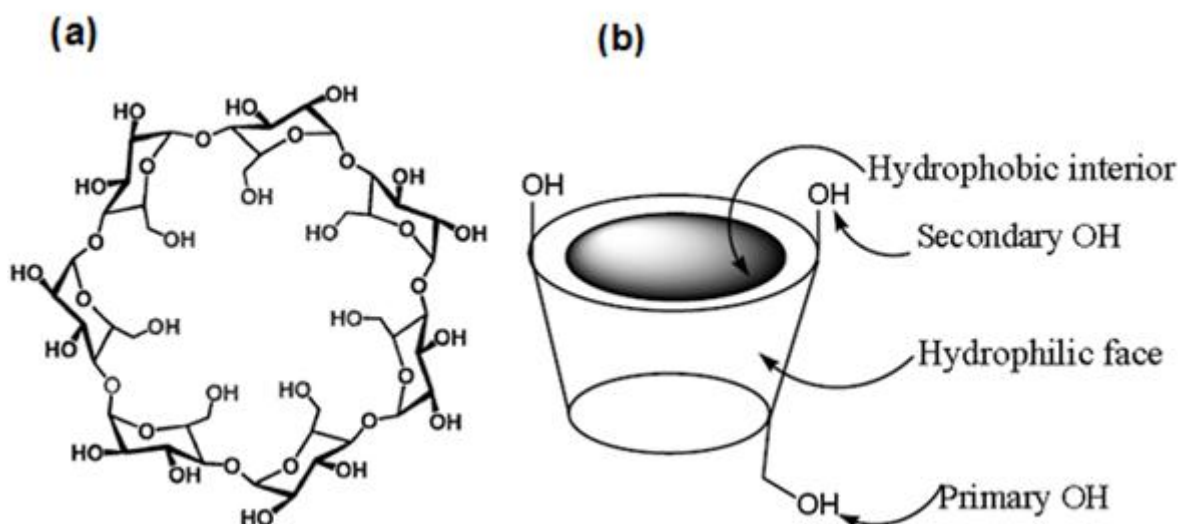


Figure 2.4: The structures of β -cyclodextrin [79].

The high solubility of cyclodextrins (CDs) limits their application in the removal of organic pollutants from water. To make them insoluble, they need to be converted into highly cross-linked polymers by polymerising with suitable bifunctional linkers such as hexamethylene diisocyanate [79]. Most modifications of CDs take place at the hydroxyl groups (OHs). According to Szejtli [1998], an electrophilic reagent attacks at the most reactive OH [80].

Bender and Komiyama, [1978] further report that the binding between organic contaminants and the nanoporous polymer is 100,000 times greater than the binding between organic contaminants and activated carbon, which is commonly used in wastewater treatment [78].

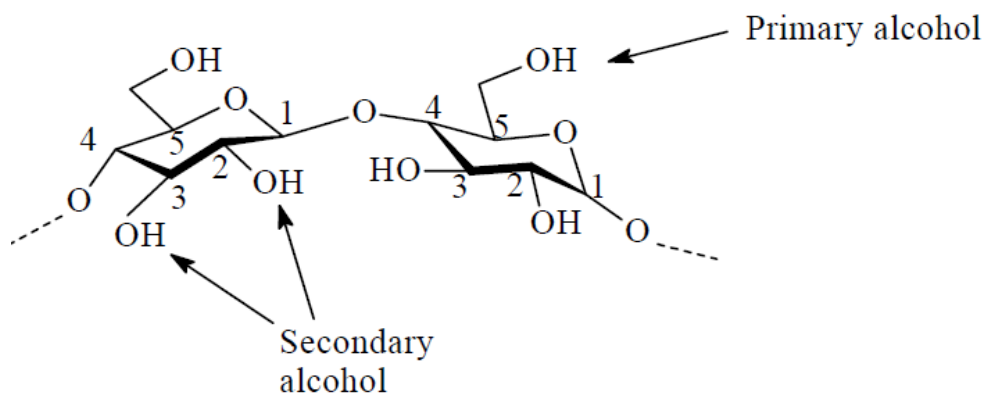


Figure 2.5: The three different types of hydroxyl groups of a CD [80].

Most modifications of CDs take place at the hydroxyl groups (Figure 2.5). The C-6 hydroxyl groups are the most basic and thus most nucleophilic, the C-2 hydroxyls are most acidic and the C-3 hydroxyls are the most inaccessible because they are sterically hindered. Therefore, under normal circumstances, an electrophilic reagent attacks at the most reactive C-6 OHs. The C-2 OH's are the most susceptible to deprotonation, and the oxyanion formed is considered to be more nucleophilic than the non-deprotonated OH's at the C-6 [80].

Thin film composite (TFC) membranes modified with amine functionalized β -cyclodextrins have been used both in desalination and the removal of organic pollutants from water. The incorporation of CDs into thin film composite membranes had improved their hydrophilicity and flux whilst maintaining the high rejection capacity of a variety of dissolved salts [81].

2.4.4 Application of nanocomposite materials and filtration membranes to contaminated water

Silver nanoparticles have been immobilised on carbon materials such as activated carbon and carbon nanotubes. They have been used as bactericidal materials. Metal loaded polymers were able to reduce bacterial counts in spiked water, therefore enhancing the nanocomposites' antibacterial characteristic [82]. Ag-MWCNTs hybrids have offered an effective destruction of both the Gram-positive and Gram-negative bacteria to afford a wide antimicrobial activity. This insoluble carbon

nanotube-based nanohybrid can be easily filtered on a porous filter to separate them from the aqueous phase that it disinfects [83].

Carbon nanoporous materials exhibit high surface areas, large pore volumes and uniform mesopores. The nanoporous polymers have shown good absorption abilities, which compared favourably to their unfunctionalised counterparts [84]. Carbon nanotubes have also exhibited excellent adsorption properties in the removal of lead, cadmium and organic 1, 2-dichlorobenzene from water, being a promising candidate in wastewater treatment. The morphologies of the CNTs can affect their adsorption capabilities greatly [85].

Mamba *et al.* (2007) demonstrated that polymerised cyclodextrins with functionalised carbon nanotubes had an enhanced absorption capacity for p-nitrophenol compared to activated carbon and native cyclodextrin polymers [86]. The synthesised nanocomposites (5% MWCNTs/ β -CD) were able to remove close to 100% of trichloro ethylene and up to 99% of p-nitrophenol from water samples [86].

2.5 CHARACTERISATION TECHNIQUES

Metal nanoparticles, carbon nanotubes and nanoporous materials are generally characterised by employing the following instruments:

2.5.1 Transmission electron microscopy (TEM)

Transmission electron microscopy is a microscopic technique whereby a fast moving beam of electrons is transmitted through an ultra-thin specimen, interacting with the specimen as it passes through [87]. An image is formed from the interaction of the electrons transmitted through the specimen which is then projected onto a fluorescent screen. The magnified image is then recorded by means of an imaging device, such as a photographic film, or detected by a sensor such as a CCD camera [87].

A transmission electron microscope is capable of imaging at a significantly higher resolution than light microscopes, with magnification capabilities usually in the 100 000 to 400 000 times range in a conventional 120 kV instrument [88]. Transmission electron microscopy is an important means of analysis employed in a range of scientific fields, including the physical and biological sciences. Transmission electron microscopy can further be used to observe modulations in chemical identity, crystal orientation, electronic structure and sample induced electron phase shift through many mechanisms such as crystallography, diffraction and X-ray analysis [88].

2.5.2 Scanning electron microscope (SEM)

A scanning electron microscope on the other hand, magnifies the sample surface area by scanning it with a high-energy beam of electrons in a raster scan pattern. The electrons interact with the atoms that make up the sample producing signals which contain information about the sample's surface topography, composition and other properties such as electrical conductivity [89]. The types of signals produced by SEM include secondary electrons, back-scattered electrons, characteristic X-rays, light, and transmitted electrons [90].

The signals result from interactions of the electron beam with atoms at or near the surface of the sample. In the most common or standard detection mode, the SEM can produce very high-resolution images of a sample surface, revealing details less than 1 to 5 nm in size. Due to the very narrow electron beam, SEM micrographs have a large depth of field yielding a characteristic three-dimensional appearance useful for understanding the surface structure of a sample. Characteristic X-rays are emitted when the electron beam removes an inner shell electron from the sample, causing a higher energy electron to fill the shell with a resultant release of energy [90].

2.5.3 Ultraviolet/Visible spectrophotometer (UV/Vis)

Spectrophotometry is one of the branches of spectroscopy where absorption of light by dissolved molecules or ions is measured. It investigates the absorption of the different substances between the wavelength limits of 190 nm and 800 nm. Ultraviolet light is measured between 190 and 400 nm, and visible light is measured between 400 and 800 nm. The absorption or reflectance in the visible range directly affects the perceived colour of the chemicals involved. In this region of the electromagnetic spectrum, molecules undergo electronic transitions [91].

Spectrophotometry is used for both qualitative and quantitative investigations of samples. The wavelength at the maximum of the absorption band will provide information about the structure of the molecule or ion where the extent of the absorption is proportional to the amount of the species absorbing the light [92].

Quantitative measurements are based on Beer-Lambert's Law which is described as follows:

$$A = ecl$$

where **A** = absorbance [arbitrary units, because it is calculated as $A = \log_{10} (I_0/I)$,

I_0 is the incident light's intensity and I is the light intensity after it passes through the sample]

e = molar absorbance or absorption coefficient (in $\text{dm}^3 \text{mol}^{-1} \text{cm}^{-1}$)

c = concentration (molarity) of the compound in the solution (in mol dm⁻³)

l = path length of light in the sample (in cm)

UV/Vis spectrophotometry involves the absorption of ultraviolet light by a molecule causing the elevation of an electron from a ground electronic state to an excited electronic state. The light intensity measured by the detector is converted into an electric signal and is displayed as a certain absorbance on the readout [91].

The concentration is calculated from the results by using the molar absorptivity found in the literature. The unknown concentration can be determined by comparing the results with a working curve of absorbance versus concentration (calibration curve) derived by using various accredited standards [91].

2.5.4 Fourier transform Infrared spectroscopy (FTIR)

Infrared spectroscopy (IR spectroscopy) deals with the infrared region of the electromagnetic spectrum that is light with a longer wavelength and lower frequency than visible light, and can be used to identify and investigate chemicals. Infrared spectroscopy is used to determine the functional groups present in a molecule. The infrared portion of the electromagnetic spectrum is usually divided into three regions; the near-, mid- and far-infrared, named for their relation to the visible spectrum. The higher energy near-IR, approximately 14000-4000 cm⁻¹ (0.8-2.5 μm wavelength) can excite overtone or harmonic vibrations [93].

The mid-infrared, approximately 4000-400 cm⁻¹ (2.5-30 μm) may be used to study the fundamental vibrations and associated rotational-vibrational structure. The far-infrared, approximately 400-10 cm⁻¹ (30-1000 μm), lying adjacent to the microwave region, has low energy and may be used for rotational spectroscopy. Infrared spectroscopy is widely used in both research and industry as a simple and reliable technique for measurement, quality control and dynamic measurement [93].

2.5.5 Brunauer-Emmett -Teller (BET)

Brunauer-Emmett-Teller (BET) surface area analysis is a technique used to determine the surface area of powders, solids and granules, the values are expressed in meter square per gram [94]. Brunauer-Emmett-Teller method is based on adsorption of gas on a surface and the amount of gas adsorbed at a given pressure allows determination of the surface area [94].

The BET equation:

$$\frac{1}{v \left[\left(\frac{p_0}{p} \right) - 1 \right]} = \frac{c - 1}{v_m c} \left(\frac{p}{p_0} \right) + \frac{1}{v_m c}$$

P = equilibrium pressure of adsorbates

p_0 = saturation pressure of adsorbates

v = adsorbed gas quantity

v_m = monolayer adsorbed gas quantity

c = BET constant

The BET surface area measurement is vital in understanding the behaviour of a specific material, as materials react with the environment via the surface. A higher surface area material is more likely to react faster, dissolve faster and adsorb more gas than a similar material with a lower surface area [95].

2.5.6 Powder X-ray diffraction (PXRD)

Powder X-ray diffraction (PXRD) is the most commonly used technique for characterising solid materials. Powder XRD consists of fine grains in the form of single crystallites, where each crystalline substance has a unique X-ray diffraction pattern. X-Ray beams that collide with the solid, causes an interaction with electrons of a particular solid. Interference is possible when the wavelength of the incoming X-ray is comparable to the separation between the atoms. When ordered arrays of scattering centres are present, the reflected X-rays will show interference maxima

and minima. Typical wavelengths used for X-ray experiments are between 0.6 and 1.9 Å. The d -spacing of the observed peaks relate to the repeating distances between planes of atoms in the structure [96].

Powder diffraction patterns are typically plotted as the intensity of the diffracted X-rays against the angle 2θ . The intensity of each peak is caused by the crystallographic structure, i.e. the position of the atoms within the unit cell and their thermal vibration. Peaks will appear in the diffraction pattern at 2θ values when constructive interference is at a maximum, that is, when Bragg's Law (eq. 1) is satisfied [96].

$$n\lambda = 2d \sin \theta$$

The positions and the intensities of the peaks can be used for identifying the structure of a solid material, verify the purity of a solid product, follow the status of a solid-state synthesis, determine or refine the lattice parameters of a solid and to determine the crystallite size of a sample [97].

The Scherrer equation (in the appendices) explains peak broadening in terms of incident beam divergence which makes it possible to satisfy the Bragg condition for non-adjacent diffraction planes. Crystallite size can also cause peak broadening. Once instrument effects have been excluded, the crystallite size is easily calculated as a function of peak width (specified as the full width at half maximum peak intensity (FWHM)), peak position and wavelength. A shape factor is used in X-ray diffraction to relate the size of crystallites [98].

2.6 REFERENCES

1. Hawley, E.L., Deeb, R.A., Mitch, W.A., Durbin, T.D. Sedlak, D.L., Mowbray, S. and Carr, S. 2005. Sources and fate of nitrosodimethylamine and its precursors in municipal wastewater treatment plants. *Water environment research journal*, 77. 32 - 39.
2. Gerecke, A.C. and Sedlak, D.L. 2003. Precursors of *N*-nitrosodimethylamine in natural waters. *International journal of environmental science and technology*, 37. 1331 - 1336.
3. Backer, L.C., Ashley D.L., Bonin, M.A., Cardinali FL., Kieszak, SM. and Wooten J.V. 2000. Household exposures to drinking water disinfection by-products: whole blood trihalomethanes levels. *Journal of exposure analysis and environmental epidemiology*, 10. 321 - 6.
4. Gordon, G.W., Cooper, J., Rip, G., and Gilbert E. Pacey. 1987. Disinfectant residual measurement methods. AWWA research foundation. *American water works association*.
5. Calderon, R.L. 2000. The epidemiology of chemical contaminants of drinking water. *Food and chemical toxicology*, 38. 13 - 20.
6. Weber, R., Tysklind, M. and Gaus, C. 2008. Dioxin, contemporary and future challenges of historical legacies. *Environmental science and pollution research*, 15. 96 - 100.
7. Macalady, D.L, Ranville, J.F. 1998. *The chemistry and geochemistry of natural organic matter*. New York: Oxford University press. 95 - 130.
8. Connell, D.W. 1997. Basic concepts of environmental chemistry. New York: Lewis Publishers. 205 - 216.
9. Marce, R.M. and Borrull, F. 2000. Solid-phase extraction of polycyclic aromatic compounds. *Journal of chromatography A*, 885. 273 - 290.
10. Fetzer, J. C. 2000. The chemistry and analysis of the large polycyclic aromatic hydrocarbons and polycyclic aromatic compounds. New York: Wiley, 27. 143 - 145.
11. Larsson, B.K., Sahlberg, GP, Eriksson, A.T, Busk, L.A. 1983. Polycyclic aromatic hydrocarbons in grilled food. *Journal of agricultural and food chemistry*, 31. 867 - 873.

12. Porta, M. and Zumeta, E. 2002. Implementing the stockholm treaty on POPs. *Occupational & environmental medicine*, 59. 651 - 652.
13. Safe, S and Hutzinger, O. 1984. Polychlorinated biphenyls (PCBs) and polybrominated biphenyls (PBBs): Biochemistry, toxicology, and mechanism of action. *Critical reviews in toxicology*, 13. 319 - 95.
14. Riedel D., Tremblay, N. and Tompkins, E.1997. *State of knowledge report for environmental contaminants and human health in the great lakes*. Basin, Ottawa.147 - 148.
15. Centeno, J.A., Mullick, F.G, Martinez, L., Page, N.P., Gibb, H., Longfellow, D., Thompson, D. and Ladich, E.R. 2002. Pathology related to chronic arsenic exposure. *Environmental health perspectives*. 110. 883 - 886.
16. Tchounwou, P.B, Patlolla, A.K, Centeno, J.A. 2003. Carcinogenic and systemic health effects associated with arsenic exposure. *Toxicologic pathology*, 31. 575 - 588.
17. Van Gosen, B.S., Lowers, H.A, Bush, A.L, Meeker, G.P, Plumlee, G.S, Brownfield, I.K. and Sutley, S.J. 2002. Reconnaissance study of the geology of U. S. vermiculite deposits. Are asbestos minerals common constituents? U. S. *Geological survey bulletin*, 2192. 12 - 15.
18. Charles, J., Kopf, P.W. and Toby, S. 1966. The Reaction of pyrophoric lead with oxygen. *Journal of physical chemistry*, 70. 1478 - 1480.
19. Howard, H. 1991. Knowledge of diagnosis and reproductive history among survivors of childhood plumbism. *American journal of public health*, 81. 1070 - 1072.
20. Greet, S., Elly, D.H., Willem, D., Van Larebeke, N. and Marike, L. 2008. Endocrine disruptors and abnormalities of pubertal development. *Basic & clinical pharmacology & toxicology*, 102. 168 - 175.
21. Green, J. and Damji, S. 2007. Why is mercury a liquid at STP? *Chemistry*. Melton: IBID Press, 3rd Ed.
22. Droste, R.L. 1997. Theory and practice of water and wastewater treatment. John Wiley and Sons, Toronto.
23. Momba, M.N.B. Broukovert, B.M. 2005. Water Dis-infection Using Novel Cyclodextrin Polyurethanes Containing Silver Nanoparticles Supported on Carbon Nanotubes. *Water research commission report*. TT249/05.

24. Vogt, R.L., Dippold, L. 2005. Escherichia coli O157:H7 Outbreak associated with consumption of ground beef, June - July 2002". *Public Health Rep*, 120 (2). 174 - 178.
25. Todar, K. 2004. The good, the bad, and the deadly. *Science magazine*, 304.1421 - 1423.
26. Craun, G.F. 1986. Waterborne disease in the United States. CRC Press, Inc. Boca Raton, FL.
27. Havelaar, A. and Bartram, J. 1996. World health organization: Guidelines for drinking water quality. *World health organisation*, 2. 29 - 31.
28. Gomez, A.L., Volek, J.S., Love, D.M., Weyers, A.M., Hesslink, R. Jr., Wise, J.A. and Kraemer, W.J. 2002. Effects of an eight-week weight-loss program on cardiovascular disease risk factors and regional body composition. *European journal of clinical nutrition*, 56. 585 - 592.
29. Kramer, M.A, Roopun, A.K, Carracedo, L.M, Traub, R.D, and Whittington, M.A. 2008. Rhythm generation through period concatenation in Rat Somatosensory Cortex. *PLOS computational biology journal*, 4. 5 - 15.
30. Ryan, K.J. and Ray, C.G. 2004. Sherris Medical Microbiology. McGraw Hill.
31. Howard, J.N. 1984. Robert Koch and the cholera vibrio: a centenary. *British medical journal*, 288. 379 - 381.
32. Doyle, M.P. and Erickson, M. C. 2006. Closing the door on the faecal coliform assay. *Microbe journal*, 1. 162 - 163.
33. Daniels, B. and Mesner, N. 2010. Drinking water facts: Coliform bacteria. Utah state university. USA. 1 - 6.
34. John DeZyane, P.E. 1990. Handbook of drinking water quality. Van Nostrand Reinhold, NY.
35. Dennehy, P.H. 2000. Transmission of rotavirus and other enteric pathogens in the home. *Paediatric infectious disease journal*, 19. S103 - 105.
36. Bishop, R.F. 1996. Natural history of human rotavirus infection. *Archives of virology, supplement journal*, 12. 119 - 28.
37. Rheingans, R.D., Heylen, J. and Giaquinto, C. 2006. Economics of rotavirus gastroenteritis and vaccination in Europe: what makes sense? *Pediatric infectious disease journal*, 25. 48 - 55.

38. Holland, R.E. 1990. Some infectious causes of diarrhoea in young farm animals. *Journal of clinical microbiology*, 3. 345 - 375.
39. Lindesmith, L., Moe, C. and Marionneau S. 2003. Human susceptibility and resistance to Norwalk virus infection. *Nature medicine*, 9. 548 - 53.
40. Widdowson, M.A., Sulka, A. and Bulens, S.N. 2005. Norovirus and foodborne disease, United States. *Emerging infectious disease journal*, 11. 95 - 102.
41. Hutson, A.M., Atmar, R.L., Graham, D.Y. and Estes, M.K. 2003. Norwalk virus infection and disease is associated with ABO histo-blood group type. *Journal of infectious diseases*, 188 .176 - 177.
42. Noda, M., Fukuda, S., Nishio, O. 2007. Statistical analysis of attack rate in norovirus foodborne outbreaks. *International Journal of food microbiology*, 122. 216 - 220.
43. Koski, T.A., Stuart, L.S. and Ortenzio, L.F. 1966. Comparison of chlorine, bromine, iodine as disinfectants for swimming pool water. *Applied Microbiology*, 14 (2). 276 - 279.
44. Gribble, G.W. 1998. Naturally occurring organohalogen compounds. *Accounts of chemical research journal*, 31. 141 - 152.
45. Connell, D. 1999. Introduction to Ecotoxicology. Blackwell Science. 68 - 70.
46. Arnold, W.R. and Rainbow A.J. 1996. Host cell reactivation of irradiated adenovirus in UV-sensitive Chinese hamster ovary cell mutants. *Mutagenesis journal*, 11. 89 - 94.
47. Altic, L.C., Rowe, M.T., Grant, I.R. 2007. UV light inactivation of Mycobacterium avium subsp. paratuberculosis in milk as assessed by fast plaque TB phage assay and culture. *Applied and environmental microbiology journal*, 73. 3728 - 3733.
48. Crittenden, J., Trussell, R.H. and Howe, K. and Tchobanoglous, G. 2005. Water Treatment Principles and Design. 2nd edition. John Wiley and Sons. New Jersey.
49. Pomerantz, N., Ladizhansky, Y., Korin, E., Waisman, M., Daltrophe, N. and Gilron, J. 2006. Prevention of scaling of reverse osmosis membranes by “zeroing” the elapsed nucleation time. *Chemistry research journal*, 45. 2008 - 2016.

50. Bartman, A., McFall, C., Christofides, P. and Cohen. Y. 2009. Model-predictive control of feed flow reversal in a reverse osmosis desalination process. *Journal of process control*, 19. 433 - 442.
51. Mulder, M. 1996. Basic Principles of Membrane Technology. Kluwer Acad. Publ, Dordrecht.
52. Thorsen, T. 1999. Fundamental Studies on Membrane Filtration of Coloured Surface Water. Ph.D. thesis, NTNU, Trondheim, November.
53. Mallevalle, J., Odendaal, P.E. and Wiesner, M.R. 1996. Water treatment membrane processes, McGraw-Hill New York 1996.
54. Bimber, B. and Guston, D. 1997. Technology assessment: The end of OTA. *Technology forecasting and social changes*, 54. 233 - 250.
55. Behari, J., Dharmendra, K., Prasenjit, S. and Tiwari, R.P. 2008. Nanoparticles in waste water treatment. *World applied sciences journal*, 3. 419 - 430.
56. Schmid, G. and Chi, L. F. 1998. Metal clusters and colloids. *Advanced materials journal*, 10. 515 - 518.
57. El-Sayed, M. A. 2001. Why gold nanoparticles are more precious than pretty gold. *Accounts of Chemical Research journal*, 34. 257 - 260.
58. Weller, H. 1993. Precisions synthesis of nanocrystals and their use in biomedical applications. *Angewandte chemie international journal* 32. 41 - 45.
59. Furno, F., Morley, K.S., Bong, B., Sharp, B.L., Arnold, P.L., Howdle, S.M., Bayston, R., Brown P., Winship, P.D. and Reid, H.J. 2004. Silver nanoparticles and polymeric medical device: A new approach to prevention of infection. *Journal of antimicrobial chemotherapy*, 54. 1019 - 1024.
60. Holladay, R., Moeller, W., Mehta D., Brooks J., Roy, R. and Mortenson, M. 2006. Silver/water, silver gels and silver-based compositions; and methods for making and using the same *application number* WO2005US47699 20051230. European patent office.
61. Baker, C., Pradhan, A., Pakstis, L., Pochan, D.J., Shah, S. I.J. 2005. Synthesis and antimicrobial properties of silver nanoparticles. *Journal of nanoscience and nanotechnology*, 5. 244.
62. Lee, D., Cohen, R.E. and Rubner, M.F. 2005. Antibacterial properties of Ag nanoparticle loaded multilayers and formation of magnetically directed antibacterial microparticles. *Langmuir journal*, 21. 9651.

63. Doraiswamy, N. and Marks, L. D. 1996. Nanotechnology in medicine and antibacterial effect of silver nanoparticles. *Applied surface science journal*, 348. 67.
64. Jeong, S.H., Yeo, S.Y., and Yi, S.C.J. 2005. Antibacterial effect of nanosized silver colloidal solution on textile fabrics. *Journal of materials science*, 40. 5407.
65. Leopold, N. and Lendl, B. 2003. A new method for fast preparation of highly surface-enhanced raman scattering active silver colloids at room temperature by reduction of silver nitrate with hydroxylamine hydrochloride. *Journal of physical chemistry B*, 107. 5723.
66. Jain, P. and Pradeep, T. 2005. Potential of silver nanoparticle-coated polyurethane foam as an antibacterial water filter. *Journal of bioscience and bioengineering* 90. 59 - 63.
67. McDowall, L. 2005. Degradation of toxic chemicals by zero-valent metal nanoparticles. Defence science and technology organisation. *DSTO-GD-0446*. Australia. 8 - 15.
68. Brittany, L., Carino, V., Kuo J., Leong L. and Ganesh, R. 2006. Adsorption of organic Compounds to metal oxide nanoparticles. *World applied science journal*, 3. 20 - 35.
69. Srivastava, A., Srivastava O.N., Talapatra, S., Vajtai, R., and Ajayan, P.M. 2004. Carbon Nanotube Filters. *Nature materials journal*, 3. 610 - 614
70. Iijima, S. 1991 Atoms in carbon cages: The structure and properties of endohedral fullerenes. *Journal of nature*, 354. 56 - 60
71. Kuzmany, H., Kukovecz, A., Simon, F., Holzweber, M., Kramber, C. and Pilcher, T. 2004. Functionalization of carbon nanotubes. *Synthetic metals journal*, 141. 113 - 118.
72. Ajayan, P.M. 1991. Substrate and size effects on the coalescence of small particles. *Chemical review*, 99. 1787.
73. Peng X., Luan Z., Din J., Li. and Tian B. 2005. Removal of Dyes from Water by Carbon Nanotubes. *Materials letter*, 59. 399.
74. Park, K.D. 1998. Bacterial adhesion on PEG modified polyurethane surfaces. *Journal of biomaterials*, 19. 851 - 859.

75. Pan, B. Lin, D. Mashayekhi H. and Xing, B. 2008. Adsorption of Organic Compounds by Carbon Nanomaterials in Aqueous Phase. *International journal of environmental science and technology*, 42. 5480.
76. Lu, Y., Chung, L.C.S. and Chang, K. F. 2005. Pollution prevention and treatment using nanotechnology. *Water research journal*, 39. 1183.
77. Roco, M.C. 1999. Nanoporous polymers for water purification. *Journal of nanoscale science & technology*, 1. 143 - 153.
78. Bender, M.L. and Komiyama, M. 1978. Cyclodextrin chemistry. Springer Verlag, New York. 786 - 787.
79. Croft, A.P and Bartsch, R.A. 1983. Synthesis of chemically modified cyclodextrins. *Tetrahedron journal*, 39. 1417 - 1474.
80. Szejtli, J. 1998. Introduction and general overview of cyclodextrin chemistry. *Chemical review*, 98. 1443 -1753.
81. Mbuli, B.S., Krause, R.W., Pillay, V.L., Oren, Y., Linder, C. and Mamba B.B. 2013. Preparation and characterization of thin film composite membranes using functionalized cyclodextrins for the purification of water. *Journal of applied polymer science*. 549 - 558.
82. Yua, W., Jiang, G., Che, J., Qi, X. and Chang, M.W. 2008. Deposition of silver nanoparticles on multiwalled carbon nanotubes grafted with hyperbranched poly (amidoamine) and their antimicrobial effects. *Journal of physical chemistry C*. 18754 - 18759.
83. Lukhele, L.P., Mamba, B.B., Momba, N.B., Krause, R.W.M. 2010. Water disinfection using novel cyclodextrin supported on carbon nanotubes. *Journal of applied sciences*, 10 (1): 65 - 70.
84. Li, Y.H., Zhao, Y.M., Hu, W.B., Ahmad, I., Zhu, Y.Q., Peng, X.J. and Luan, Z.K. 2007. Carbon nanotubes - the promising adsorbent in waste water treatment. *Journal of physics: Conference series*, 61. 698 - 691.
85. Lee, J., Han, S. and Hyeon, T. 2004. Synthesis of new nanoporous carbon materials using nanostructured silica materials as templates. National creative research initiative centre for oxide nanocrystalline materials and school of chemical Engineering. Seoul national university. Korea. 151 - 156.

86. Mamba, B.B., Krause, R.W. Malefetse, T.J. 2007. Monofunctionalised cyclodextrin polymers for the removal of organic pollutants from water. *Environmental chemistry letters*, 5. 79 - 84.
87. Ruska, E. 2000. The early development of electron lenses and electron microscopy. *Journal of science*, 60. 28 - 32.
88. Crewe, A.V., Wall, J. and Langmore, J. 1970. Visibility of a single atom. *Journal of science*, 68. 1338 - 1340.
89. Knoll, M. 1935. Aufladepotential und Sekundäremission elektronenbestrahlter Körper. *Zeitschrift für technische physik*, 16. 467 - 475
90. Von Manfred, A. 1939. Das elektronen-rastermikroskop. Theoretische Grundlagen". *Zeitschrift für physik*, 108. 9 - 10, 553 - 572
91. Skoog, D.A., West D.M and Holler F.J. 1992. Fundamentals of analytical chemistry. Saunders college publishing, Fort Worth, US. 169 -173.
92. Kenkel J. 1994. Analytical chemistry for technicians. Lewis publishers, Boca Raton, US.
93. Laurence, M., Harwood C.J., and Moody. 1989. Experimental organic chemistry: Principles and practice (Illustrated Ed.). Wiley-Blackwell. 292 - 295.
94. Lowell, S., Shields, J.E., Thomas, M.A., and Thommes, M. 2004 Characterization of porous solids and powders: surface area, pore size and density. Dordrecht, South Holland, the Netherlands: Kluwer academic publishers. 67 - 70.
95. Sing, K.S.W., Fraissard, J.P. and Conner, C.W. 1997. *Physical Adsorption: Experiment, Theory and Applications*. Dordrecht, South Holland, the Netherlands: Kluwer Academic Publishers. 6 - 10.
96. Geselbracht, M.J. 2008. *Introduction to X-ray powder diffraction*. Reed College. 1 - 9.
97. Jenkins, R. and Snyder, R.L. 1996. *Introduction to X-ray powder Diffractometry*. John Wiley & Sons Inc. 89 - 91.
98. Cullity, B.D. and Stock, S.R. 2001. Elements of X-Ray Diffraction. 3rd Ed. Prentice-Hall Inc. 167 - 171.

CHAPTER 3

RESEARCH METHODOLOGY

3.1 INTRODUCTION

In this study, different materials were prepared for application in water purification. Cyclodextrin polymers and nanocomposites were synthesised and characterised. The prepared materials were then tested *in-vivo* using water contaminated with organic contaminants as well as water contaminated with *E. coli* bacteria.

3.2 REAGENTS AND CHEMICALS

All chemicals were of Analytical Reagent (AR) grade and were used as received, whilst some were further purified when required. Sodium dodecyl sulphate ($\text{NaC}_{12}\text{H}_{25}\text{SO}_4$), dimethylformamide ($\text{C}_3\text{H}_7\text{NO}$), nitric acid (HNO_3), sulphuric acid (H_2SO_4), silver nitrate (AgNO_3), calcium hydride (CaH_2), hydrazine hydrate (N_2H_4), trisodium citrate ($\text{Na}_3\text{C}_6\text{H}_5\text{O}_7$), 4-hydroxynitrobenzene ($\text{C}_6\text{H}_5\text{NO}_3$), β -cyclodextrin ($\text{C}_{42}\text{H}_{70}\text{O}_{35}$), benzoyl chloride ($\text{C}_7\text{H}_5\text{ClO}$), sodium hydride (NaH), acetone ($\text{C}_3\text{H}_6\text{O}$), allyl bromide ($\text{C}_3\text{H}_5\text{Br}$), hexamethylene diisocyanate ($\text{C}_8\text{H}_{12}\text{N}_2\text{O}_2$) and MWCNTs (> 95% purity) were purchased from Sigma- Aldrich™ (South Africa).

Escherichia coli (*E. coli*), ATCC 25922 bacteria, bacteriological agar and nutrient broth were also purchased from Sigma-Aldrich. Sterilised distilled water and the nutrient agar plates used in growing and maintaining the bacterial cultures were supplied by Microbiology Laboratories, university of Limpopo, Turfloop. Dimethylformamide (DMF) (200 mL) was dried over 2 g of calcium hydride for 48 h before usage. After 48 h, DMF was distilled over calcium sulphate under inert (argon) conditions for purification purposes. Multi-walled carbon nanotubes were functionalised first before they were incorporated on to the nanocomposites.

3.3 CHARACTERISATION TECHNIQUES

3.3.1 Field Emission Scanning Electron Microscopy (FE-SEM)

Figure 3.1 shows the sputter coater model Q150T ES (Quorum Technologies, USA) that was used in this research. A thin layer of Tungsten was evaporated onto the surface of the specimen to make them conductive so that electrons that come into contact with them can be reflected and then scattered.



Figure 3.1: Sputter coater.

The scattered electrons were then attracted towards the detector. Thereafter the electrons were converted to form an image that was observed on the display monitor. The conversion of electrons was facilitated by the photo-multiplier tube on the side of the column.

Figure 3.2 shows the FE-SEM Zeiss Supra 55VP (Carl Zeiss, Germany) operated between 2 kV and 3 kV that was used in this research.

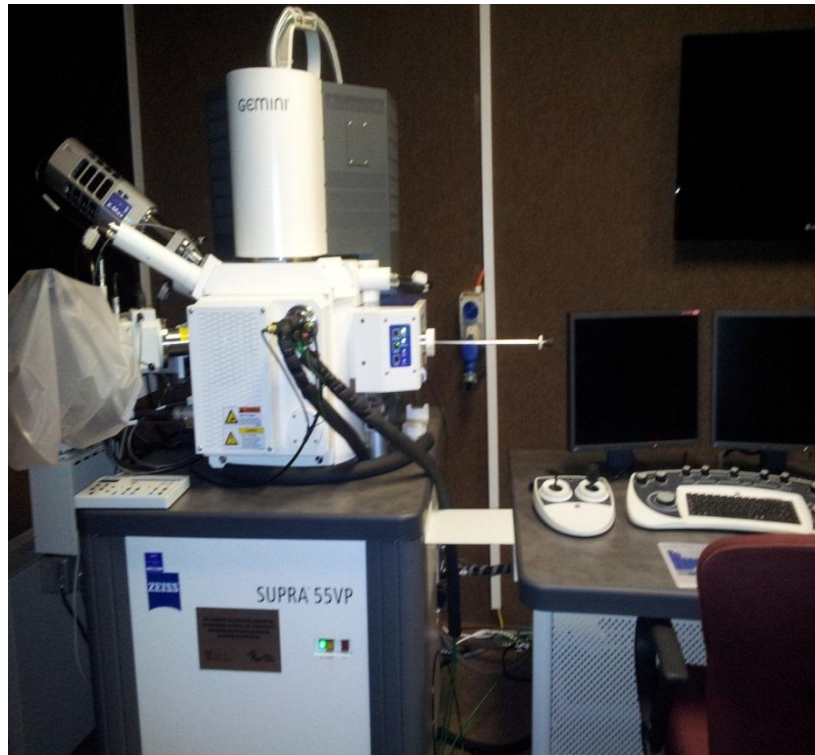


Figure 3.2: Field Emission Scanning electron microscope.

Materials such as MWCNTs, Ag nanoparticles, cyclodextrins, functionalised cyclodextrin polymers as well as the nanocomposites were sputter coated before analysis with the FE-SEM.

3.3.2 Transmission electron microscopy

The electron microscope shown in Figure 3.3 used was a Jeol (Tokyo, Japan) JEM-1010 transmission electron microscope. Specimens to be viewed in TEM were prepared using a negative staining technique with formvar coated grids. Concentrated aqueous suspensions of *E. coli* cells were exposed to an aqueous 3% phosphotungstic acid (PTA) solution for 1 minute. After that, a minute solution was deposited on *formvar*-coated copper grids and allowed to settle for a further 2 minutes.



Figure 3.3: Transmission electron microscope.

The copper grids of materials such as MWCNTs, Ag nanoparticles and cyclodextrin nanocomposites were dispersed in ethanol, placed on *formvar* coated copper grids, and thereafter viewed by means of TEM. The projected images were photographed by means of the SiS Megaview III digital camera and the software used was Soft Imaging Systems from Olympus Germany.

3.3.3 X-Ray diffraction

X-Ray powder diffraction (XRD) patterns of the synthesised nanocomposite materials were determined on a Bruker D2 Phaser X-Ray diffractometer which is a bench-top type with high intensity Cu-K α radiation ($\lambda = 1.54 \text{ \AA}$) and a graphite monochromator at a scanning rate of 0.02 s^{-1} ranging from 10 to 120° . The diffractometer was operated at 30 kV and 10 mA current. The results obtained were exported and then plotted using Origin 6.1 software program.

3.3.4 Fourier transform Infrared spectroscopy

Agilent Cary 600 series FTIR spectrophotometer was used in these studies. The instrument was calibrated by running the background first, followed by collecting the sample which was loaded as received on the sampling plate. The results obtained were exported and then plotted using Origin 6.1 software program.

3.3.5 Brunauer-Emmett-Teller analysis

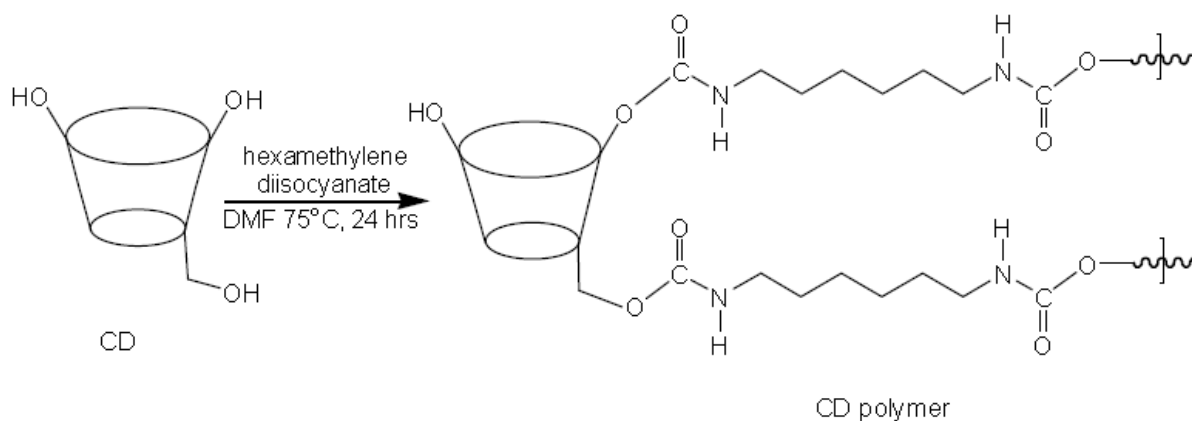
BET analysis of the synthesised nanocomposite materials was done using an automated Trister 3000 V6.05 gas adsorption analyser. The samples were degassed with nitrogen gas for 12 h at a flow rate of 60 cm³/min using Micrometrics Degassing System at 150 °C prior to the determination of their surface areas and pore volumes. The analysis was performed under liquid nitrogen. The standard multi-point BET measurements were followed.

3.4 EXPERIMENTAL

3.4.1 Synthesis of functionalised β -cyclodextrin nanocomposites

3.4.1.1 Synthesis of the insoluble β -cyclodextrin nanocomposites

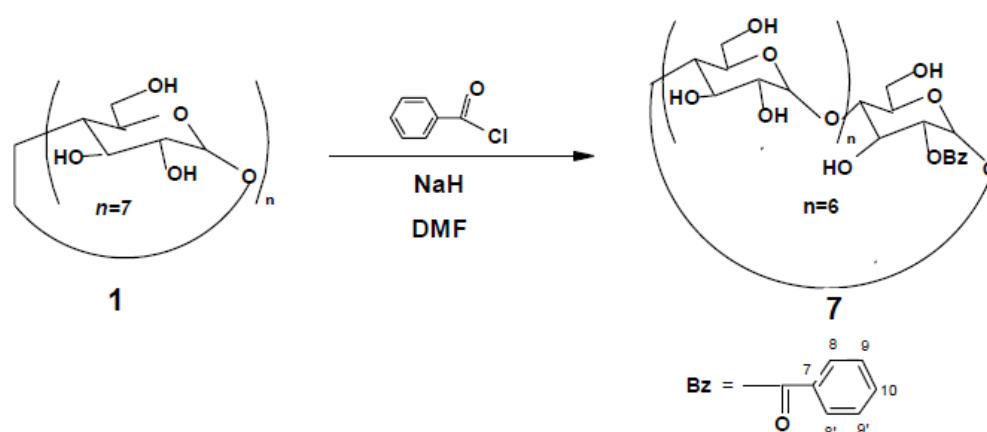
β -cyclodextrin (1 g, 0.88 mmol) was dissolved in 20 mL of DMF while stirring. The solution was heated to 75 °C followed by drop-wise addition of hexamethylene-diisocyanate (2 mL) in a 1:8 molar ratio. The mixture was stirred at 75 °C for 24 h under argon gas (see Scheme 3.1). The polymer formed was washed with acetone followed by drying under vacuum at room temperature.



Scheme 3.1: Conversion of cyclodextrin soluble polymer to an insoluble polymer using HMDI.

3.4.1.2 Mono-2-substituted benzoyl β -cyclodextrin polymer

β -cyclodextrin (1 g, 0.88 mmol) was dissolved in 20 mL of DMF followed by addition of sodium hydride (63 mg, 2.64 mmol) while stirring until all the sodium hydride was dissolved. The reaction was left stirring for 18 h at room temperature. Benzoyl chloride (0.31 mL, 0.372 g, 2.64 mmol) was then added to the resulting clear solution. The reaction was stirred for a further 24 h at room temperature under argon atmosphere (Scheme 3.2).

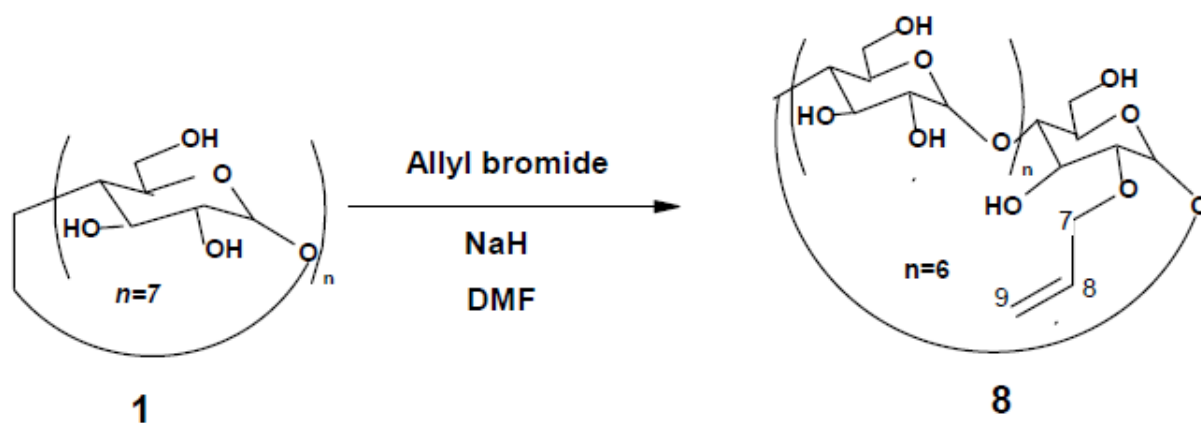


Scheme 3.2: Preparation of the benzoyl substituted β -cyclodextrin.

Addition of 100 mL acetone precipitated the compound which was then filtered. After drying under vacuum, white solid granules were obtained. The product obtained was dissolved in 20 mL DMF with stirring. The solution was heated to 75 °C followed by the drop-wise addition of hexamethylene diisocyanate (2mL). The mixture was allowed to stir at 75 °C under argon gas for an additional 24 h. The polymer formed was washed with acetone followed by drying under vacuum at room temperature [1].

3.4.1.3 Mono-2-substituted allyl β -cyclodextrin polymer

β -cyclodextrin (1 g, 0.88 mmol) was dissolved in 20 mL DMF followed by addition of NaH (0.063 g, 2.64 mmol) while stirring until sodium hydride was dissolved. The reaction was allowed to stir for 18 h at room temperature under argon atmosphere. Allyl bromide (0.319 g, 0.23 mL, 2.64 mmol) was added to the resulting clear solution and the temperature was raised to 60 °C. After 5 h, acetone (100 mL) was added to precipitate the allyl derivative (Scheme 3.3).



Scheme 3.3: Preparation of the allyl substituted β -cyclodextrin.

The white paste formed was then filtered off and washed further with large quantities of acetone to remove residual DMF followed by drying under high vacuum. The product obtained was dissolved in DMF (20 mL) with stirring. The solution was heated to 75 °C followed by the drop-wise addition of hexamethylene diisocyanate (2 mL). The mixture was stirred at 75 °C under argon gas for 24 h. The polymer thus

formed was washed with acetone followed by drying under vacuum at room temperature [1].

3.4.2 Functionalisation of carbon nanotubes

Approximately 1 g of multi-walled carbon nanotubes were oxidised in a (1:3 ratio) mixture of 30 mL concentrated sulphuric acid and 10 mL of nitric acid for 30 minutes to incorporate -COOH and -OH functional groups onto the MWCNTs. After 30 minutes, the mixture was diluted with 500 mL of distilled water. Functionalised carbon nanotubes (fMWCNTs) were washed until a neutral pH was achieved [2].

3.4.3 Synthesis of β -CD/MWCNT nanocomposites

Three portions of β -cyclodextrin (2 g, 1.76 mmol) were dissolved in 18 mL of DMF while stirring. Functionalised MWCNTs (0.01 g, 0.02 g and 0.04 g) were agitated in DMF respectively for 15 minutes and then added to each β -CD solution. The mixtures were heated to 75 °C followed by a drop-wise addition of the hexamethylene diisocyanate. The mixtures were allowed to stir at 75 °C under argon gas for 24 h. After 24 h, the nanocomposites were precipitated and washed with acetone. The remaining solvent was removed under vacuum at room temperature [3]. From these reactions, 1 wt. %, 2 wt. % and 3 wt. % MWCNTs/ β -CD were prepared respectively. Calculations are shown in the appendices.

3.4.4 Synthesis of silver nanoparticles

Silver nanoparticles were synthesised by a wet chemical method [4]. Briefly 50 mL of silver nitrate solution (0.014 M) and 9 % (w/w) sodium dodecyl sulphate (SDS) was prepared in a round bottom flask. A mixture of hydrazine hydrate (25 mL, 0.0027M) and sodium citrate (25 mL, 0.001M) was added to the silver nitrate and sodium dodecyl sulphate solution drop-wise while observing the colour change with constant stirring. The resulting nanoparticles solution was washed with distilled water and ethanol several times to remove impurities [5]. The UV/Vis spectrophotometer

was used to confirm the formation of nanoparticles under water atmosphere at room temperature.

3.4.5 Synthesis of silver nanoparticles on functionalised MWCNTs (Ag-MWCNTs)

A mixture of sodium dodecyl sulphate (SDS) (9 %, w/w) and silver nitrate (0.0014 M) was prepared. About 50 mL of this mixture was added to a round bottom flask containing 20 mg of fMWCNTs. Mixtures of hydrazine hydrate (25 mL, 0.0027 M) and sodium citrate (25 mL, 0.001 M) was added drop-wise to a mixture of SDS, fMWCNTs and silver nitrate solution for 2 h while stirring at room temperature. The mixture was left to stir for an additional 24 h. After 24 h, the precipitates were filtered and washed with distilled water [5].

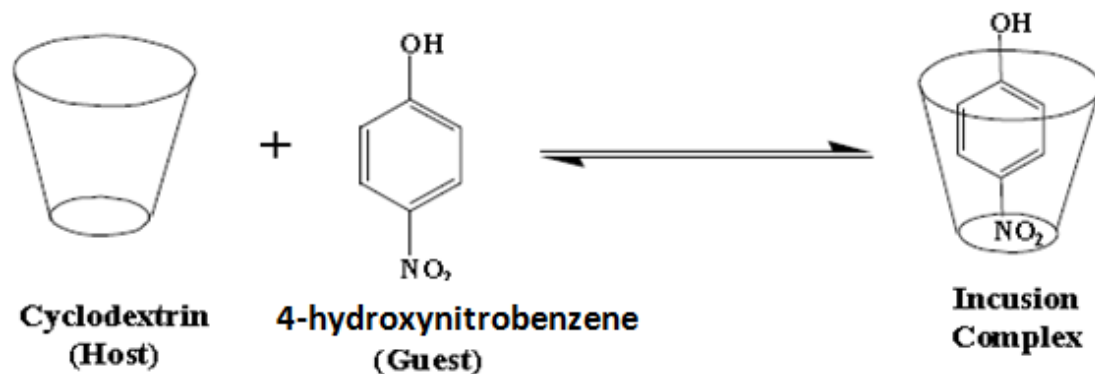
3.4.6 Polymerisation of Ag-MWCNTs onto β -cyclodextrin polymers

Ag-MWCNTs (0.02 g) were mixed with 2 mL of DMF and stirred at room temperature for 15 minutes. β -cyclodextrin (2 g, 1.76 mmol) polymer was dissolved in DMF (40 mL) in a round bottom flask. The Ag-MWCNTs (0.02 g) solution was added to the round bottom flask and the reaction mixture was allowed to stir at 70 °C for 1 h. Hexamethylene diisocyanate (HMDI) (4 mL) was added drop-wise and the mixture was refluxed at 75 °C under argon gas for 24 h. The resultant nanocomposite material was precipitated, washed with acetone and dried under vacuum [6].

3.4.7 Investigation of 4-hydroxynitrobenzene (PNP) using UV-Vis spectrophotometry

A stock solution of 4-hydroxynitrobenzene was prepared by dissolving 20 mg of 4-hydroxynitrobenzene in 1 L of distilled water and then filled to the mark. From this solution, different concentrations were prepared to obtain a standard curve of 4-hydroxynitrobenzene. A standard curve is a quantitative research tool, and a method of plotting assay data that is used to determine the concentration of a substance.

The standard solutions were used to determine the best absorption wavelength for 4-hydroxynitrobenzene. Solid phase extraction was carried out in order to determine the amount of pollutant that can be absorbed by the newly synthesized nanocomposite materials (see Scheme 3.4).



Scheme 3.4: Mechanism of absorption of 4-hydroxynitrobenzene.

The extraction was carried out using a small column into which the polymer was packed. The column was conditioned with distilled water followed by water contaminated with 4-hydroxynitrobenzene. The filtrate was collected and its absorbance was measured at 318 nm using a UV/Vis spectrophotometer Ultraspec 3000 Pro, (Figure 3.4). Finally, the calibration curve obtained was used to determine the concentration of the pollutants of each sample [1, 3]. All experimental procedure reported in this section were at least repeated 3 times.



Figure 3.4: UV/Vis spectrophotometer used to analyse 4-hydroxynitrobenzene samples.

3.4.8 Antibacterial Application

3.4.8.1 Preparation of nutrient agar plates

A mixture of 15 g bacteriological agar and 25 g nutrient broth was diluted in 1000 mL of distilled water. The solution was then heated while stirring until it reached its boiling point. The resulting clear solution was autoclaved for 2 h, poured into petri-dishes (Figure 3.5) and allowed to set.



Figure 3.5: Nutrient agar plate.

3.4.8.2 Preparation of nutrient broth and growth of biomass

The nutrient broth (10 g) was dissolved in 400 mL of distilled water and then divided into 4 Erlenmeyer flasks each containing 100 mL distilled water (Figure 3.6 a and b). The flasks were sterilised in an autoclave and one loop of *Escherichia coli* (ATCC 25922) was transferred to each flask. *Escherichia coli* (0.2 mL) from all flasks containing the broth media was transferred to agar plates and incubated at 37 °C for 24 h.

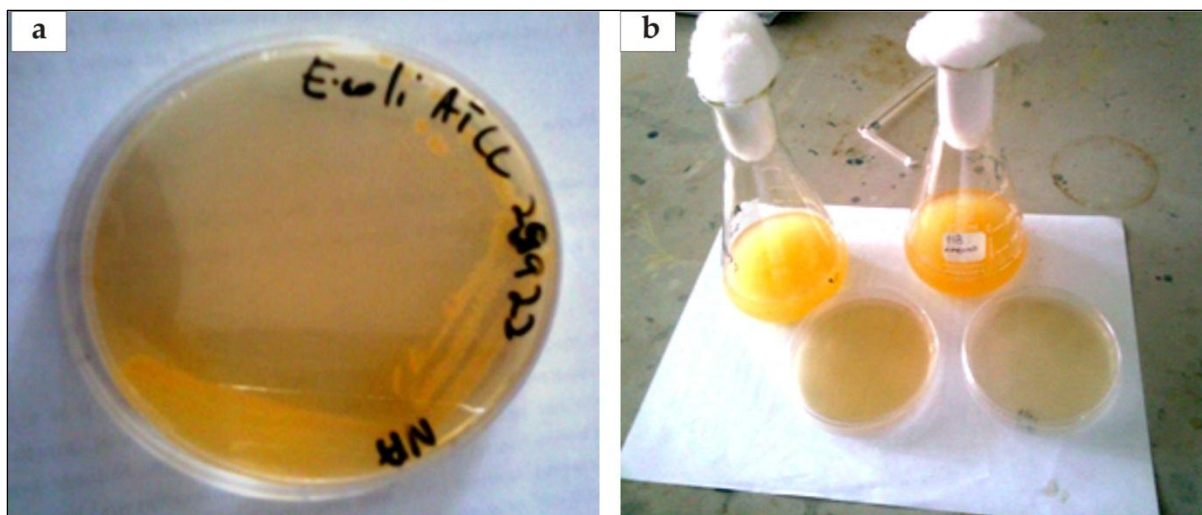


Figure 3.6: Preparation of nutrient broth.

3.4.8.3 Preparation of water samples by micro-dilution

The broth inoculated with *E. coli* (1 mL) was pipetted and transferred to the first flask containing 99 mL of distilled water. From the first flask, 1 mL was again drawn out and pipetted in the second flask containing 99 mL of distilled water. A similar procedure was followed to inoculate the third, fourth and fifth flask respectively. The resulting diluted solutions had 10^{-1} , 10^{-2} , 10^{-3} , 10^{-4} , and 10^{-5} dilution factors respectively.

3.4.8.4 Dis-infection of water

Approximately 20 mL of water contaminated with known concentration of bacteria was transferred into 9 bottles each containing magnetic stirring bars. About 150 mg sample of each of the following were analysed (unless otherwise stated): Ag nanoparticles, raw MWCNTs, MWCNTs/ β -CD, Ag-MWCNTs, functionalised-MWCNTs β -CD, Ag-MWCNTs/ β -CD, Ag/ β -CD, benzoyl substituted β -CD and allyl substituted β -CD. The bottles were closed securely to ensure that no further contamination occurred (Figure 3.7). All experimental procedure reported in this section were at least repeated 3 times.



Figure 3.7: The process of water dis-infection from bacteria at controlled temperature.

The mixtures were allowed to stir while a small amount was taken from the bottles after several minutes, filtered with a filter paper and plated on agar plates. The plates were incubated for 24 h to perceive if any bacterial growth occurred. After incubation, the number of colonies observed on plates were counted and recorded. The colony forming units and percentage inactivation of the bacteria for all the samples were calculated from the visible number of colonies. The above procedure was again followed in order to investigate both the time and concentration effect of the nanocomposite materials on the structure of the bacteria. The investigation was also undertaken at various temperatures to monitor the bacterial activity in the presence of nanocomposites.

3.4.8.5 Kinetics of bacterial growth rate in the presence of Ag-MWCNTs/ β -CD nanocomposites

To examine the bacterial growth rate and to determine the growth curve in the presence of Ag-MWCNTs/ β -CD nanocomposites, *E. coli* bacteria were cultured in 100 mL of nutrient broth (NB) medium supplemented with 5, 10, and 100 mg of these prepared nanocomposites material. The cylindrically shaped sample containers were placed horizontally on an orbital shaker platform and agitated at 225 rpm. Growth rates and bacterial concentrations were determined by measuring the optical density (OD) at 600 nm for 4 h. The bacterial samples were fixed in Karnovsky's fixative made up in phosphate buffer at pH 7.4 after each 30 minutes interval. This was followed by running the OD in a UV/Vis spectrophotometer in the Microbiology laboratory at Turfloop campus, University of Limpopo.

At the Electron Microscope Unit (Medunsa campus, University of Limpopo), the bacterial solution was filtered using Whatman Nucleopore™ filters with 13 mm diameter and 5.0 μ m pore size. These were rinsed with phosphate buffer to remove all excess fixative for 15 minutes. To dehydrate the bacteria, the specimen was rinsed for 7 minutes each in ascending concentrations ranging from 50%, 70%, 80%, 90%, and 95% to 100% of ethanol. For complete dehydration, the bacteria were rinsed and evaporated using hexamethyldisilane reagent. Once the bacteria were dry, filters were mounted directly onto aluminium pin-type stubs and sputter coated with a thin layer (4 nm) of tungsten at least 3 times. For SEM analysis, samples of bacteria at 60, 120, 150 and 210 minute intervals were investigated for morphological changes.

3.5. REFERENCES

1. Mamba, E, Krause R.W.M., Malefetse, T.J. and Nxumalo, N. 2006 Monofunctionalized cyclodextrin polymers for the removal of organic pollutants from water. *Environmental Chemistry Letter*, 5. 79 - 84.
2. Salipira, K.L., Mamba, B.B., Krause, R.W. and Durbach, S.H. 2008. Polymerisation of cyclodextrins and multi-walled carbon nanotubes for use in water purification. *Water SA*, 1. 113 - 118.
3. Esumi, K., Ishigami, M., Nakajima, A., Sawada, K., and Honda, H. 1995 Chemical treatment of carbon nanotubes. *Carbon journal*, 34 (2). 279 - 281.
4. Gleiter, H. and Mater, A. 2000. DOI 10.1016/S1359-6454(99)00285 - 2.
5. Guzman, M.G., Dille, J. and Godet, S. 2008. Synthesis of silver nanoparticles by chemical reduction method and their antibacterial activity. Proceedings of World Academy of Science. *Engineering and technology journal*, 33.
6. Lukhele, L.P., Mamba, B.B., Momba M.N.B. and Krause, R.W.M. 2010. Water disinfection using novel cyclodextrin polyurethanes containing silver nanoparticles supported on carbon nanotubes. *Journal of applied sciences*, 10: 65 - 70.

CHAPTER 4

RESULTS AND DISCUSSION

4.1 INTRODUCTION

Results obtained in this research are presented and discussed in this chapter. The results include characterisation of the synthesised nanomaterials, organic contaminants absorption tests as well as bacterial tests.

4.2 CHARACTERISATION OF SYNTHESISED NANOCOMPOSITE MATERIALS

4.2.1 FTIR results

4.2.1.1 The FTIR spectra of raw and functionalised MWCNTs

Figure 4.1 shows the FTIR spectra of raw and functionalised MWCNTs. MWCNTs were characterised by FTIR to confirm the attachment of the hydroxyl and carboxyl group on the walls of carbon nanotubes after functionalisation. The FTIR spectrum of raw MWCNTs (Figure 4.1a) appeared slightly different from the FTIR of functionalised MWCNTs (Figure 4.1b). Functionalised MWCNTs (Figure 4.1b) showed additional peaks due to their acid treatment with sulphuric and nitric acid. The peaks at positions 1217 and 1340 cm^{-1} are due to the C-O bond of the carboxylic acid.

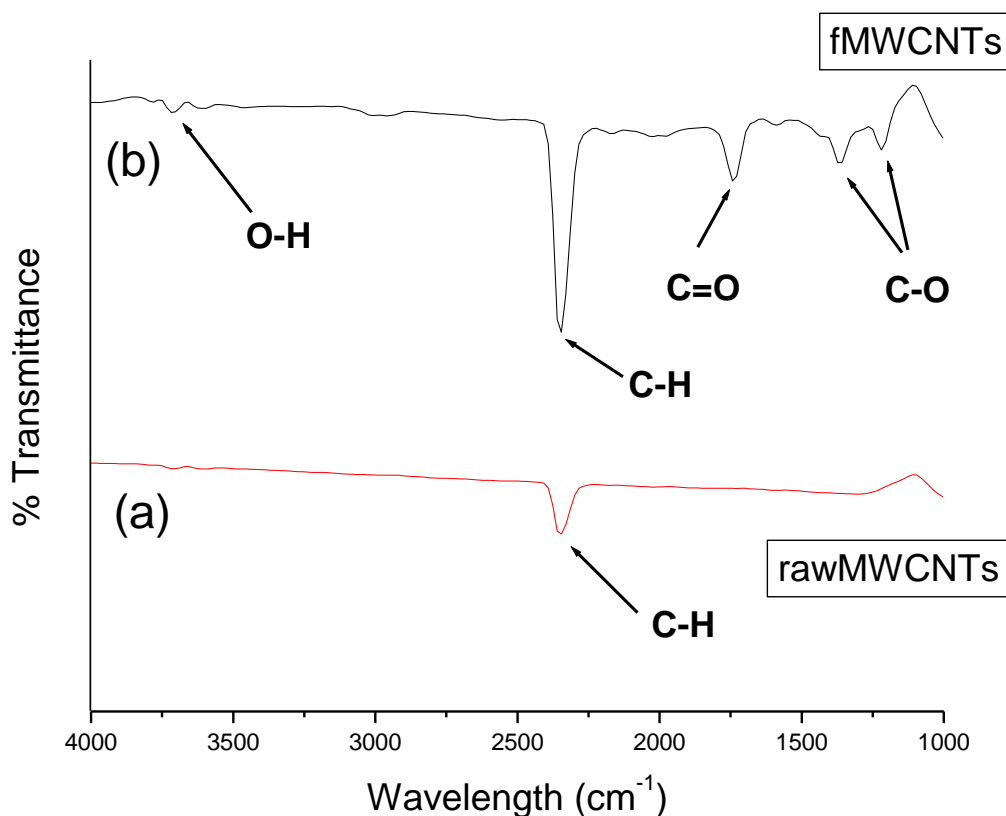


Figure 4.1: FTIR spectra of (a) raw MWCNTs and (b) functionalised MWCNTs.

The peaks at 1733 cm^{-1} presented the C=O group, whereas the peaks at 3688 cm^{-1} are due to the O-H bending distortion mode of the carboxylic acid which was also previously reported by Buang *et al.* (2012) [1]. The increase in the peak intensity of the C-H stretching mode at 2341 cm^{-1} suggests that oxidation of the MWCNTs successfully introduced the carboxylic group (-COOH) on the walls of carbon nanotubes. The C-H signal also confirmed that the carbon atoms were now sp^3 hybridised instead of being sp^2 hybridised as in the case of raw MWCNTs [2].

4.2.1.2 The FTIR spectra of mono-2-substituted benzoyl β -cyclodextrin polymer

Figure 4.2 shows the FTIR spectra of mono-2-substituted benzoyl β -cyclodextrin polymer. The FTIR spectra of mono-2-substituted benzoyl β -cyclodextrin polymer in Figure 4.2 showed the absorption band at 1646 cm^{-1} , described as the C=O of the

polymer, introduced by functionalisation with the benzoyl group from benzoyl chloride. The FTIR spectra (Figure 4.2) also showed a characteristic C-O stretching at 1000 cm^{-1} . The absorption band at 1373 cm^{-1} indicates the characteristic C-N stretching which confirmed the presence of the amine group of the cyclodextrin polymer. Similar findings were observed by Mamba *et al.* (2006) [3]. The development of the vibration band of O-H at 3415 cm^{-1} and C-H at 3049 cm^{-1} also confirmed the successful synthesis of the resulting nanosponge.

The C-2 hydroxyl groups are more acidic than the C-6 hydroxyl groups of β -cyclodextrin. This characteristic was exploited by using sodium hydride (NaH) as a strong base under anhydrous conditions to deprotonate the C-2 secondary hydroxyl groups of the β -cyclodextrin macrocycle [3]. The reaction involved dissolving β -cyclodextrin in small amounts of DMF, followed by the addition of small amounts of the deprotonating reagent. The resultant milky mixture was then stirred vigorously at room temperature for 1 day in an inert atmosphere. Addition of benzoyl chloride to the oxyanion produced the corresponding ester called mono-2-substituted benzoyl β -cyclodextrin polymer [3].

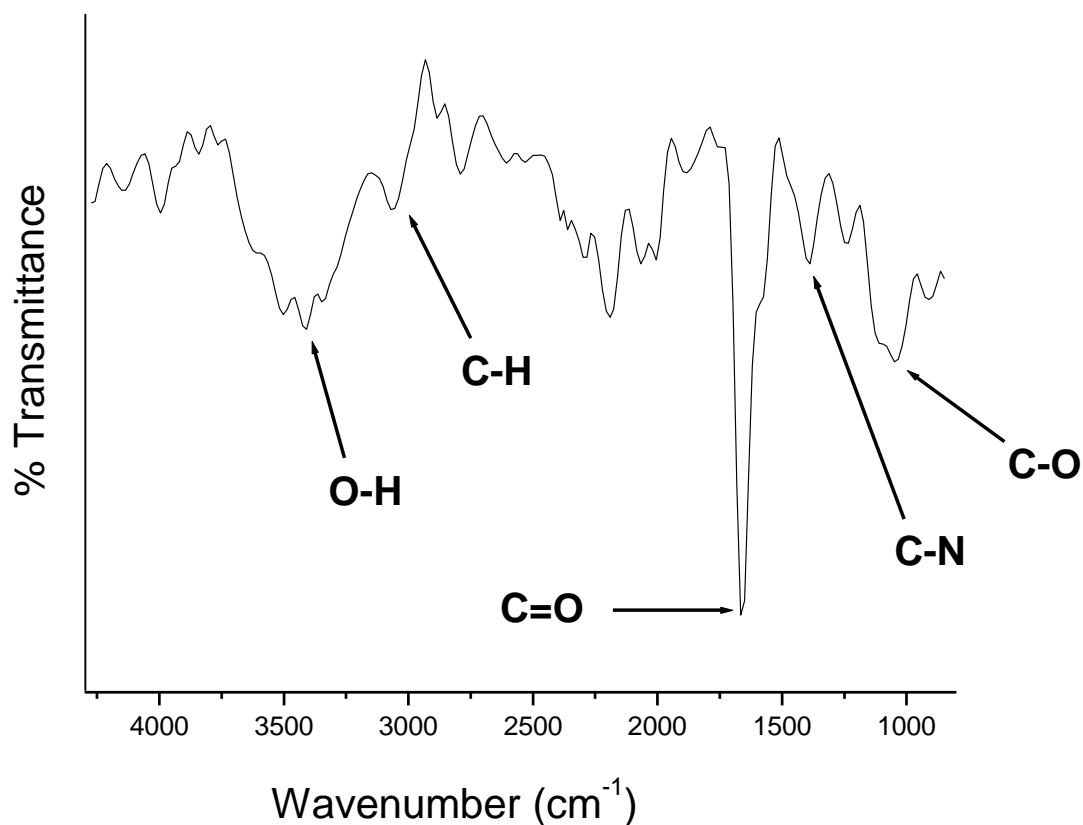


Figure 4.2: FTIR of the synthesised benzoyl substituted β -CD polymer.

4.2.1.3 The FTIR spectra of mono-2-substituted allyl β -cyclodextrin polymer

Figure 4.3 shows the FTIR spectra of mono-2-substituted allyl β -cyclodextrin polymer. The allylated β -CD polymer (Figure 4.3) showed an absorption band at 1596 cm^{-1} credited to the C=C stretch of the allyl group. The vibration band of O-H at 3414 cm^{-1} and C-H at 3061 cm^{-1} also confirmed the synthesis of the resulting polymer. Similar findings were observed by Mamba *et al.* (2006) [3].

The addition of methyl iodide to the deprotonated CD yielded the methyl ether. The treatment of the CD oxyanion with allyl bromide yielded the allyl derivative [3].

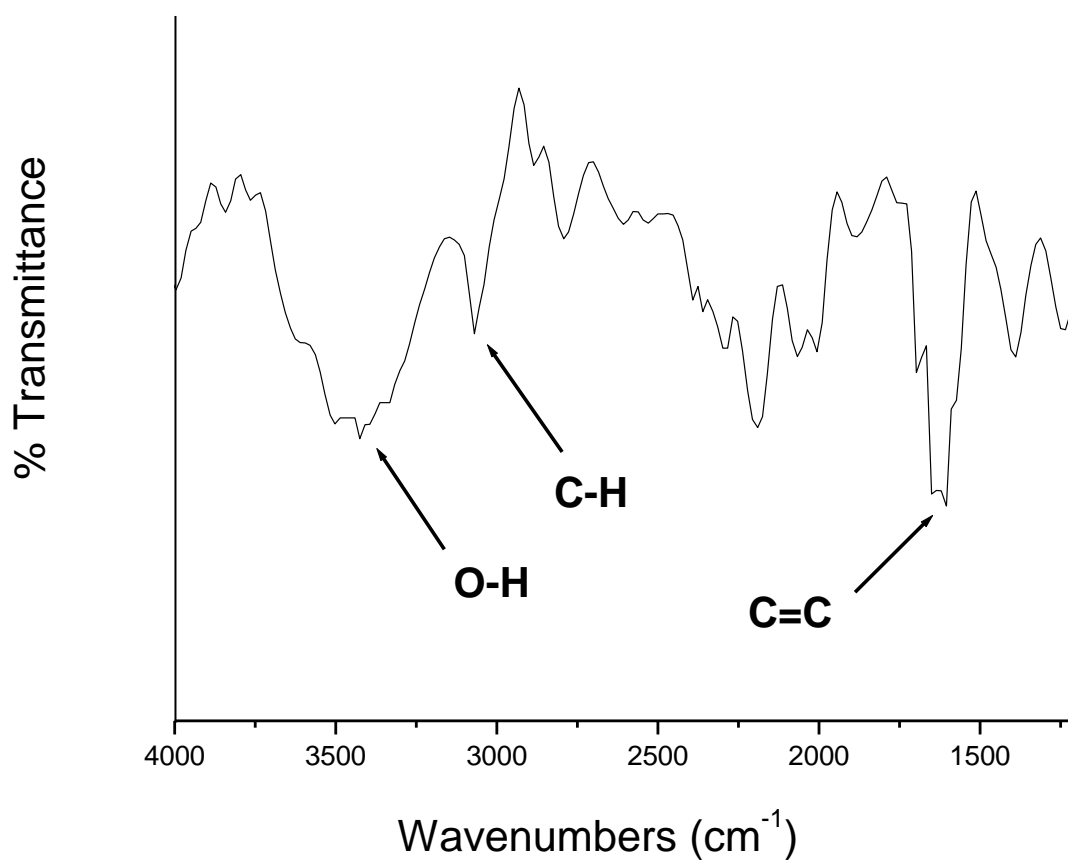


Figure 4.3: FTIR spectrum of the synthesised Allyl substituted β -CD polymer.

Both the benzoylated (Figure 4.2) and the allylated polymer (Figure 4.3) showed relatively related FTIR data, with minor differences since they were all synthesised from β -cyclodextrin. The major differences was with the characteristic C=O of the benzoylated and the C=C of the allylated polymer.

4.2.2 Characterisation of the synthesised nanocomposite materials and cyclodextrin polymers by FE-SEM and TEM

4.2.2.1 FE-SEM and TEM of multi-walled carbon nanotubes (MWCNTs)

Figure 4.4 show the FE-SEM and TEM images of MWCNTs before and after functionalisation. Figure 4.4a and b show the MWCNTs before functionalisation being bundled with lesser dispersion amongst them. Carbon nanotubes are hydrophobic due to their carbonic nature and also presence of van-der-Waals attraction between tubes. As a result, they exhibit low dispersion in water and organic solvents [4]. MWCNTs treated in an acid mixture of H_2SO_4 and HNO_3 (Figure 4.4c and d) showed a better dispersion in comparison with the unfunctionalised MWCNTs (Figure. 4.4b). This was due to the OH groups formed in the functionalised MWCNTs [5]. The morphology of the MWCNTs revealed both open and closed tubes (Figure. 4.4d). Similar observations have been made by Kim *et al.* (2005) on this type of CNTs [6].

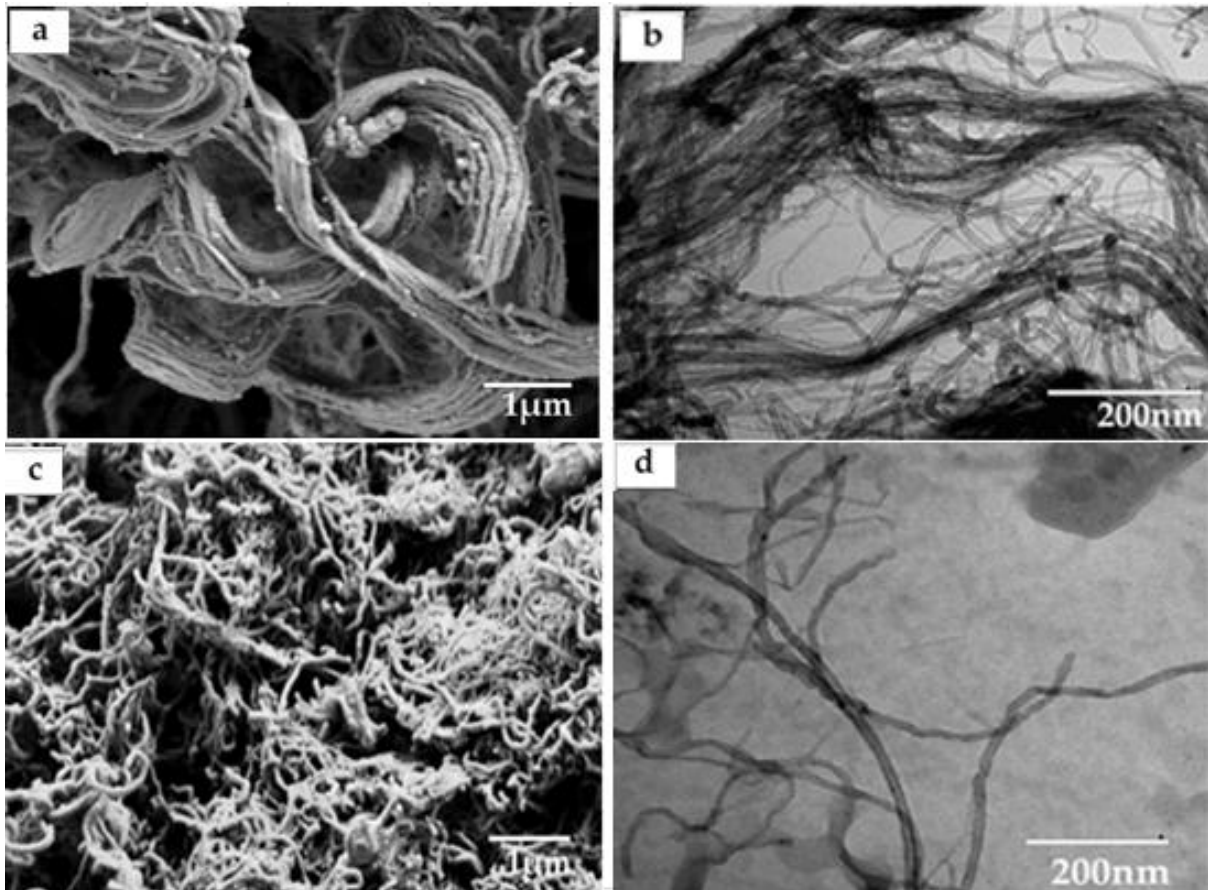


Figure 4.4: (a) FE-SEM images for unfunctionalised MWCNTs, (b) TEM images for unfunctionalised MWCNTs (c) FE-SEM of functionalised MWCNTs, and (d) TEM of functionalised MWCNTs.

The diameter of the tubes lie in the range of 2 - 5 nm with the maximum length of 1 μm determined from TEM micrograph in Figure 4.4d. Raw commercial MWCNTs were disordered and had some impurities; these were viewed as dark areas suspected to be amorphous carbon by TEM in Figure 4.4b. After purification of MWCNTs (Figure 4.4d), most of the previously observed dark areas were notably clear and more dispersed suggestive of functionalisation of MWCNTs.

4.2.2.2 FE-SEM and TEM of cyclodextrin polymer (β -CD HMDI)

Figure 4.5 show the FE-SEM and TEM of β -cyclodextrin polymers. The surface morphology (Figure 4.5a and b) of the polymer appeared to be spongy. The results are in agreement with those observed by Salipira *et al.* (2006) [2].

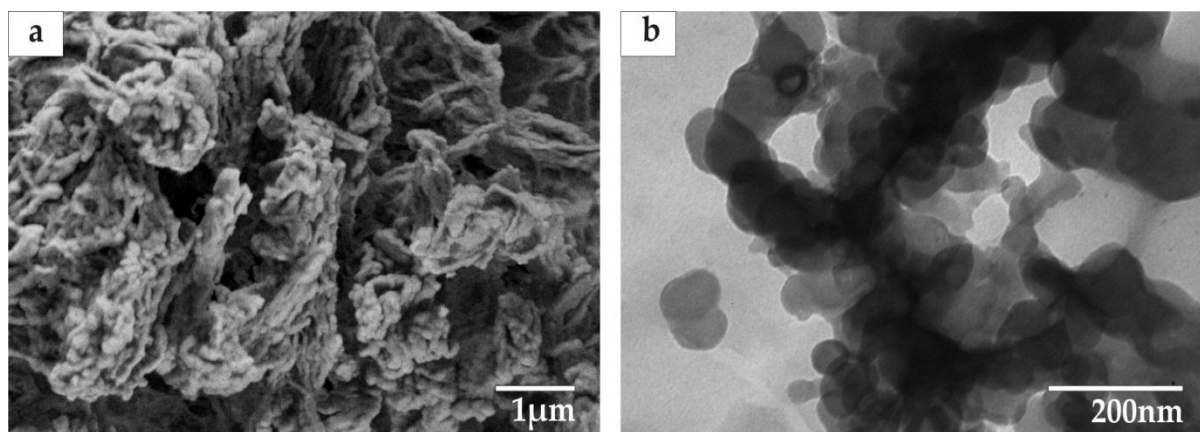


Figure 4.5: (a) FE-SEM micrograph of β -CD polymer and (b) TEM micrograph of β -CD polymer.

The morphology (Figure 4.5.a and b) indicated that the polymer would possibly be an efficient filter for water impurities.

4.2.2.3 FE-SEM and TEM micrographs of cyclodextrin polymers incorporated with 1 wt. % multi-walled carbon nanotubes

Figure 4.6 shows the FE-SEM and TEM of MWCNTs/ β -CD nanocomposite material. The FE-SEM micrograph (Figure 4.6a) confirms the presence of nanotubes in cyclodextrin polymers. Higher magnifications of the FE-SEM results (Figure 4.6a) revealed that the nanotube sheets were in fact rather rough, and the tubes formed a random, heavily interconnected micro-porous system which is in agreement with previous results by Salipira *et al.* (2006) [2].

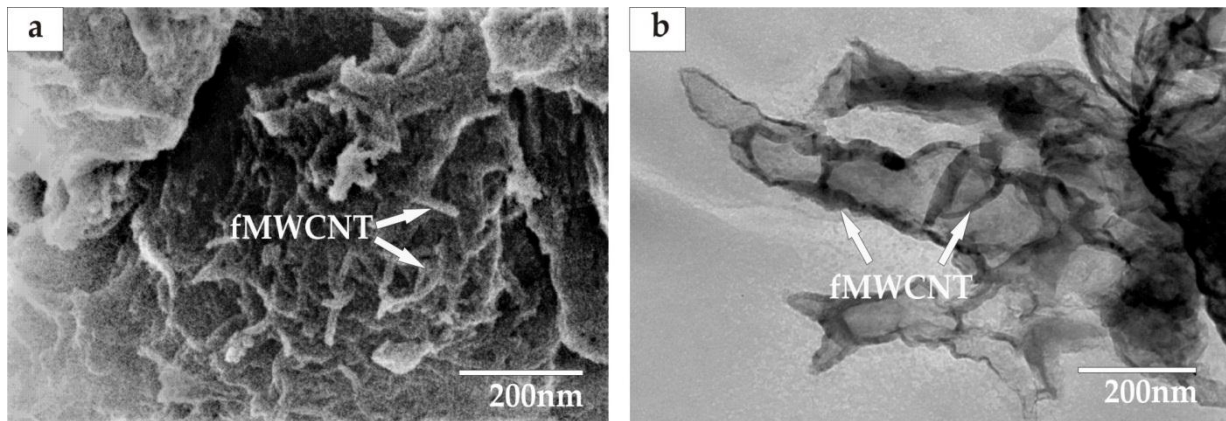


Figure 4.6: (a) FE-SEM of 1 wt. % MWCNTs/ β -CD nanocomposites and (b) TEM of 1 wt. % MWCNTs/ β -CD nanocomposites. The arrows indicate the CNTs.

TEM micrograph (Figure 4.6b) also confirms the orientation of fMWCNTs on β -CD. Analysis of TEM results (Figure 4.6b) show that the apparent pore diameter of MWCNTs in this nanocomposite is 3 - 6 nm. The results show also clearly long tubes representing MWCNTs dispersed in cyclodextrin polymers.

4.2.2.4 FE-SEM and TEM micrographs of silver nanoparticles

Figure 4.7 show the FE-SEM and TEM micrographs of silver nanoparticles. The FE-SEM and TEM image in Figure 4.7a and b showed that the silver nanoparticles are agglomerated and almost spherical in shape as observed by Guzman *et al.* (2009) [7].

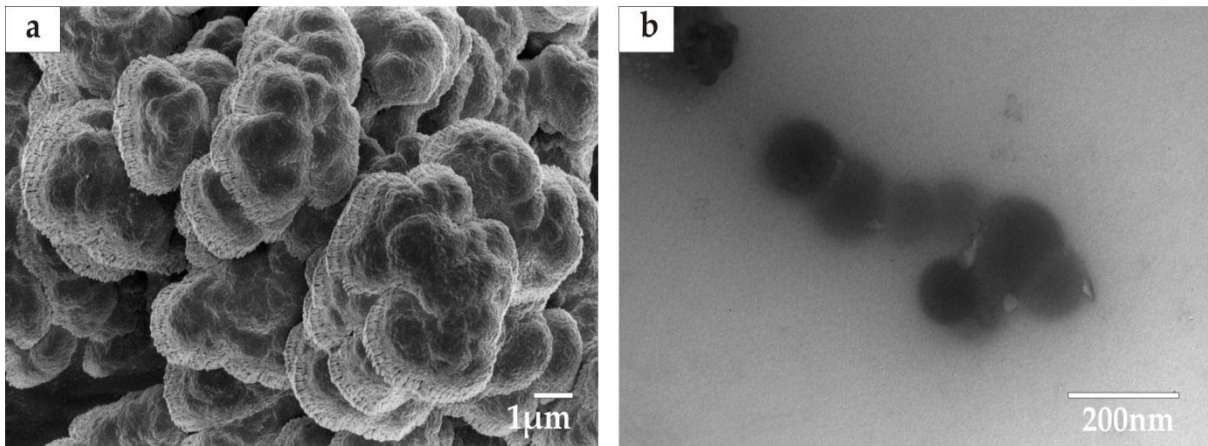


Figure 4.7: (a) FE-SEM micrograph of silver micro-particles and (b) TEM micrograph of silver nanoparticles.

The diameter of the particles was estimated to be between 70 - 100 nm from Figure 4.7b showing that the prepared nanoparticles were quite large.

Figure 4.8 shows the EDX of silver nanoparticles. FE-SEM was used to run the EDX spectrum of a pure silver nanoparticle sample. In the middle part of the presented spectrum (Figure 4.8), one peak is seen located between 2.5 keV and 4 keV which is directly related to the silver characteristic peak as indicated in the spectrum.

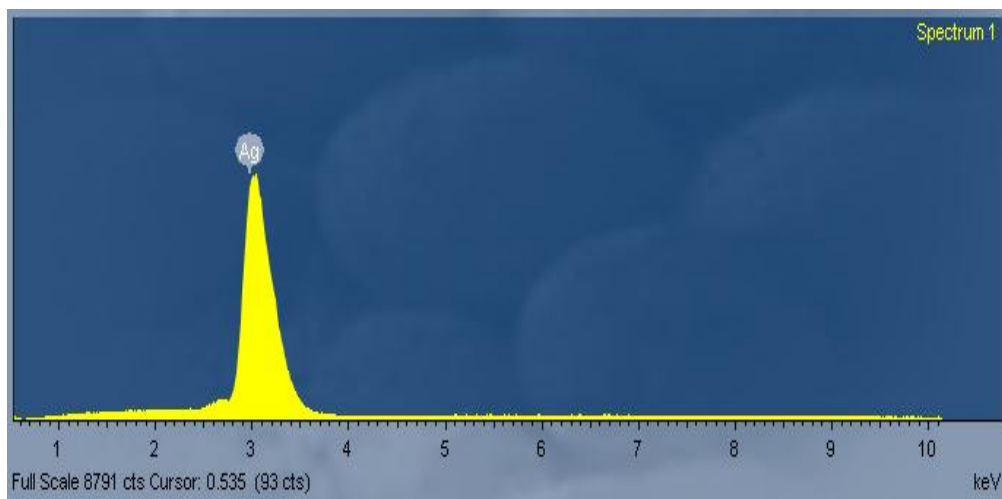


Figure 4.8: EDX spectrum of silver nanoparticles.

The results confirmed the presence of silver nanoparticles (Figure 4.7b); the EDX spectrum is similar to that obtained by Puchalski *et al.* (2007) [8].

4.2.2.5 FE-SEM and TEM micrographs of 32 wt. % Ag-MWCNTs nanocomposite material

Figure 4.9 show the FE-SEM and TEM of 32 wt. % Ag-MWCNTs nanoparticles. Both FE-SEM (Figure 4.9a) and TEM (Figure 4.9b) micrographs confirm that silver nanoparticles was decorated on carbon nanotubes. The arrows in Figure 4.9a indicate areas of carbon nanotubes linking to silver nanoparticles and the arrows in Figure 4.9b of the TEM micrograph confirms the presence of silver nanoparticles attached to the walls of the carbon nanotubes.

FE-SEM image (Figure 4.9a) of the MWCNTs deposited with silver show formation of a few aggregated Ag nanoparticles with a bright contrast on the surface of MWCNTs. It is evident that silver was dispersed on the surface of MWCNTs with a thin layer of coating. Due to the distinctive difference in contrast, silver nanoparticles can be readily identified as dark spots (Figure 4.9b) superimposed on MWCNTs background.

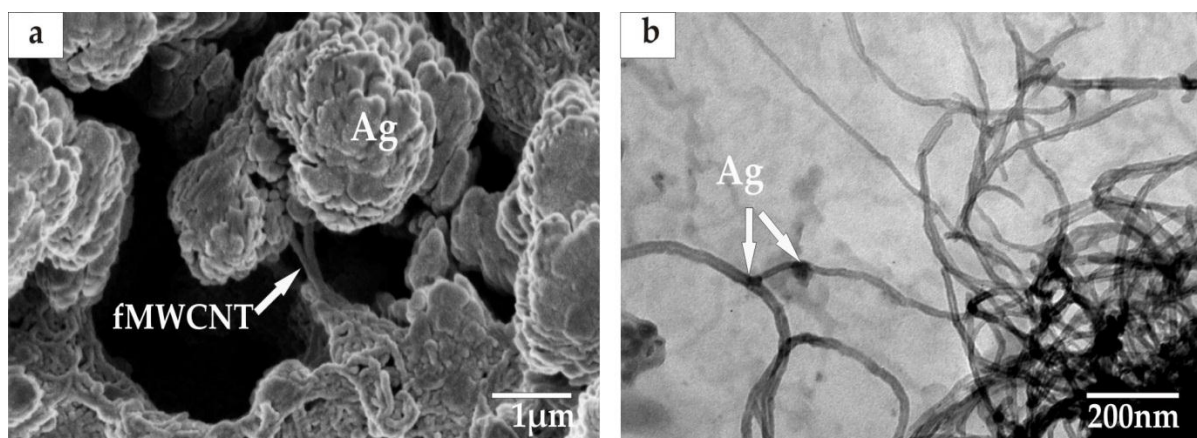


Figure 4.9: (a) FE-SEM micrograph of 32 wt. % Ag-MWCNTs nanocomposite and (b) TEM micrograph of 32 wt. % Ag-MWCNTs nanocomposites.

With the nanotubes as backbone, the silver nanoparticles were attached (Figure 9b), which indicated that there were active sites on the acid-treated MWCNTs walls which aided the nucleation and growth of silver nanoparticles on the surface [9]. Also the

nanoparticles can only anchor on certain nanotubes, indicating an inhomogeneous distribution of the nanoparticles on the walls of carbon nanotubes [5].

In order to determine the chemical composition of the 32 wt. % Ag-MWCNTs, the energy dispersive X-ray was used. Figure 4.10 shows the EDX of 32 wt. % Ag-MWCNTs. EDX analysis confirmed that Ag nanoparticles were deposited on MWCNTs. The results also illustrate efficient interactions and compatibility between MWCNTs and Ag nanoparticles leading to the presence of silver on the surface of the MWCNTs.

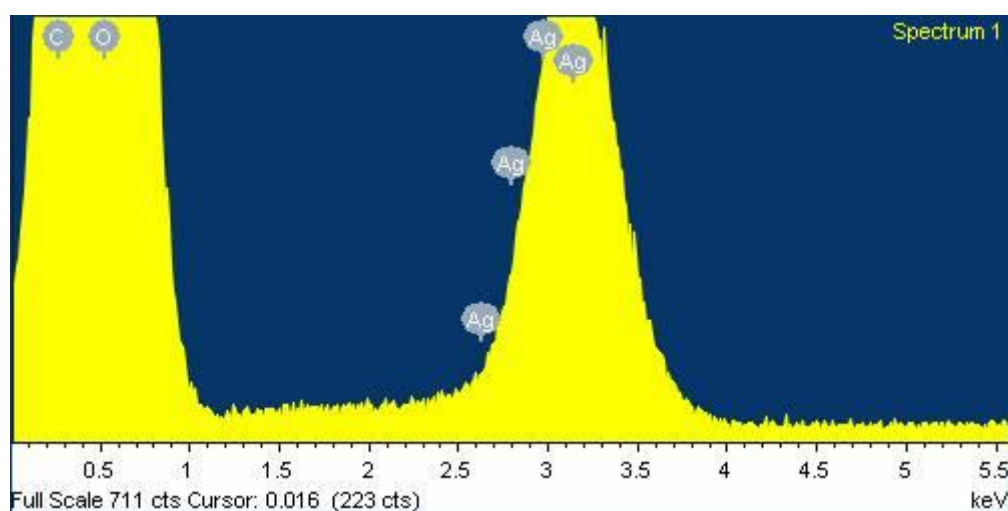


Figure 4.10: EDX of Ag-MWCNTs nanocomposites.

4.2.2.6 FE-SEM and TEM micrographs of 10 wt. % Ag/ β -cyclodextrin nanocomposites

Figure 4.11a and b show the FE-SEM and TEM of 10 wt. % Ag/ β -CD nanocomposites. FE-SEM micrograph (Figure 4.11a) displayed that the spongy cyclodextrin polymer was randomly attached to the silver nanoparticles.

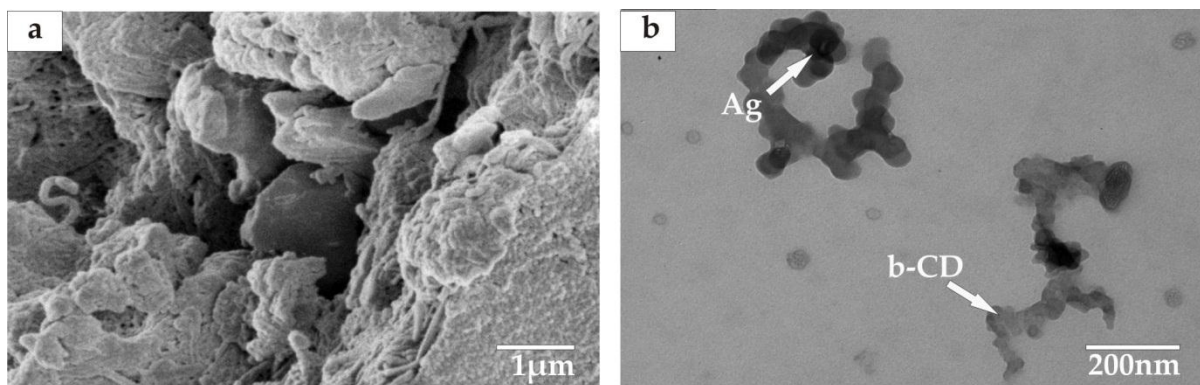


Figure 4.11: (a) FE-SEM micrograph of 10 wt. % Ag/β-CD nanocomposites and (b) TEM micrograph of 10 wt. % Ag/β-CD nanocomposites.

TEM micrograph of 10 wt. % Ag/β-CD (Figure 4.11b) showed almost spherical Ag/β-CD nanocomposite shapes, with the average size of silver nanoparticles decreasing with increasing β-CD capping. The particle size of Ag/β-CD nanocomposites ranged from 30 nm to 40 nm.

4.2.2.7 FE-SEM and TEM micrographs of 1 wt. % Ag-MWCNTs/β-CD nanocomposites

Figure 4.12 show the FE-SEM and TEM of 1 wt. % Ag-MWCNTs/β-CD nanocomposites material. A closer look at the nanocomposite materials in Figure 4.12a showed MWCNTs attached to cyclodextrin and silver nanoparticles. This should allow for efficient contact between polluted water and the nanocomposites.

The TEM micrograph (Figure 4.12b) shows the presence of dark spots on the outer wall of the carbon nanotubes which is indicative of successful impregnation of silver nanoparticles into MWCNTs. The silver nanoparticles size ranged from 20 nm to 60 nm.

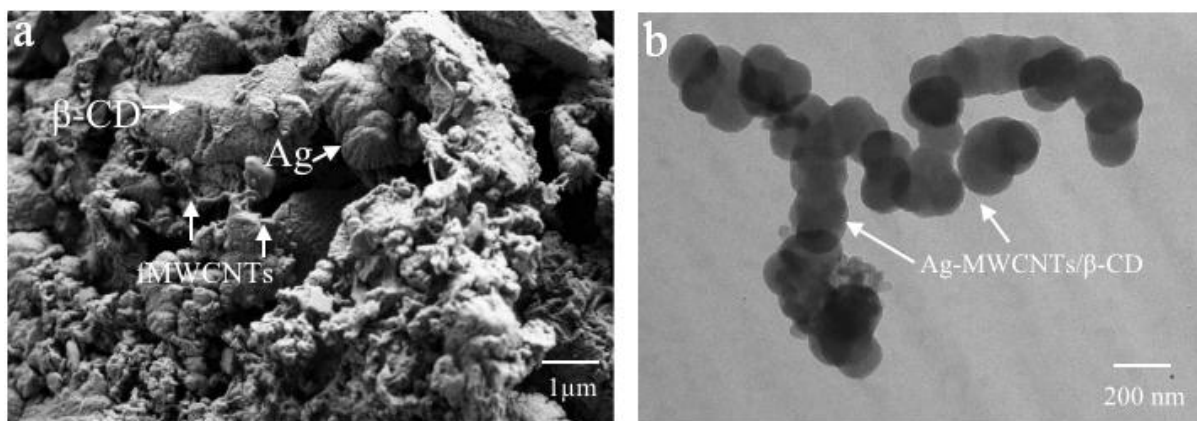


Figure 4.12: (a) FE-SEM micrograph of 1 wt. % Ag-MWCNTs/ β -CD nanocomposites and (b) TEM micrograph of 1 wt. % Ag-MWCNTs/ β -CD nanocomposites.

Figure 4.13 shows the EDX of 1 wt. % Ag-MWCNTs/ β -CD nanocomposites. The elemental composition by EDX confirms the presence of silver in the 1 wt. % Ag-MWCNTs/ β -CD nanocomposites. The results also suggest that silver was loaded in low quantities.

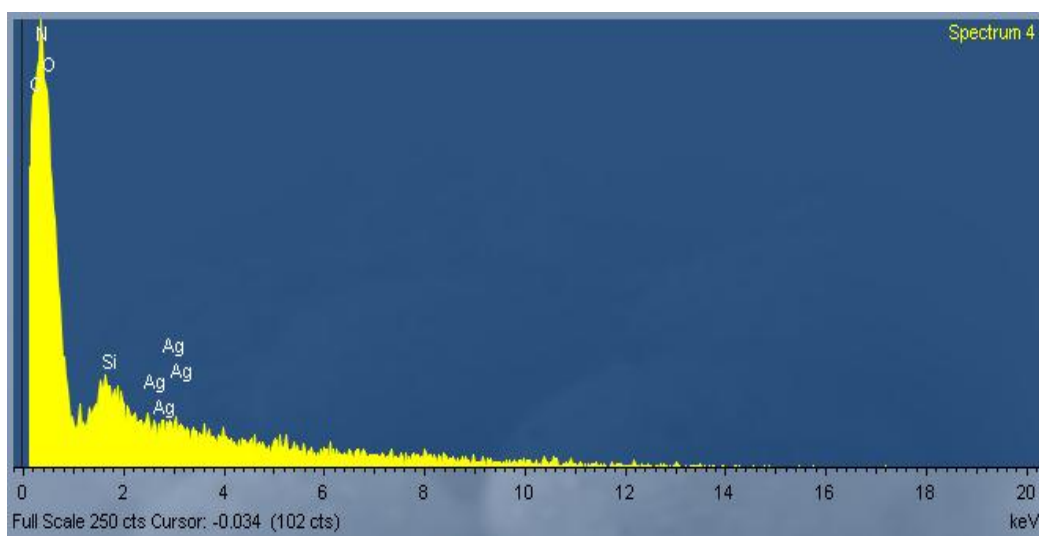


Figure 4.13 EDX of 1 wt. % Ag-MWCNTs/ β -CD nanocomposites.

4.2.2.8 FE-SEM micrographs of mono-2-substituted benzoyl β -cyclodextrin polymer and mono-2-substituted allyl β -cyclodextrin polymer

Figure 4.14a and b show the FE-SEM of the mono-2-substituted benzoyl β -cyclodextrin polymer and mono-2-substituted allyl β -cyclodextrin polymer respectively. Chemical modification of β -CDs in Figure 4.14a and b were specifically undertaken by varying their solubility behaviour to modify their complex properties and to introduce functional groups that can achieve specific functions. Functionalisation of β -CD (Figure 4.14a and b) was achieved by a reaction of the hydroxyl groups with an electrophile in both cases.

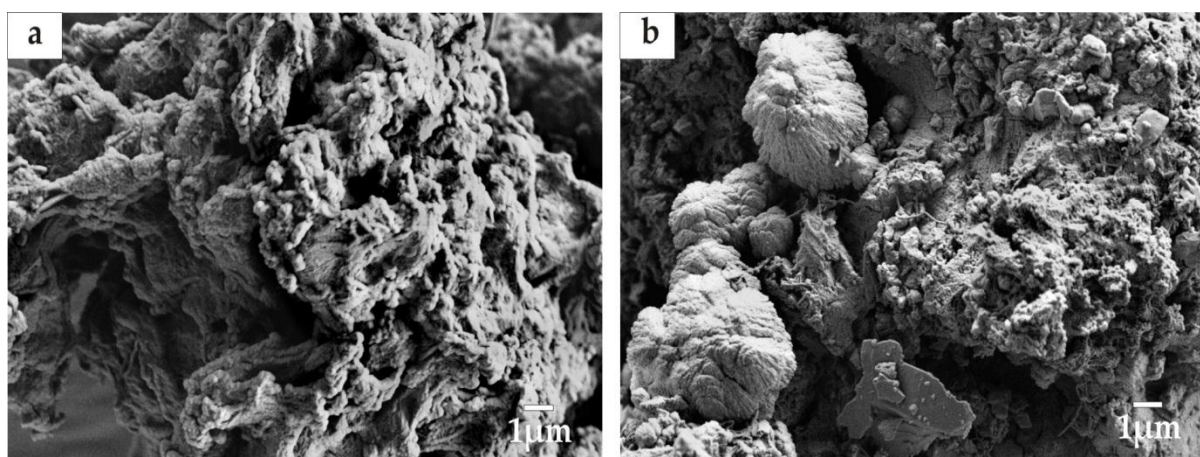


Figure 4.14: (a) FE-SEM micrograph of benzoyl substituted β -CD polymer and (b) FE-SEM micrograph of allyl substituted β -CD polymer.

Reactions of the hydroxyl group of the CDs with acid chlorides, benzoyl chloride yielded an ester. The structures of the functionalised cyclodextrin polymers (Figure 4.14a & b) show a slight difference in their morphology though both seem to be spongy as observed by Mamba *et al.* (2006) [3]. This is due to the difference in the functional groups that were introduced. Both the benzoyl- and the allyl- substituted β -CD polymer (Figure 4.14a and b) were reported to enhance the absorption of organic contaminants in water samples [3].

4.2.3 Characterisation of the synthesised nanocomposite materials by XRD

4.2.3.1 XRD profile of carbon nanotubes

Figure 4.15 shows the X-ray diffraction patterns of raw and functionalised carbon nanotubes. As described in the work done by Buang *et al.* (2012), the significant diffraction pattern for functionalised MWCNTs in Figure 4.15a and b appeared at 25.8° (2θ) [1]. The 2θ peaks corresponded to (002) reflection planes also known as interlayered spacing between adjacent graphite layers.

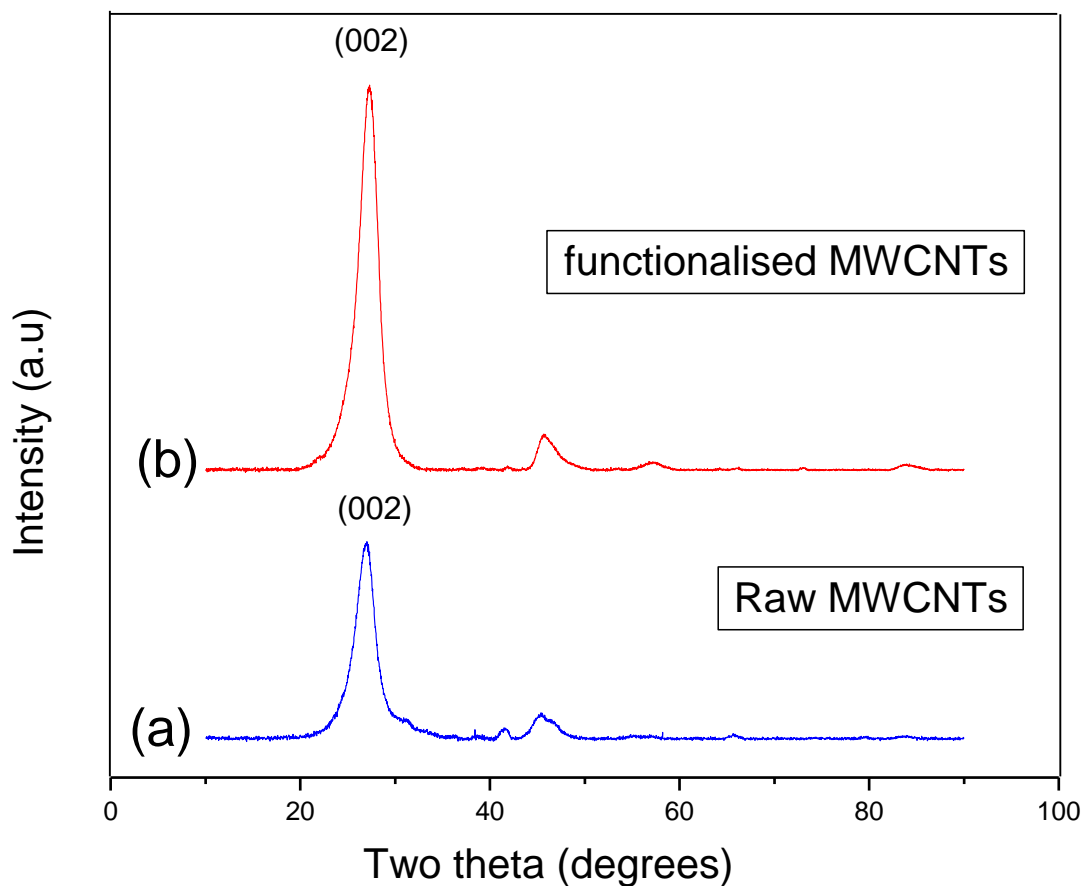


Figure 4.15: XRD patterns of (a) raw MWCNTs and (b) functionalised MWCNTs.

The intensity of the diffraction peak at (002) plane in functionalised MWCNTs (Figure 4.15a) was increased as compared to the raw MWCNTs (Figure 4.15b). This was an indication of the carbon nanotubes purity after acid treatment and formation of more ordered purified MWCNTs.

Table 4.1 shows the summarised data and calculations of the Bragg's angle, d-spacing, full-width at half maximum (FWHM) and estimated crystallite size of raw and functionalised MWCNTs. The d-spacing of MWCNTs was calculated using Bragg's law, and the crystallite size was estimated from the FWHM of the (002) peak using Scherrer's formula.

Table 4.1: Estimation of crystallite size from XRD patterns for raw and functionalised MWCNTs.

Sample	θ value (degree)	θ value (radians)	d-spacing (nm)	FWHM (radians)	Estimated crystallite size (nm)
Raw MWCNTs	12.9	0.226	0.334	0.0532	2.61
fMWCNTs	12.9	0.226	0.344	0.443	3.13

The d-spacing was calculated to be 0.334 nm for raw MWCNTs (Figure 4.15a) and 0.344 nm for functionalised MWCNTs (Figure 4.15b). From the results, it can be concluded that functionalisation of MWCNTs did not have much influence on the average d-spacing indicating that the structure of the nanotubes was preserved after functionalisation. An estimated crystallite size was calculated to be 2.61 nm for raw MWCNTs and 3.13 nm for functionalised MWCNTs, indicating that the attachment of the -OH groups (refer to FTIR, section 4.2.1.1) on the walls of the carbon nanotubes increased the crystallite size. From XRD patterns in Figure 4.15a and b, it can be concluded that functionalised MWCNTs still had the same cylinder-shaped wall structure and inter-planar spacing just as the raw MWCNTs. Thus the structure of MWCNTs is protected even after having undergone the functionalisation process [1].

4.2.3.2 XRD profile of Ag nanoparticles, MWCNTs and 32 wt. % Ag-MWCNTs nanocomposite materials

Figure 4.16a, b and c shows the powder XRD pattern of synthesised Ag nanoparticles and MWCNTs in comparison with 32 wt. % Ag-MWCNTs nanocomposites. The diffraction peaks on silver nanoparticles pattern in Figure 4.16a correspond to the (111), (200), (220) and (311) planes, which can be indexed to a face-centred cubic structure. The XRD pattern (Figure 4.16a) thus clearly shows that the silver nanoparticles are crystalline in nature [10].

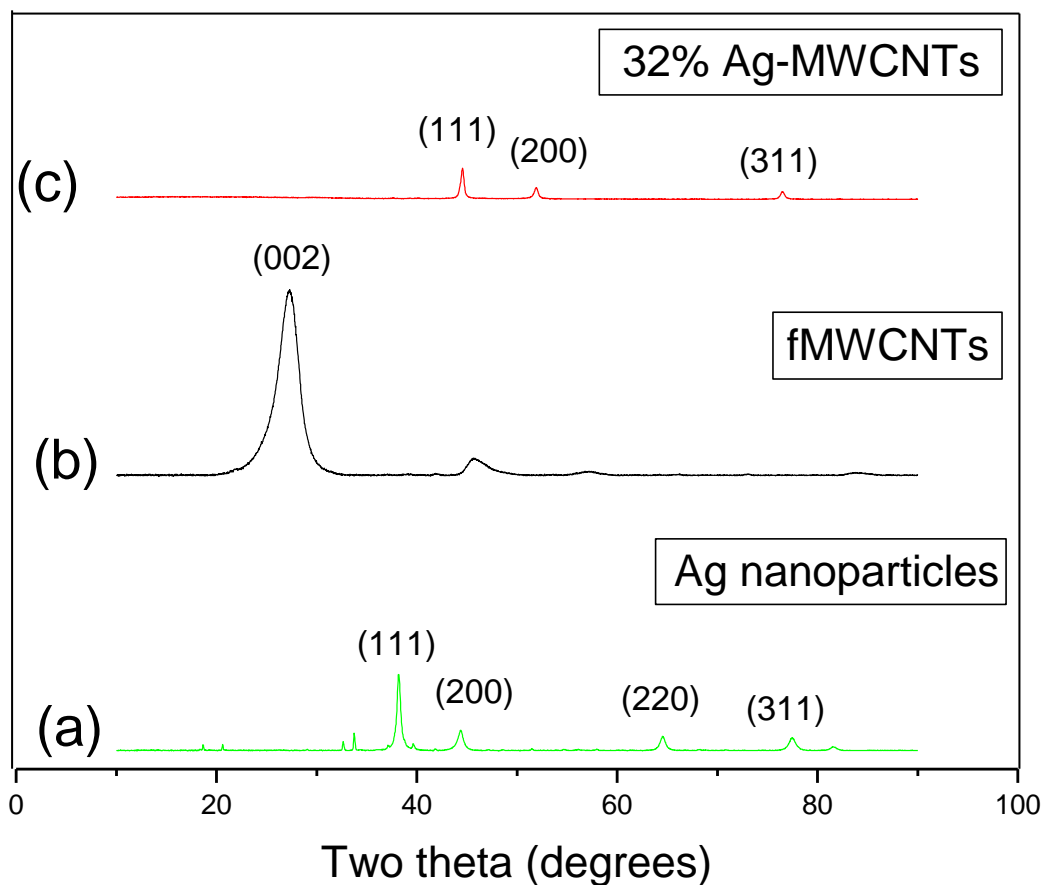


Figure 4.16: XRD patterns of synthesised Ag nanoparticles and MWCNTs, in comparison with 32 wt. % Ag-MWCNTs nanocomposite material.

Previous studies by Ma *et al.* (2008), demonstrated that the binding energy between the Ag atoms and functionalised MWCNTs was very strong after Ag decoration on MWCNTs [10]. Ag nanoparticles got strongly attached to the MWCNTs surface due to the acid treatment of the MWCNTs, and this enhanced the reactivity of MWCNTs. Figure 4.16c shows 32 wt. % Ag in MWCNTs. A slight shift on the peaks is due to sample preparation procedures, though representing the same results. The percentage loading of Ag was higher; hence the peak due to MWCNTs is small or negligible in the Ag-MWCNTs nanocomposites. The results indicated that silver nanoparticles were successfully deposited onto the walls of carbon nanotubes at large amounts.

Table 4.2 shows the summarised data and calculations of the Bragg's angle, d-spacing, FWHM and estimated crystallite size of Ag nanoparticles and 32 wt. % Ag-MWCNTs nanocomposite material. The d-spacing of silver nanoparticles (Figure 4.16c) was calculated from Bragg's law and the crystallite size was estimated from the full width at half maximum of the (200) plane using Scherrer's formula. The estimated crystallite size of silver nanoparticles was 70 nm, which is in agreement with the observed TEM data (section 4.2.2.4, Figure 4.7). An estimated crystalline size of Ag nanoparticles on the walls of MWCNTs was calculated to be 4.67 nm . This suggests that much of the Ag has been highly dispersed throughout the surface structure of MWCNTs.

Table 4.2: Estimation of crystallite size from XRD patterns for Ag nanoparticles and 32 wt. % Ag/MWCNTs nanocomposite material.

Sample	θ value (degree)	θ value (radians)	d-spacing (nm)	FWHM (radians)	Estimated crystalline size (nm)
Ag nanoparticles	19.12	0.3337	2.35	0.00488	70

32 wt. % Ag-MWCNTs	22.75	0.397	1.99	0.0296	4.67
--------------------	-------	-------	------	--------	------

4.2.3.3 XRD profile of 10 wt. % Ag/ β -CD nanocomposite material in comparison with the profile of Ag nanoparticles.

Figure 4.17a and b show the powder XRD pattern of 10 wt. % Ag/ β -CD nanocomposite material in comparison with the XRD profile of Ag nanoparticles. The appearance of (200) and (311) planes on the XRD profile of 10 wt. % Ag/ β -CD nanocomposite in Figure 4.17b, clearly confirms the incorporation of Ag nanoparticles, as compared to Figure 4.17a. The Ag nanoparticles peak intensity is related to the concentration of Ag nanoparticles introduced on the β -CD polymer (approximately 10 wt. % Ag was loaded on β -CD).

A broad peak corresponding to (002) plane is observed on the 10 wt. % Ag/ β -CD nanocomposite pattern. This broad peak is accredited to cyclodextrin molecules attached to silver nanoparticles, since a broad peak at this region is due to the carbonyl and hydroxyl groups in which cyclodextrin is mainly composed of [11].

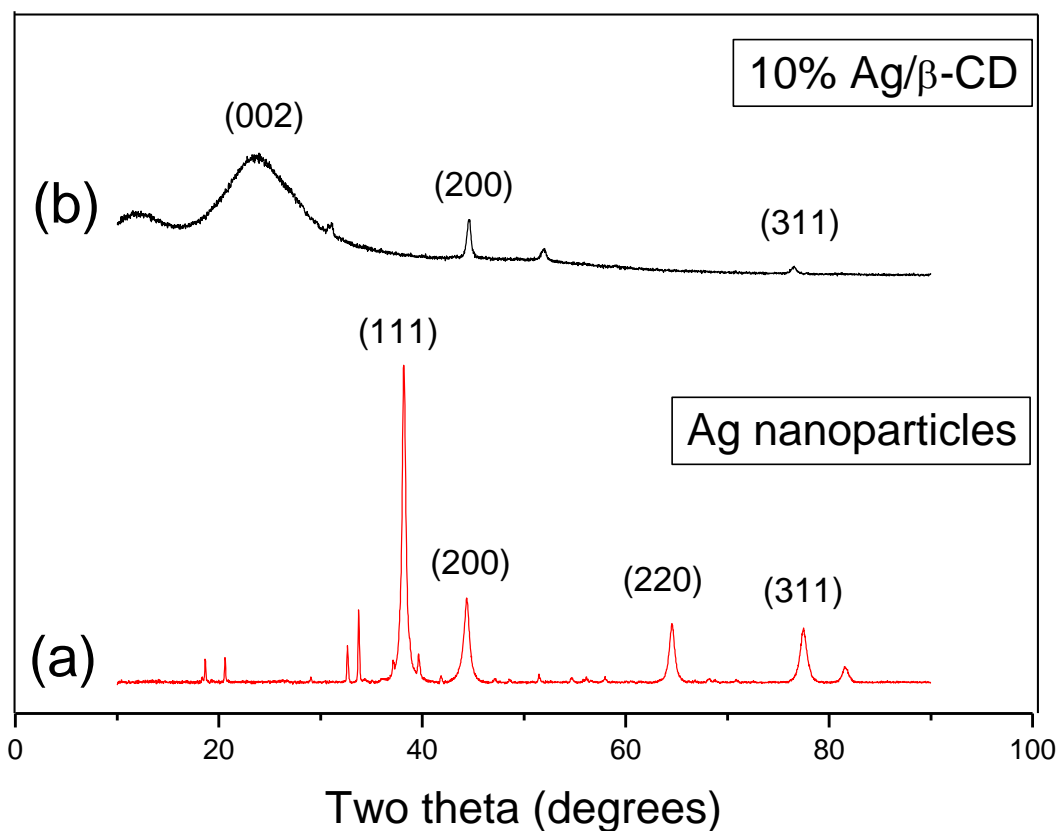


Figure 4.17: XRD patterns of synthesised silver nanoparticles and 10 wt. % Ag/β-CD nanocomposite materials.

The d-spacing of 10 wt. % Ag/β-CD nanocomposite material in Figure 4.17b was calculated from Bragg's law and the crystallite size was estimated from the full width at half maximum of the (200) plane using Scherrer's formula as shown in Table 4.3. The calculated average particles size of Ag nanoparticles in the 10 wt. % Ag/β-CD nanocomposite was 5.25 nm. Cyclodextrin polymerised with silver nanoparticles produced a good average crystallite size which is acceptable for water purification.

Table 4.3: Estimation of crystallite size from XRD patterns of 10 wt. % Ag/ β -CD nanocomposite material.

Sample	θ value (degree)	θ value (radians)	d- spacing (nm)	FWHM (radians)	Estimated crystallite size (nm)
10 wt. % Ag/ β CD	22.4	0.319	0.202	0.0264	5.25

4.2.3.4 XRD profile of 1 wt. % Ag-MWCNTs/ β -CD in comparison with the 10 wt. % Ag/ β CD and 32 wt. % Ag-MWCNTs nanocomposite material

Figure 4.18 shows the patterns of 1 wt. % Ag-MWCNTs/ β -CD in comparison with the 10 wt. % Ag/ β -CD and 32 wt. % Ag-MWCNTs nanocomposite material. The data shows a highly reduced peak intensity of Ag on 1 wt. % Ag-MWCNTs/ β -CD nanocomposites material (Figure 4.18c). A broad peak corresponding to (002) planes (Figure 4.18c) in comparison with the 32 wt. % Ag-MWCNTs (Figure 4.18a) and the 10 wt. % Ag/ β -CD (Figure 4.18b) signify the presence of cyclodextrin polymer and carbon nanotubes. The observed Ag as shown by the (111) plane on the XRD of 1 wt. % Ag-MWCNTs/ β -CD is related to the amount of Ag introduced on this nanocomposites materials (i.e. approximately 1 wt. % Ag on MWCNTs/ β -CD).

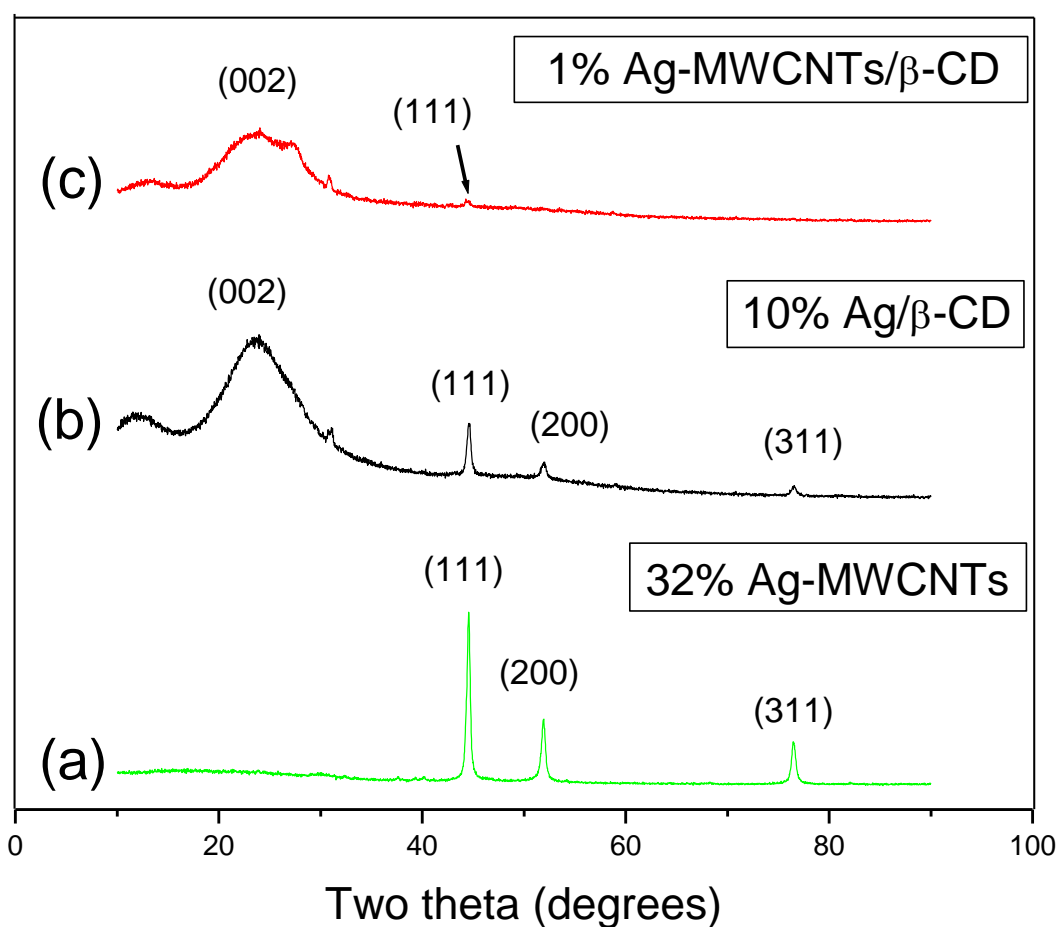


Figure 4.18: The XRD pattern of Ag-MWCNTs/β-CD nanocomposite material.

The calculated d-spacing of silver nanoparticles in 1 wt. % Ag-MWCNTs/β-CD nanocomposite material is 0.202 nm. This value is closely related to the d-spacing of the Ag on Ag-MWCNTs. The estimated size of Ag crystallites using X-ray diffraction was approximately 4.67 nm for Ag on MWCNTs and approximately 5.25 nm for Ag on β-CD, and 2.93 nm for Ag on 1 wt. % Ag-MWCNTs/β-CD. The estimated sizes of Ag by X-ray diffraction on different materials are not related to the observed TEM data (section 4.2.2.7). However, the XRD data is related to the TEM data when comparing the particle size of Ag before and after it has been incorporated on different nanocomposites materials. Similar trends were observed on the bacterial activity (see section 4.5.4) of these Ag doped nanocomposite materials (i.e. 32 wt. % Ag-MWCNTs, 10 wt. % Ag/β-CD and 1 wt. % Ag-MWCNTs/β-CD).

Table 4.4: Estimation of crystallite size from XRD patterns for 1 wt. % Ag-MWCNTs/ β -CD nanocomposite material.

θ value (degree)	θ value (radians)	d-spacing (nm)	FWHM (radians)	Estimated crystallite size (nm)
22.2	0.454	0.202	0.0473	2.93

4.2.4 Characterisation of Ag nanoparticles using UV-Vis spectrophotometer

Figure 4.19 shows the UV/Vis absorption spectra of AgNO_3 solution and silver nanoballs in the presence of sodium dodecyl sulphate as a capping agent. During the synthesis, silver nitrate and sodium dodecyl sulphate (SDS) was used as metal salt precursor and stabilising agent to produce stable nanoparticles. The best absorption of pure silver nitrate (Figure 4.19a) was observed at 300 nm. The absorption spectrum of the pale yellow-brown silver colloids prepared by sodium citrate and hydrazine hydrate reduction showed a surface plasmon absorption band with a maximum of 400 nm, indicating the presence of spherical or roughly spherical nanoparticles (Figure 4.19b). The findings are related to those obtained from TEM (section 4.2.2.4) and also correspond to what was reported by Wang *et al.* (2010) [12].

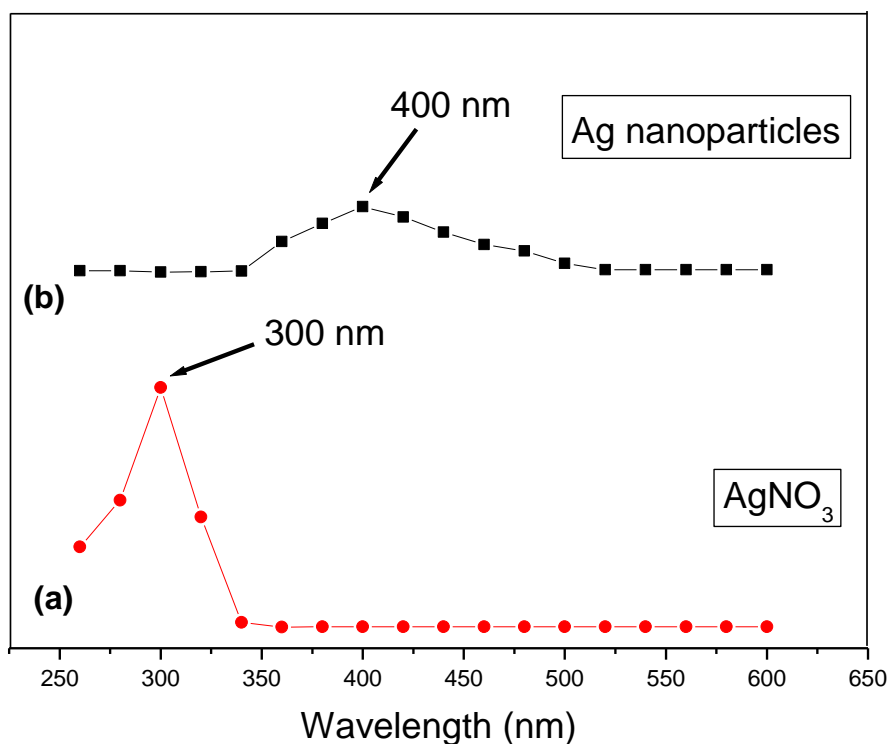


Figure 4.19: UV-visible absorption spectra of AgNO_3 solution and silver nanoparticles.

4.2.5 BET results of the nanocomposite materials

BET surface area analysis is a technique used to determine the specific surface area of powders, solids and granules [13]. The higher the surface area, the better will be the performance of the nanomaterials in water purification [13]. Table 4.5 shows the surface area and pore volume data of the synthesised nanocomposite materials.

Table 4.5: BET surface area and pore volume analysis of nanocomposite materials.

Sample no:	Sample name	Surface area (m ² /g)	Pore volume (cm ³ /g)
1	1 wt. % MWCNTs/ β -CD	3.65	0.00876
2	2 wt. % MWCNTs/ β -CD	2.23	0.00871
3	3 wt. % MWCNTs/ β -CD	1.76	0.00634
4	Ag nanoparticles	0.994	0.00301
5	β -CD polymer	1.27	0.00347
6	32 wt. % Ag-MWCNTs	4.73	0.0431
7	10 wt. % Ag/ β -CD	0.0391	0.00221
8	1 wt. % Ag-MWCNTs/ β -CD	0.652	0.000237

From sample 1 to 3 (Table 4.5), it can be seen that the surface area decreased with an increase in carbon nanotubes loading. Similar results were also observed on the pore volume. These results suggests that a small amount of carbon nanotube

addition in cyclodextrin polymers is generally required in order to achieve a high surface area of the nanocomposite materials. It is interesting to note that the high surface area recorded on sample 1 correlate with the high performance observed on water purification studies (section 4.3.4). Ag nanoparticles also had a reduced surface area compared to those of carbon nanotubes with cyclodextrin. It was also notable that the 1 wt. % Ag-MWCNTs/ β -CD and 10 wt. % Ag/ β -CD polymers had a reduced surface area and pore volume when compared to that of MWCNTs/ β -CD nanocomposite materials. This suggested that the processing of the materials during synthesis as well as the loading of metal nanoparticles might have reduced the surface area and pore sizes. However the results corroborate those observed by Lukhele *et al.* 2008 [14].

4.3 PURIFICATION OF WATER SAMPLES CONTAMINATED WITH 4-HYDROXYNITROBENZENE

4.3.1 Determination of the absorbance wavelength of 4-hydroxynitrobenzene

Figure 4.20 shows the spectra displaying the absorption wavelength region of which 4-hydroxynitrobenzene absorbs. From Figure 4.20, the highest absorption region of 4-hydroxynitrobenzene was observed at 318 nm. This wavelength was used in all the experiments. A solution of 4-hydroxynitrobenzene had a pale yellow colour, fading from the highest to the lowest concentration.

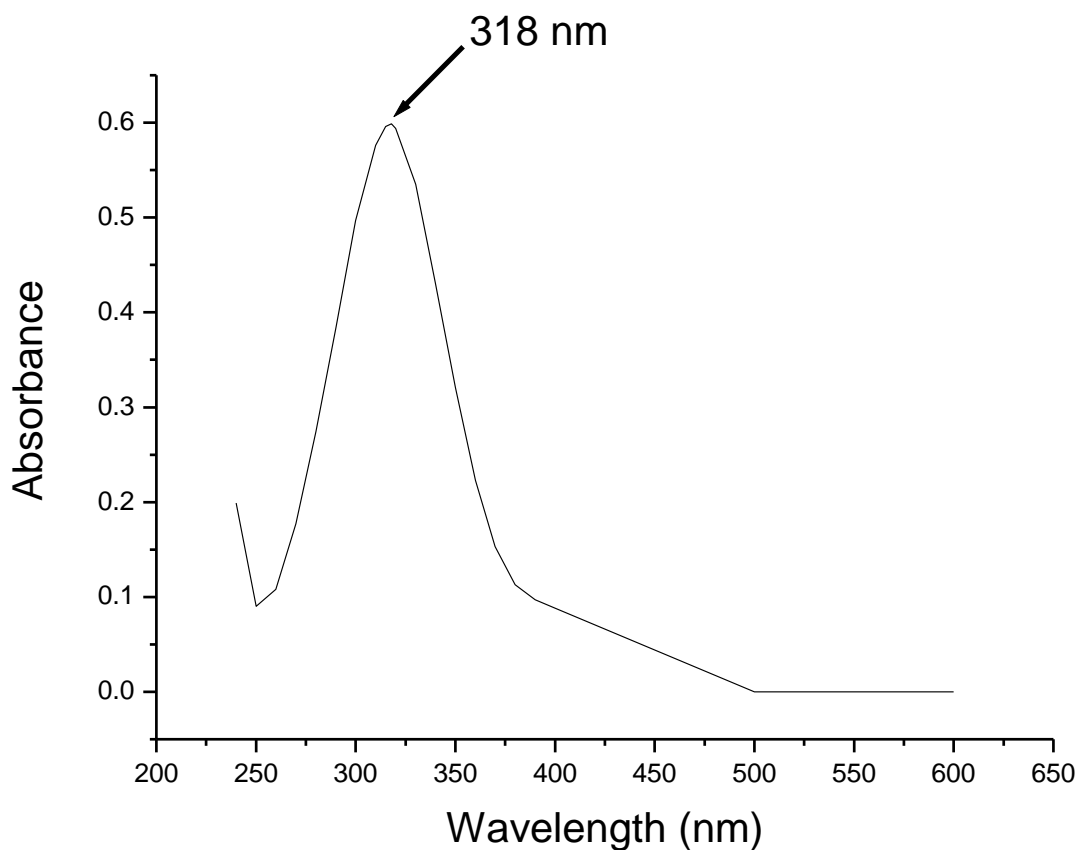


Figure 4.20: A plot showing absorbance against wavelength of 4-hydroxynitrobenzene.

4.3.2 Calibration curve of 4-hydroxynitrophenol at 318 nm

Figure 4.21 shows the calibration curve of 4-hydroxynitrobenzene at 318 nm. The calibration curve was used to determine the best linear fit for 4-hydroxynitrobenzene. From the calibration curve, the unknown concentrations can be determined. $R^2 = 0.9996$

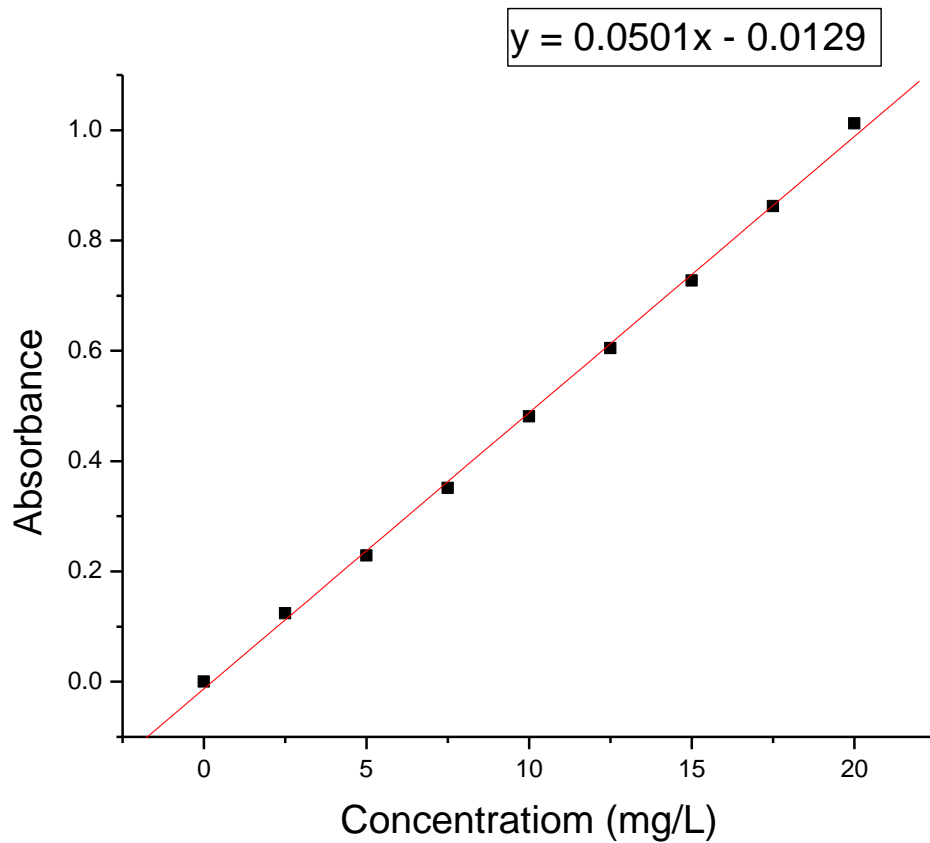


Figure 4.21: The standard curve of 4-hydroxynitrobenzene at 318 nm.

4.3.3 Effect of mono-2-substituted benzoyl β -cyclodextrin polymer and mono-2-substituted allyl β -cyclodextrin polymer on the removal of organic contaminants from water

Table 4.6 shows the percentage of 4-hydroxynitrobenzene absorbed by the mono-functionalised cyclodextrin polymers and their final concentrations. The highest absorption efficiency of the 4-hydroxynitrobenzene contaminant was found to be 88% by the allyl-substituted β -CD polymer, followed by 82% by the benzoyl-substituted β -CD polymer, with 74% of β -CD polymer being the least. The data clearly suggests that mono-functionalisation of β -cyclodextrin by the two substituted groups had a slight enhancement on the absorption efficiency of β -CD during water purification analysis. Since the results could not give higher absorption efficiencies, other nanocomposites incorporated with MWCNTs were prepared.

Table 4.6: Results showing the percentage of 4-hydroxynitrobenzene absorbed by the polymers and their final concentrations.

Sample no.	Sample name	Initial concentration (mg/L)	Final concentration (mg/L)	4-hydroxynitrobenzene absorbed (%)
1	β -CD polymer	10	0.96	74
2	Benzoyl substituted β -CD	10	1.83	82
3	Allyl substituted β -CD	10	1.24	88

4.3.4 Effect of MWCNTs loadings on the β -cyclodextrin polymers for removal of organic contaminants from water

Table 4.7 shows the percentage of 4-hydroxynitrobenzene absorbed by the MWCNTs/ β -CD nanocomposites during water purification. Three samples were prepared in such a way that the loading of MWCNTs were increased while leaving β -CD constant.

Table 4.7: Results showing the percentage of 4-hydroxynitrobenzene absorbed by MWCNTs nanocomposites and their final concentrations.

Sample no.	Sample name	Initial concentration (mg/L)	Final concentration (mg/L)	4-hydroxynitrobenzene absorbed (%)
1	1 wt. % MWCNTs/ β -CD	10	0.337	97
2	2 wt. % MWCNTs/ β -CD	10	0.437	96
3	3 wt. % MWCNTs/ β -CD	10	0.516	95

The results displayed in Figure 4.22 shows a comparison that was done over time using different MWCNTs/ β -CD nanocomposite concentrations in water purification. It was observed that the 1 wt. % MWCNTs/ β -CD (sample 1) was the fastest in reducing 4-hydroxynitrobenzene contaminant in water. The absorbance reading was observed to be less than 0.004 after 12 minutes (i.e. up to 97% removal of the contaminant). This data indicates that less time will be required during the actual water purification process. The results are further supported by the BET data

(section 4.2.4) which confirmed that this nanocomposite (sample 1) had a higher surface area compared to sample 2 and 3.

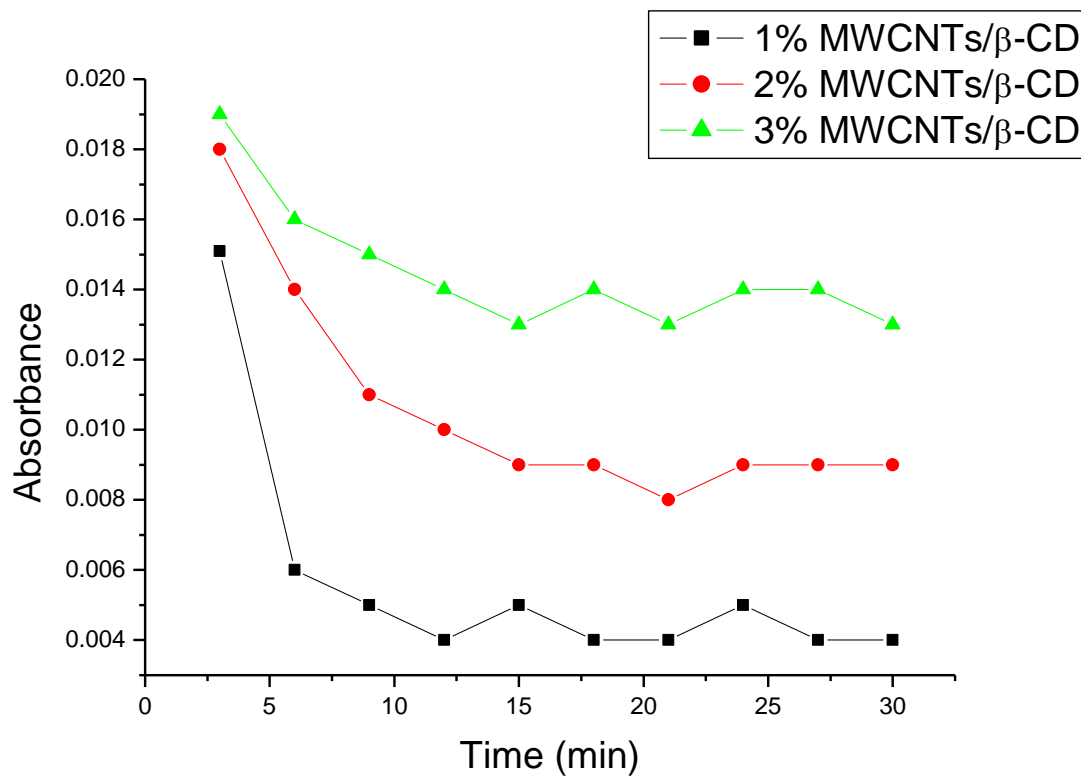


Figure 4.22: Comparison of different masses of MWCNTs/β-CD nanocomposites during water treatment at 318 nm wavelength.

4.3.5 Comparative studies of β -CD, MWCNTs, 10 wt. % Ag/ β -CD and 1 wt. % Ag-MWCNTs/ β -CD for removal of organic contaminants from water

Table 4.8 shows the comparative studies undertaken on β -CD, MWCNTs, 10 wt. % Ag/ β -CD and 1 wt. % Ag-MWCNTs/ β -CD for removal of 4-hydroxynitrobenzene from water. It was observed that carbon nanotubes alone were able to purify water samples with high absorption efficiency than β -CDs and Ag doped nanocomposites. The MWCNTs were incorporated onto cyclodextrin because they are more costly, whilst cyclodextrin is less expensive. Cheaper and yet effective materials are advantageous for industries and municipalities.

Table 4.8: Results showing the percentage of 4-hydroxynitrobenzene absorbed by β -CD, MWCNTs, 10 wt. % Ag/ β -CD and 1 wt. % Ag/MWCNTs/ β -CD nanocomposites and their final concentrations.

Sample no.	Sample name	Initial concentration (mg/L)	Final concentration (mg/L)	4-hydroxynitrophenol absorbed (%)
1	B-CD polymer	10	2.653	74
2	MWCNTs	10	0.557	94
3	10 wt. % Ag/ β -CD	10	6.585	34
4	1 wt. % Ag-MWCNTs/ β -CD	10	4.21	58

Metal loaded nanocomposites had lower absorption of 4-hydroxynitrobenzene compared with MWCNTs/ β -CD nanocomposites and β -CD polymers. This can be attributed to their low surface area (section 4.2.4). However they show excellent results on bacterial studies due to the antibacterial effect of the loaded Ag nanoparticles (section 4.4.4). Similar observations were made by Lukhele, *et al.* (2008) [14].

4.4 PURIFICATION OF WATER SAMPLES CONTAMINATED WITH ESCHERICHIA COLI BACTERIA USING DIFFERENT NANOMATERIALS

4.4.1 Determination of the initial colony forming unit

Figure 4.23 shows results which were obtained after micro-dilutions of broth containing *E. coli* in distilled water. The results display the number of colonies obtained before introduction of nanocomposites to the bacteria.

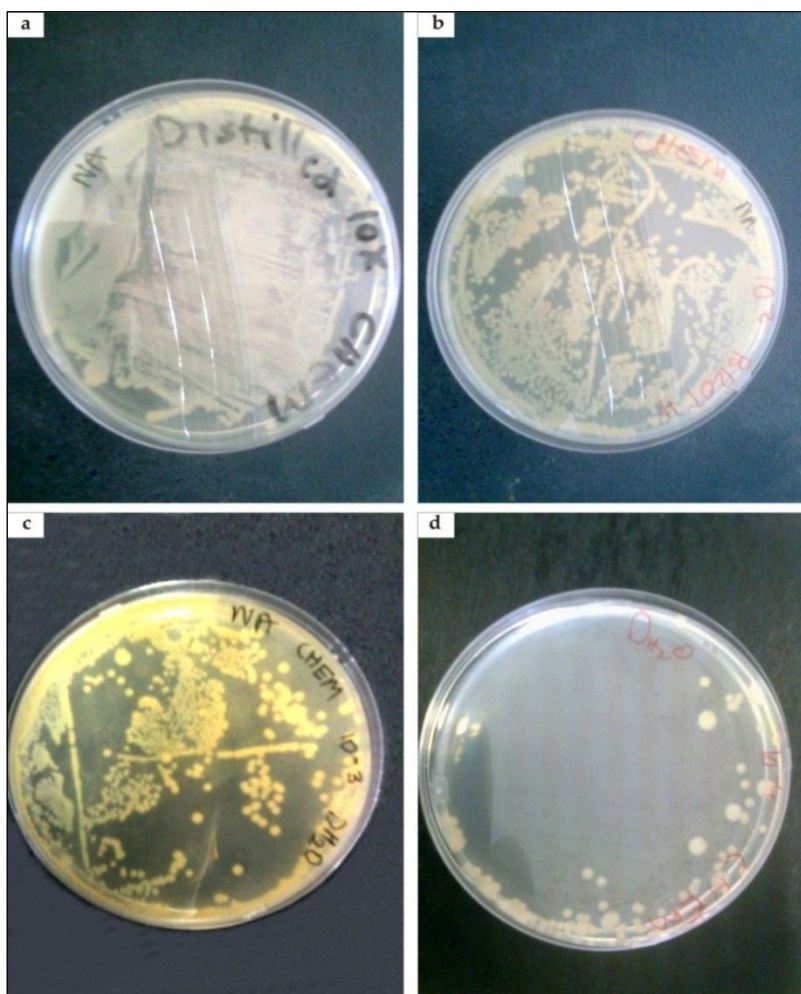


Figure 4.23: Results obtained after 24 h incubation of (a) 10^{-1} dilution, (b) 10^{-2} dilution, (c) 10^{-3} dilution and (d) 10^{-4} *E. coli* dilution standards.

The results displayed that the bacterial growth of plate A, B and C were excessively concentrated with the bacterial culture showing too many colonies which couldn't be easily counted, hence plate D was selected and its initial colony forming unit was used in this section.

Micro-dilutions of the bacteria were done to obtain the initial colony forming unit or the concentration of the bacteria that can be used as a standard before and after introducing the nanocomposites to the bacteria. The initial colony forming unit calculated for the plate with 10^{-4} dilution was found to be 117×10^5 . Both the initial colony forming unit calculations and the percentage reduction were calculated as shown in the appendices.

Table 4.9: Number of colonies obtained after micro-dilutions.

Plate	Number of colonies
10^{-1}	TNTC
10^{-2}	TNTC
10^{-3}	TNTC
10^{-4}	117 ± 0.1

Key: TNTC= Too Numerous To Count

4.4.2 Effect of Ag nanoparticles on removal of bacteria from water

4.4.2.1 Treatment of water using 300 mg of Ag nanoparticles

Table 4.10 and Figure 4.24 shows results obtained after investigation of the antibacterial performance of Ag nanoparticles (300 mg) on *E. coli* contaminated water over 30 minutes. The results were obtained after exposure of the silver nanoparticles to contaminated water over a selected period. From these data, it was observed that silver nanoparticles at higher concentrations can destroy bacteria in water even from as little time as 30 seconds. This is the reason why no colony was observed at all.

Table 4.10: Water purification results after introducing 300 mg silver nanoparticles to contaminated water with *E. coli* bacteria. Initial cfu = 117×10^5 .

Time	Colony forming unit (cfu/mL)	*Percentage inactivity of the bacteria (%)
0.5	0	100
5	0	100
10	0	100
15	0	100
20	0	100
25	0	100
30	0	100

*100% inactivity means that all the bacteria was inactivated or killed in water samples.

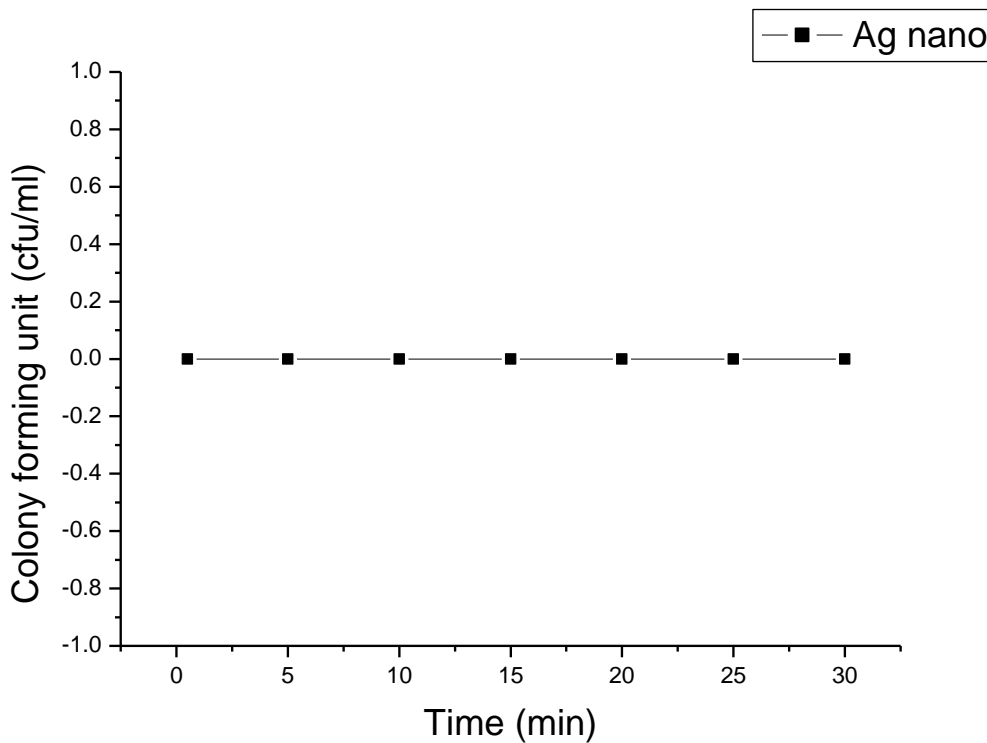


Figure 4.24: Antibacterial performance of silver on *E. coli* over 30 minutes.

4.4.2.2 Treatment of water using 150 mg of Ag nanoparticles

Table 4.11 and Figure 4.25 shows results obtained after investigation of the antibacterial performance of Ag nanoparticles (150 mg) on *E. coli* contaminated water over 20 minutes.

Table 4.11: Water purification results after introducing 150 mg of silver nanoparticles for the removal of *E. coli* bacteria. Initial cfu = 62000.

Time (min)	Colony forming unit (cfu/mL)	*Percentage inactivity of the bacteria (%)
0.5	2900 ± 0.1	95.3

2	800 ± 0.1	98.7
4	300 ± 0.1	99.5
6	300 ± 0.1	99.5
8	300 ± 0.1	99.5
10	300 ± 0.1	99.5
12	200 ± 0.1	99.7
14	200 ± 0.1	99.7
16	200 ± 0.1	99.7
18	0	100
20	0	100

*100% inactivity means that all the bacteria was inactivated or killed in water samples.

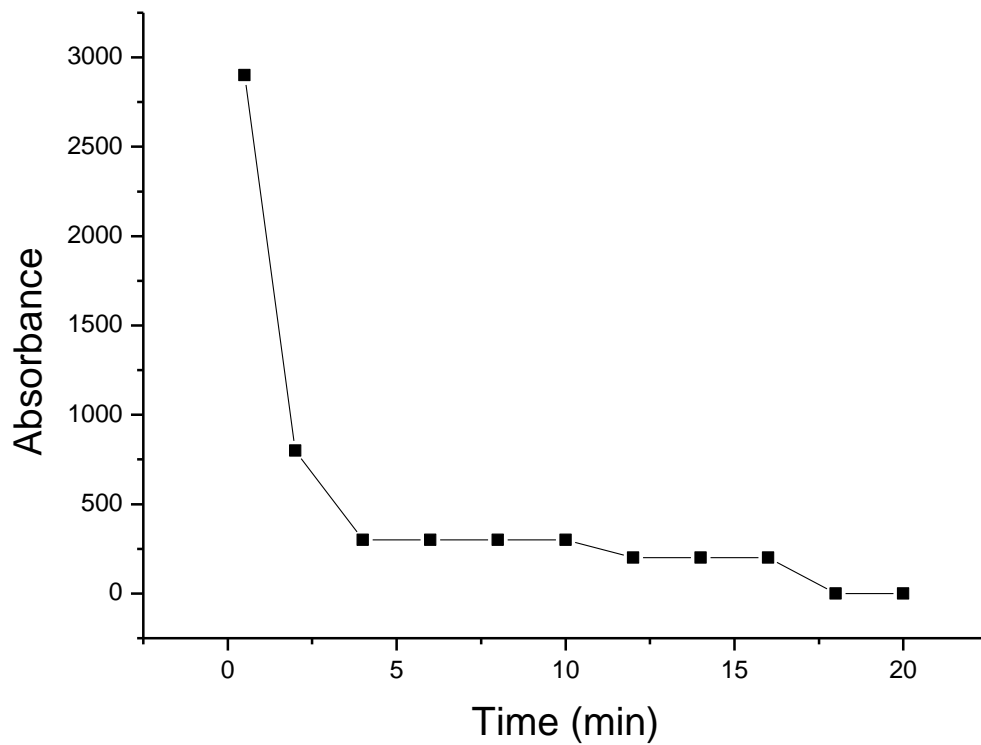


Figure 4.25: Antibacterial performance of silver nanoparticles on *E. coli* over 20 minutes.

It was necessary to investigate the exact time at which the bacteria were destroyed; therefore, the exposure time of the bacteria in the contaminated water was reduced and measured in 2 minute intervals. It was observed that after 18 minutes most of the bacteria were killed in water.

4.4.3 Comparative studies of cyclodextrin polymers and MWCNTs on removal of *E. coli* bacteria from water samples

Table 4.12 (1 and 2) and Figure 4.26 shows results obtained after investigation of the antibacterial performance of cyclodextrin polymers (150 mg) on *E. coli* contaminated water over 90 minutes.

Table 4.12: Colony forming units obtained after introduction of cyclodextrin polymers and MWCNTs on removal of *E. coli* bacteria from water samples. Initial cfu = 62000.

Time (min)	Colony forming unit (cfu/mL)				
	Benzoyl substituted β -CD	Allyl substituted β -CD	Raw MWCNTs	fMWCNTs	β -CD
30	100	4000	2000	1000	1400
60	100	500	300	0	600
90	0	200	0	0	100

Table 4.13: Percentage inactivity of *E. coli* bacteria obtained after introduction of cyclodextrin polymers and MWCNTs.

*Percentage inactivity of the bacteria (%)				
Benzoyl substituted β -CD	Allyl substituted β -CD	Raw MWCNTs	fMWCNTs	β -CD
99.8	93.5	96.8	98.4	97.7
99.8	99.2	99.5	100	99.0

100	99.7	100	100	99.8
-----	------	-----	-----	------

*100% inactivity means that all the bacteria was inactivated or killed in water samples.

Figure 4.26 shows a graphical representation of the data collected over a 90 minutes interval shown in Table 4.12 and Table 4.13. The mono-2-substituted benzoyl β -cyclodextrin and mono-2-substituted allyl β -cyclodextrin were investigated on how effectively they can destroy *E. coli* bacteria in water. The benzyl-substituted β -CD showed better results compared to the allyl-substituted β -CD since after 90 minutes, bacteria were killed in water. A comparison was also made between the functionalised and non-functionalised MWCNTs, on their efficiency of killing the bacteria.

The functionalised MWCNTs showed good results since bacteria were killed after 60 minutes. This could be due to the fact that functionalised carbon nanotubes were pure and highly reactive when compared with non-functionalised MWCNTs. Cyclodextrin alone still showed that after 90 minutes, the bacteria were still alive and therefore cyclodextrin could not be used alone since the time it required to remove contaminants was prolonged and would not be effective in water purification.

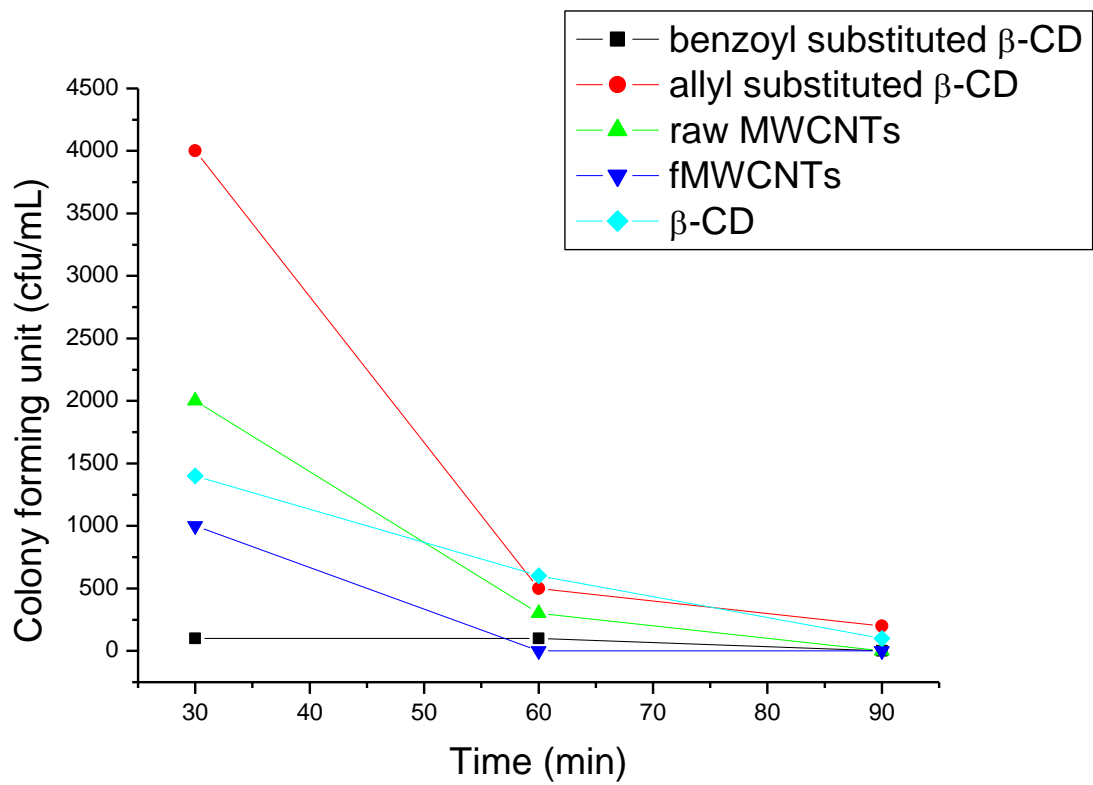


Figure 4.26: Comparison of colony forming units versus time of different nanocomposite materials used for water purification.

4.4.4 Comparative studies of different nanocomposite materials on removal of *E. coli* bacteria from water samples

The data in Table 4.14 and 2 gives a summary of the results on the activity of different nanocomposite materials.

Table 4.14: The colony forming unit of nanocomposite materials obtained during the removal of *E. coli* bacteria from water samples. Initial cfu = 15400.

Time (min)	Colony forming unit (cfu/mL)			
	32 wt. % Ag-MWCNTs	1 wt. % MWCNTs/ β -CD	10 wt. % Ag/ β -CD	1 wt. % Ag-MWCNTs/ β -CD
0.5	1700	3000	2500	1000
2	1100	2300	1500	600
4	1000	2300	900	300
6	1000	1800	500	300
8	1000	1800	400	300
10	700	1800	400	0
12	700	1800	400	0
14	700	1000	300	0
16	300	1000	200	0
18	0	300	200	0
20	0	300	0	0

Figure 4.27 shows a graphical representation of the bacterial activity of different nanocomposite materials. It can be noticed that both 32 wt. % Ag-MWCNTs and 10 wt. % Ag/ β -CD gave a closely related and better bacterial activity compared to the 1 wt. % Ag-MWCNTs/ β -CD. This clearly shows that the 1 wt. % MWCNTs/ β -CD is

mainly effective at removing organic pollutants in water. However, it is worth noting that this mixture (1 wt. % MWCNTs/ β -CD), when doped with Ag nanoparticles has an enhanced bacterial activity.

After just 10 minutes of nanocomposites interaction with the bacteria, the percentage inactivation of the bacteria reached 100. These clearly demonstrate that this nanocomposite is capable of killing *E. coli* bacteria at a very short period of time. The bacterial activity of 1 wt. % Ag doped on MWCNTs/ β -CD is even higher than the findings (approximately 95% *E. coli* was removed in 90 minutes) reported by Lukhele *et al.* (2008) [14].

Usually the surface structure of the nanocomposites plays an important role on the bacterial activity. A surface area of 0.652 m²/g of 1 wt. % Ag-MWCNTs/ β -CD was obtained as compared to 4.73 m²/g surface area of 32 wt. % Ag-MWCNTs nanocomposites. This data indicates that the bacterial activity of Ag on MWCNTs/ β -CD is different, since a drop in surface area is expected to give lower bacterial activity. It can therefore be assumed that the bacterial activity of 1 wt. % Ag-MWCNTs/ β -CD is due to the higher dispersion of Ag nanoparticles on MWCNTs/ β -CD. This assumption can be backed up by the estimated crystallite size of 2.93 nm Ag on MWCNTs/ β -CD, compared to 4.67 nm for Ag on MWCNTs and 5.25 for Ag on β -CD. However, the TEM data of 1 wt. % Ag on MWCNTs/ β -CD data do not provide a better clarity on the particle sizes of Ag on the above mentioned nano-materials.

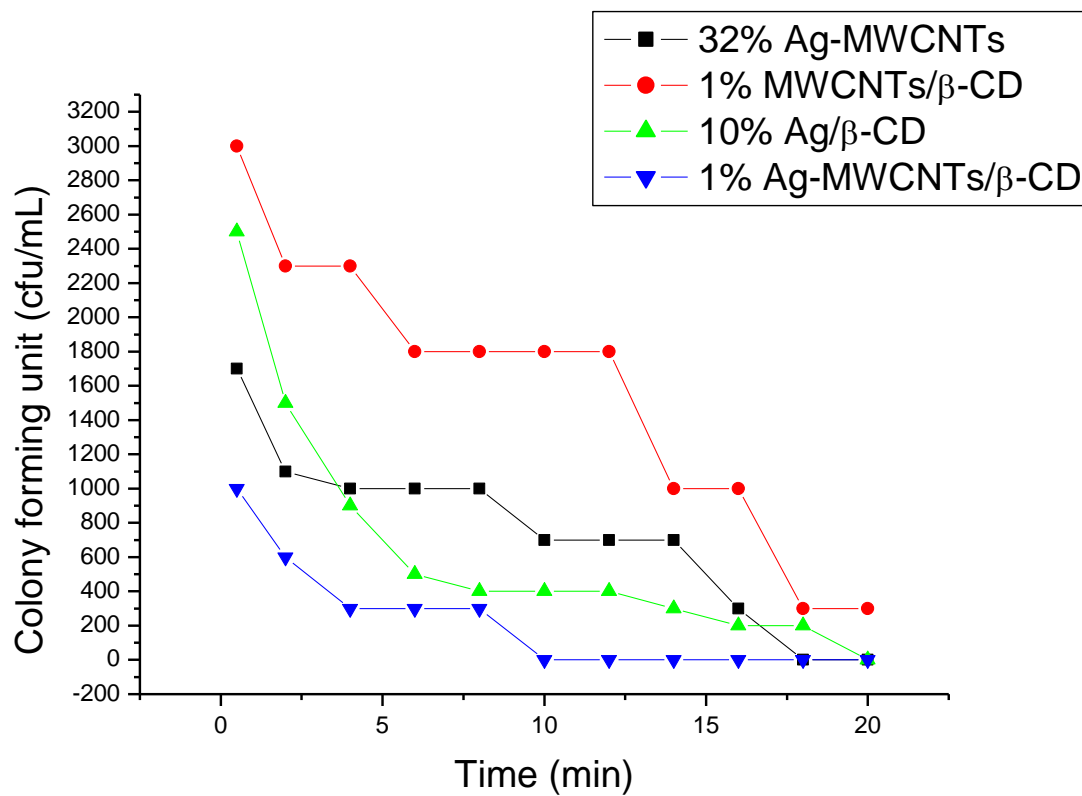


Figure 4.27: Comparison of colony forming unit versus time of different nanocomposites used for water purification.

Table 4.15: The percentage inactivity of *E. coli* bacteria by different nanocomposite materials during water purification.

*Percentage inactivity of the bacteria (%)			
32 wt. % Ag-MWCNTs	1 wt. % MWCNTs/ β -CD	10 wt. % Ag/ β -CD	1 wt. % Ag-MWCNTs/ β -CD
88.9	80.5	83.8	95.5
92.9	85.1	90.3	98.1
93.5	85.1	94.2	98.1
93.5	88.3	96.8	98.1
93.5	88.3	97.4	98.1
95.5	88.3	97.4	100
95.5	88.3	97.4	100
95.5	93.5	98.1	100
98.1	93.5	98.7	100
100	98.1	98.7	100
100	98.1	100	100

*100% inactivity means that all the bacteria was inactivated or killed in water samples

From the overall results obtained, it can be concluded that there is a slight improvement with time in the percentage inactivation of the bacteria observed when silver was doped on the nanocomposites. This is excellent because obtaining an efficient and fast method would be an added advantage. Results obtained showed the ability of the Ag doped nanocomposites with carbon surfaces to have antibacterial properties. However this material gave poor performance when tested for organic contaminants removal in water. In general, this nanocomposite material

can be a better selection for purifying water in the industries and municipality; since they seem to be efficient, even requiring less time in purifying water.

4.5 INVESTIGATION OF THE GROWTH CURVE OF *E. COLI* BACTERIA BY MEASURING THE OPTICAL DENSITY IN THE PRESENCE OF 1 wt. % Ag-MWCNTs/ β -CD NANOCOMPOSITE MATERIAL

4.5.1 Introduction

Optical density is measured in a UV/Vis spectrophotometer by monitoring the concentration of bacteria in a suspension. Measuring the optical density (OD) is a common method to quantify the concentration of substances (Beer-Lambert law), since the absorbance is proportional to the concentration of the absorbing species in the sample. Visible light passes through a cell suspension and the light get scattered. Greater scatter indicates that more bacteria are present. The amount of light scattered can be measured in a spectrophotometer at 600 nm [15].

4.5.2 Effect of 1 wt. % Ag-MWCNTs/ β -CD nanocomposite material on the optical density measurement of *E. coli* in contaminated water

The results in Table 4.16 were obtained after each 30 minutes of bacterial interaction with nanocomposites in the nutrient broth medium for 90 minutes. The bacterial growth was tested in the nutrient broth for optimal activity. Optical densities were measured and plotted as a function of time for 90 minutes at regular intervals with different concentration of 1 wt. % Ag-MWCNT/ β -CD nanocomposite material as shown in Figure 4.28.

Table 4.16: Optical density measurements of *E. coli* at 600 nm

Time (minutes)	Absorbance at 600 nm		
	5 mg of 1 wt. % Ag-MWCNTs/ β CD	10 mg of 1 wt. % Ag-MWCNTs/ β CD	100 mg of 1 wt. % Ag-MWCNTs/ β CD
0	1.088	1.085	1.09
30	1.149	1.092	1.086

60	0.949	0.843	0.842
90	0.889	0.82	0.794

Bacterial cells grow by a process called binary fission in which one cell doubles in size and splits into halves to produce two identical daughter cells. Bacterial cell growth enhances the turbidity of the liquid nutrient medium and as a result the absorption increases. The results further agree with those obtained from the colony forming method and confirmed that the activity of the bacteria decreased with time in the presence of 1 wt. % Ag-MWCNTs/ β CD nanocomposites.

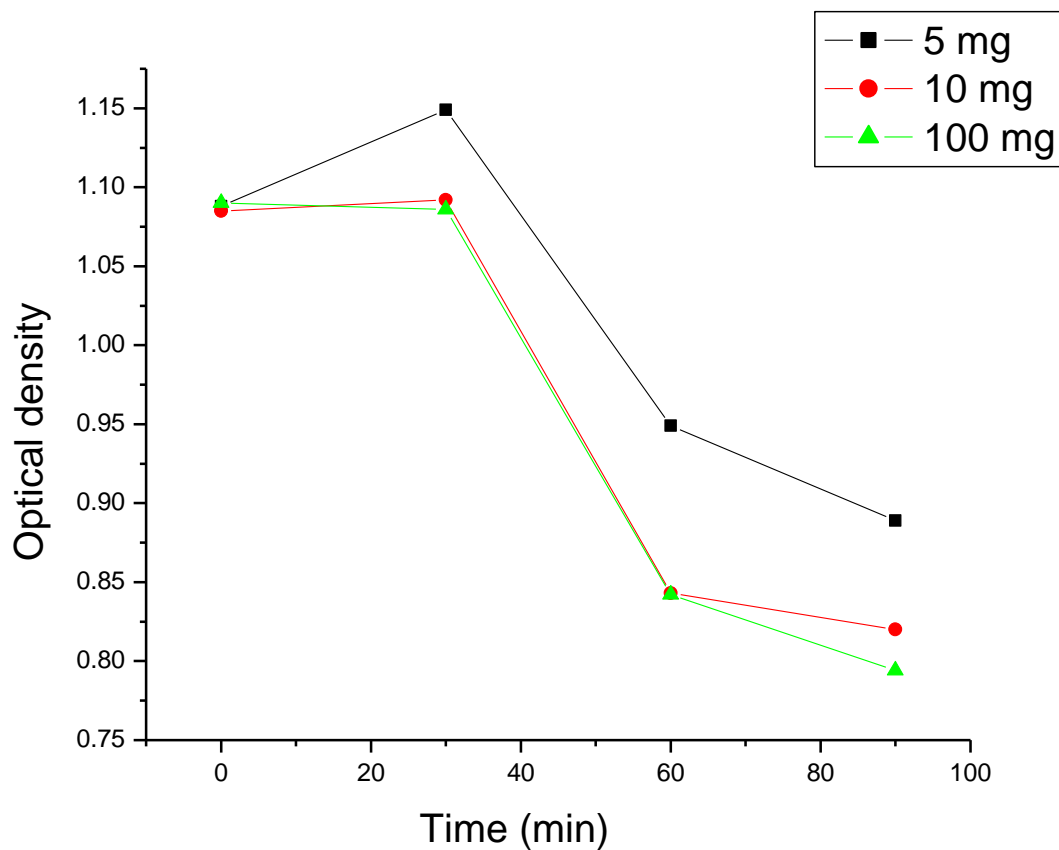


Figure 4.28: Optical density as a function of time for *E. coli* supplemented with Ag-MWCNT/ β -CD nanocomposites in nutrient broth medium.

In a nutrient medium, bacterial growth curve increases with time. In the presence of 1 wt. % Ag-MWCNTs/ β -CD nanocomposite, a slight growth was noticed (Figure 4.28), which later decreased as the nanocomposites were interacting with the bacteria. The amount of nanocomposites caused a growth delay of *E. coli*. It was also observed that after 90 minutes, 100 mg of 1 wt. % Ag-MWCNTs/ β -CD nanocomposites act as effective bactericides and there was virtually no bacterial growth on the plates which were incubated for 24 h.

4.5.3 Investigation of the interaction between 1 wt. % Ag-MWCNTs/ β -CD nanocomposite material and *E. coli* bacteria in broth medium after 90 minutes

The following results (Figure 4.29) were obtained after 90 minutes interaction of the 1 wt. % Ag-MWCNT/ β -CD nanocomposite material with *E. coli* bacteria in broth medium. The agar plate in Figure 4.29.a shows the colonies of the bacteria before introduction of the nanocomposite material. The results in Figure 4.29b, c and d confirms that no bacterial growth on plates supplemented with 5 mg, 10 mg and 100 mg after 90 minutes contact with 1 wt. % Ag-MWCNTs/ β -CD nanocomposite material after 24 h incubation at 37 °C. Bacterial destruction was found to be sustained as no colony growth was observed even after 48 h of incubation. The results suggest that the nanocomposites are bactericidal.

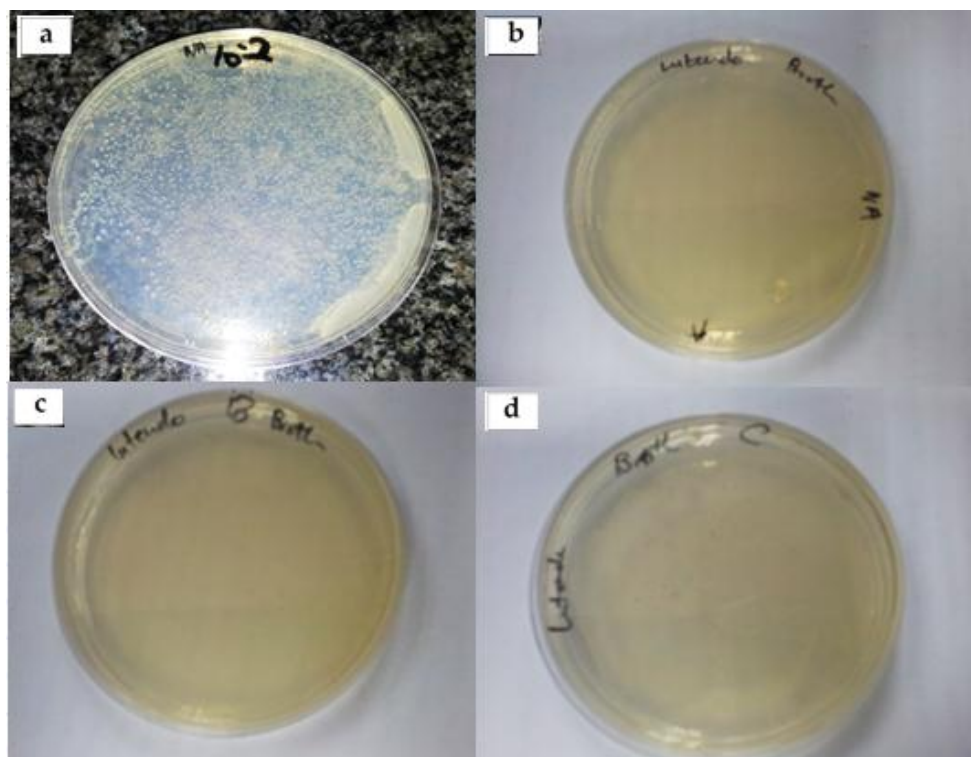


Figure 4.29: Nutrient agar plates showing (a) bacterial growth before introduction of 1 wt. % Ag-MWCNTs/ β -CD nanocomposite material, and plates supplemented with (b) 5 mg, (b) 10 mg and (c) 100 mg 1 wt. % Ag-MWCNTs/ β -CD nanocomposite material after 90 minutes of the bacterial interaction with these nanocomposites.

4.6 INVESTIGATION OF THE ROLE PLAYED BY 1 wt. % Ag-MWCNTS/ β -CD NANOCOMPOSITE MATERIALS ON THE DESTRUCTION OF *E. coli* BACTERIA IN WATER BY MEANS OF SCANNING ELECTRON MICROSCOPY

4.6.1 Introduction

Bacteria have different membrane structures and are classified as gram negative or gram positive. The structural difference lies in the organization of peptidoglycan, which is the key component of membrane structure. A gram-negative bacterium exhibits a thin layer of peptidoglycan (about 2-3 nm) between the cytoplasmic membrane and the outer cell wall. Outer membrane of *E. coli* cells are mostly constructed from tightly packed lipopolysaccharide (LPS) molecules, which provide an effective permeability barrier [15].

The overall charge of bacterial cells at biological pH values is negative because of excess number of carboxylic groups, which upon dissociation makes the cell surface negative. The opposite charges of bacteria and nanomaterials are attributed to their adhesion and bioactivity due to electrostatic forces [16].

4.6.2 The structure of *E. coli* bacteria

Figure 4.30 shows the structure of *E. coli* bacteria (ATCC 25922) studied under FE-SEM. The structure of *E. coli* bacteria was studied before interaction with the nanoparticles. At this stage, it could be observed that *E. coli* structure was surrounded by a visible capsule (Figure 4.30) and that it exhibited the morphology of a rod-shaped bacterium.

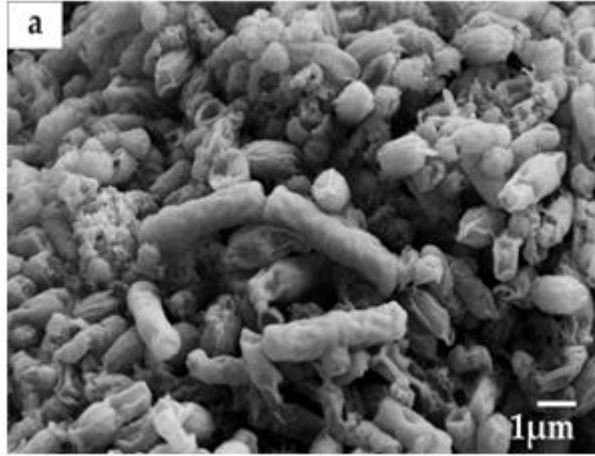


Figure 4.30: FE-SEM micrograph of *E. coli* bacteria.

4.6.3 Interaction of *E. coli* bacteria with 1 wt. % Ag-MWCNTs/ β -CD nanocomposite material over a period of 60 minutes

Figure 4.31 shows the interaction of *E. coli* bacteria with 1 wt. % Ag-MWCNTs/ β -CD nanocomposite material over a period of 60 minutes. Field emission scanning electron microscopy confirmed the incorporation of nanocomposite materials into the membrane structure (Figure. 4.31c and d). During the initial stages of interaction (Figure 4.31a and b), the bacteria was found clustered on the nanocomposites. After 2 to 4 minutes (Figure 4.31a and b) of bacterial interaction with the nanocomposite materials, the nanocomposite materials seemed not to have interacted with the bacteria as yet; nevertheless both the bacteria and nanocomposite materials are visible.

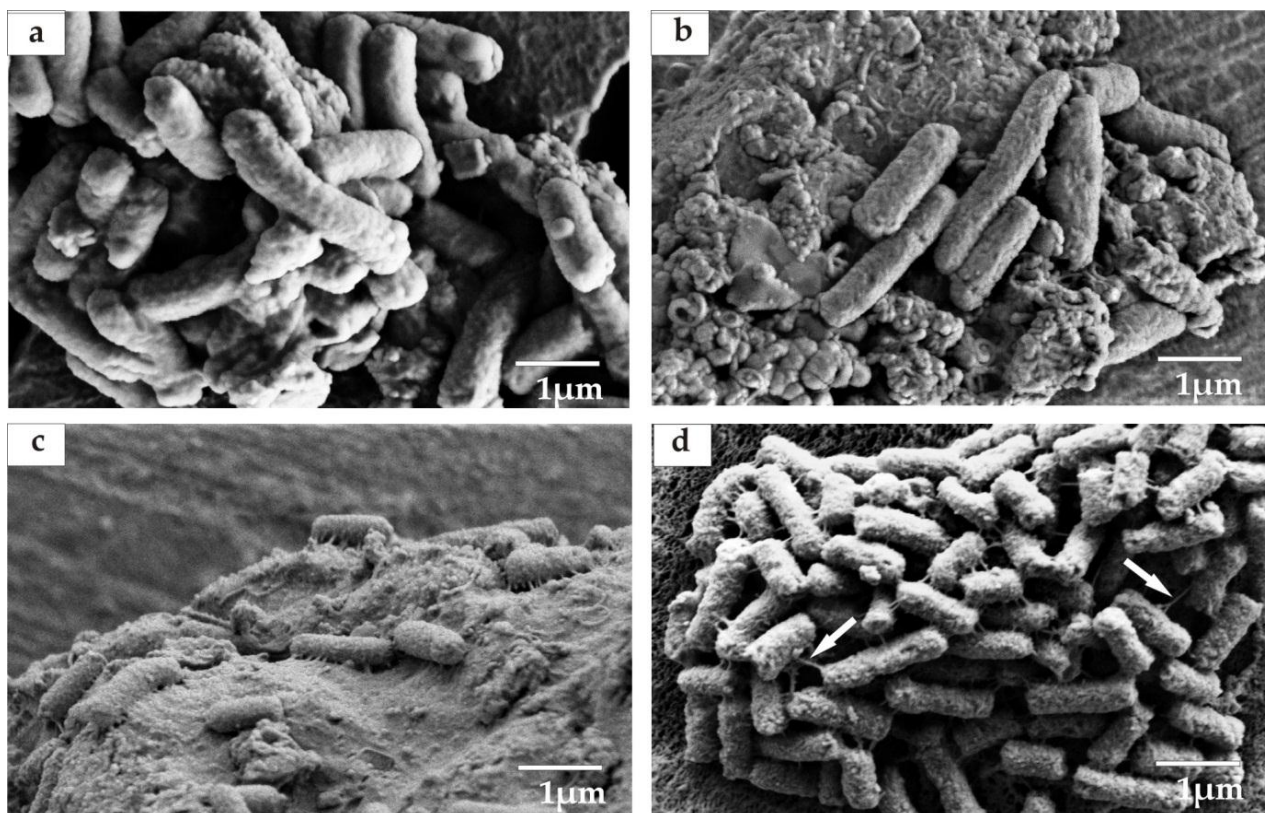


Figure 4.31: FE-SEM micrograph of *E. coli* treated with 1 wt. % Ag-MWCNTs/ β -CD nanocomposite materials (a) after 2 minutes, (b) after 4 minutes, (c) after 6 minutes and (d) after 60 minutes interaction. Arrows indicate MWCNTs.

Binding of nanocomposites to the bacteria depends on the surface area available for interaction. Nanocomposite materials have larger surface area available for

interactions, which enhances bactericidal effect and, hence they impart cytotoxicity to the microorganisms [16].

Between 6 and 60 minutes interaction (Figure 4.31 c and d), bacteria display some interaction with nanocomposites. Nanocomposite materials adhered to the bacterial cell wall surface (Figure 4.31c & d); and *E. coli* appear to have lost their outer capsule and therefore exhibited a different structure to that observed before the nanocomposite materials were introduced in Figure 4.30. Multi-walled carbon nanotubes were visibly 'trapping' *E. coli* in Figure 4.31d. As this occurred, the nanocomposite materials tends to penetrate inside the bacteria and causes damage by interacting with phosphorus and sulphur containing compounds such as DNA [16].

4.6.4 Interaction of *E. coli* bacteria with 1 wt. % Ag-MWCNTs/ β -CD nanocomposite material after 150 and 210 minutes

Figure 4.32 shows interaction of *E. coli* bacteria with 1 wt. % Ag-MWCNTs/ β -CD nanocomposite material between 150 and 210 minutes. The bacterial structure (Figure 4.32 a & b) showed critical changes and damages occurred in the membrane and the cell structure. It is possible that DNA may have lost its replication ability and cellular proteins became inactive after treatment with the nanocomposites. Another reason would be the release of silver ions from 1 wt. % Ag-MWCNTs/ β -CD nanocomposite material, which may have had an additional contribution to the bactericidal efficiency. It may also be that the nanocomposite material penetrated into the bacteria and inactivated its enzymes, generating hydrogen peroxide and causing bacterial cell death [18]. Additional ultra-structural investigation may be useful in clarifying some of these questions such as atomic force microscopy and ultra-high vacuum scanning force microscopy.

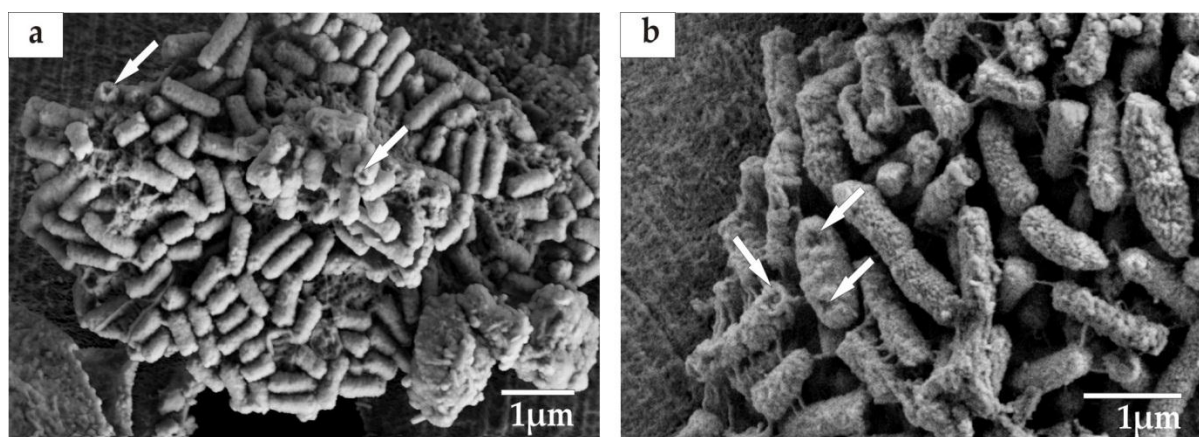


Figure 4.32: FE-SEM of *E. coli* ‘pit’ formation after (a) 150 minutes and (b) after 210 minutes interaction treatment with 1 wt. % Ag-MWCNTs/ β -CD nanocomposite material. The arrows illustrate the pits formed.

Studies by Amro *et al.* (2000) suggest that when *E. coli* is treated with silver nanoparticles, changes took place in its membrane morphology which produced a significant increase in its permeability thus affecting sufficient transport through the

plasma membrane [18]. This left the bacterial cells incapable of properly regulating transport through the plasma membrane, therefore resulting in cell death [18].

The results indicate that treated bacteria showed significant damage on the outer membranes, which are recognised by the formation of 'pits' on their surfaces (Figure 4.32). Metal depletion causes formation of irregular-shaped pits in the outer membrane of bacteria which is caused by progressive release of the lipopolysaccharides (LPS) molecules and membrane proteins [19]. In addition, it is believed that silver binds to functional groups of proteins, resulting in protein denaturation [19]. Heavy metals are toxic and react with proteins, therefore they bind protein molecules; and as a result cellular metabolism is inhibited subsequently causing death of microorganisms [20]. The overall bacterial results reflect that 1 wt. % Ag-MWCNTs/ β -CD nanocomposite material have an excellent biocidal effect and shows great potential in reducing bacterial growth for practical application.

4.7 EFFECT OF TEMPERATURE ON INTERACTION OF Ag-MWCNTS NANOCOMPOSITE MATERIAL WITH *E. coli* BACTERIA

4.7.1 Determination of the colony forming unit and percentage reduction of *E. coli* bacteria in the presence of 32 wt. % Ag-MWCNTs nanocomposite material at different incubation temperatures

The results displayed in Table 4.17 and Figure 4.33 were obtained after interacting *E. coli* bacteria in the presence of Ag-MWCNTs nanocomposite material between 10 °C and 30 °C.

Table 4.17: The colony forming unit and the percentage reduction calculated from number of colonies. Initial cfu = 15400.

Time (min)	Colony forming unit (cfu/mL)					Percentage inactivation of the bacteria (%)				
	*10 °C	*15 °C	*20 °C	*25 °C	*30 °C	*10 °C	*15 °C	*20 °C	*25 °C	*30 °C
0.5	3500	1800	1700	2000	200	77.2	88.3	89.0	87.0	98.7
2	2700	800	1100	1700	100	82.5	94.8	92.9	89.0	99.3
4	700	400	800	1100	100	95.5	97.4	94.8	92.9	99.3
6	200	200	600	800	0	98.7	98.7	96.1	94.8	100
8	100	100	600	800	0	99.3	99.3	96.1	94.8	100
10	0	100	500	800	0	100	99.3	96.8	94.8	100
12	0	0	400	700	0	100	100	97.4	95.5	100
14	0	0	400	500	0	100	100	97.4	96.8	100
16	0	0	300	300	0	100	100	98.1	98.1	100
18	0	0	0	100	0	100	100	100	99.3	100

20	0	0	0	0	0	100	100	100	100	100
----	---	---	---	---	---	-----	-----	-----	-----	-----

*All the reactions were undertaken within ± 3 °C temperatures.

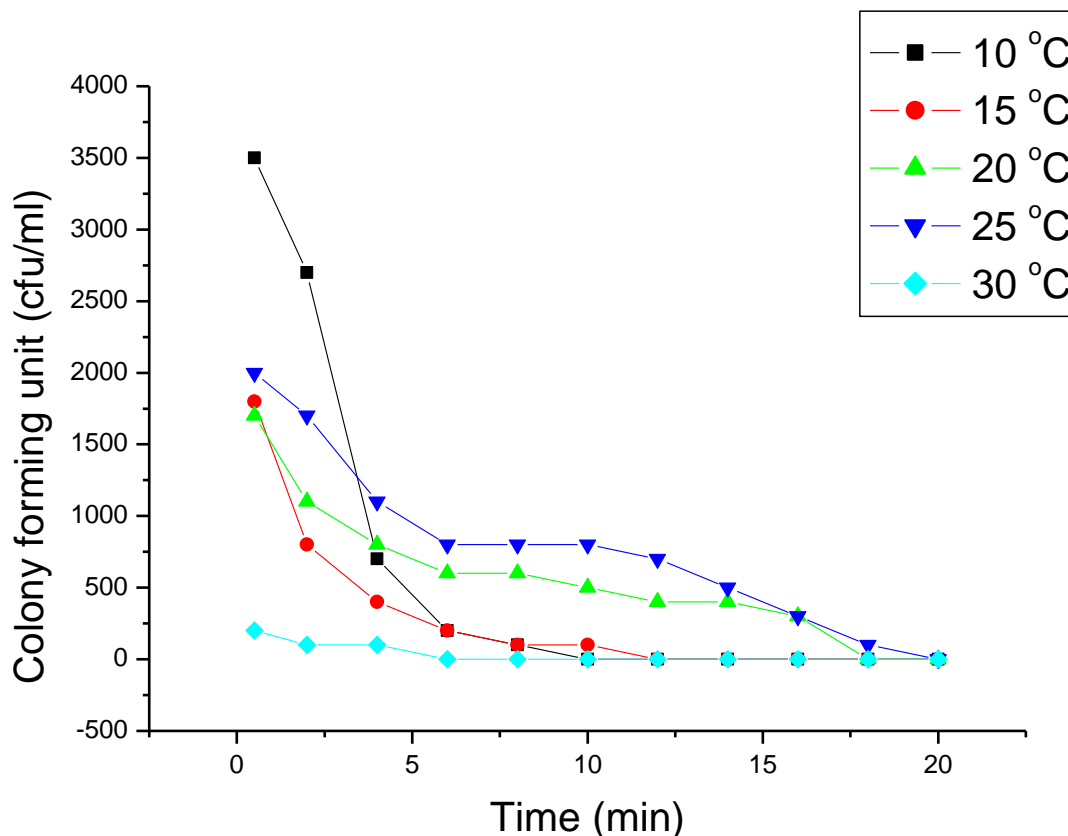


Figure 4.33: Antibacterial effect of Ag-MWCNTs at different temperatures.

As shown in the results obtained, (Figure 4.33) the activity of bacteria was varied at different temperatures. The results showed that at lower temperatures, it is easier to destroy the bacteria faster than at higher temperature due to some inhibition factors evident at lower temperatures. At a high temperature such as 30 °C, the bacteria exhibit more activity since it is closer to 37 °C which is the optimum temperature for their growth. The nanocomposite materials prepared proved to be active and was observed not to lose their activity even at lower temperatures.

4.7.2 Determination of the kinetic parameters: Interaction of 32 wt. % Ag-MWCNTs with *E. coli* bacteria at different temperatures

Assumptions were made that the reaction was first order and that the rate depended only on the colony forming unit. The rate was derived from the least-squares best fit line of $y = y_0 + A_1 e^{-(x-x_0)/t_1}$, where y_0 is the colony forming unit reading, A_1 is the frequency factor and k , the rate constant was calculated from $k = 1/t_1$. The activation energy (E_a) was derived from the least-squares best fit line of $\ln k$ vs. $1/T$, from the Arrhenius equation $\ln k = -E_a/RT + \ln A$, where the slope is equal to $-E_a/R$, the intercept is equal to $\ln A$. $R = 8.314 \text{ J.K}^{-1}.\text{mol}^{-1}$ and T is the temperature in Kelvin.

4.7.2.1 First order analysis of the antibacterial activity of 32 wt. % Ag-MWCNTs nanocomposite material at 10 °C

Figure 4.34 shows the first order graph displaying results obtained after interaction of the 32 wt. % Ag-MWCNTs nanocomposite material with *E. coli* bacteria at 10 °C. The hyperbolic graph obtained displayed the R-squared value of 0.93089 and the rate was calculated to be 0.382 min^{-1} .

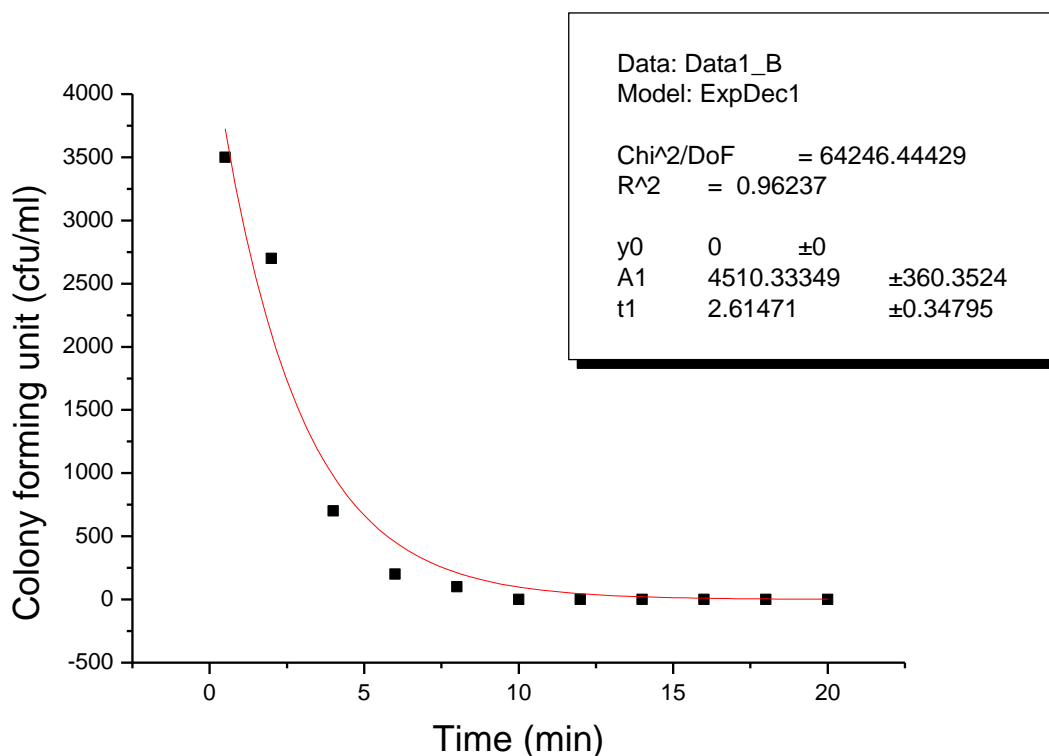


Figure 4.34: A first order analysis of showing antibacterial effect of 32 wt. % Ag-MWCNTs at 10 °C.

4.7.2.2 First order analysis of the antibacterial activity of 32 wt. % Ag-MWCNTs nanocomposite material at 15 °C

Figure 4.35 shows the first order graph displaying results obtained after interaction of the Ag-MWCNTs nanocomposite material with *E. coli* bacteria at 15 °C. The hyperbolic graph obtained displayed the R-squared value of 0.99274 and the rate was calculated to be 0.454 min⁻¹. This shows that the rate at which the bacteria are inactivated is higher than that at 10 °C.

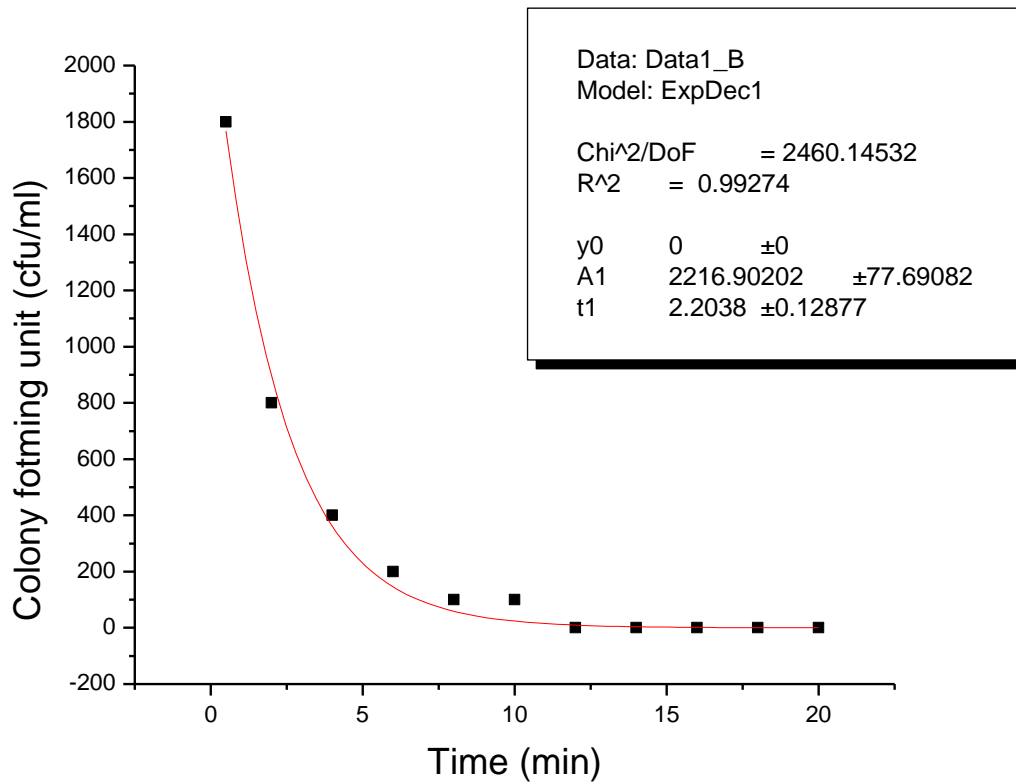


Figure 4.35: A first order analysis showing antibacterial effect of 32 wt. % Ag-MWCNTs at 15 °C.

4.7.2.3 First order analysis of the antibacterial activity of 32 wt. % Ag-MWCNTs nanocomposite material at 20 °C

Figure 4.36 shows the first order graph displaying results obtained after interaction of the Ag-MWCNTs nanocomposite material with *E. coli* bacteria at 20 °C. The hyperbolic graph obtained displayed the R-squared value of 0.92803 and the rate was calculated to be 0.137 min⁻¹. This shows that the rate at which the bacteria are inactivated is lower than that at 10 and 15 °C.

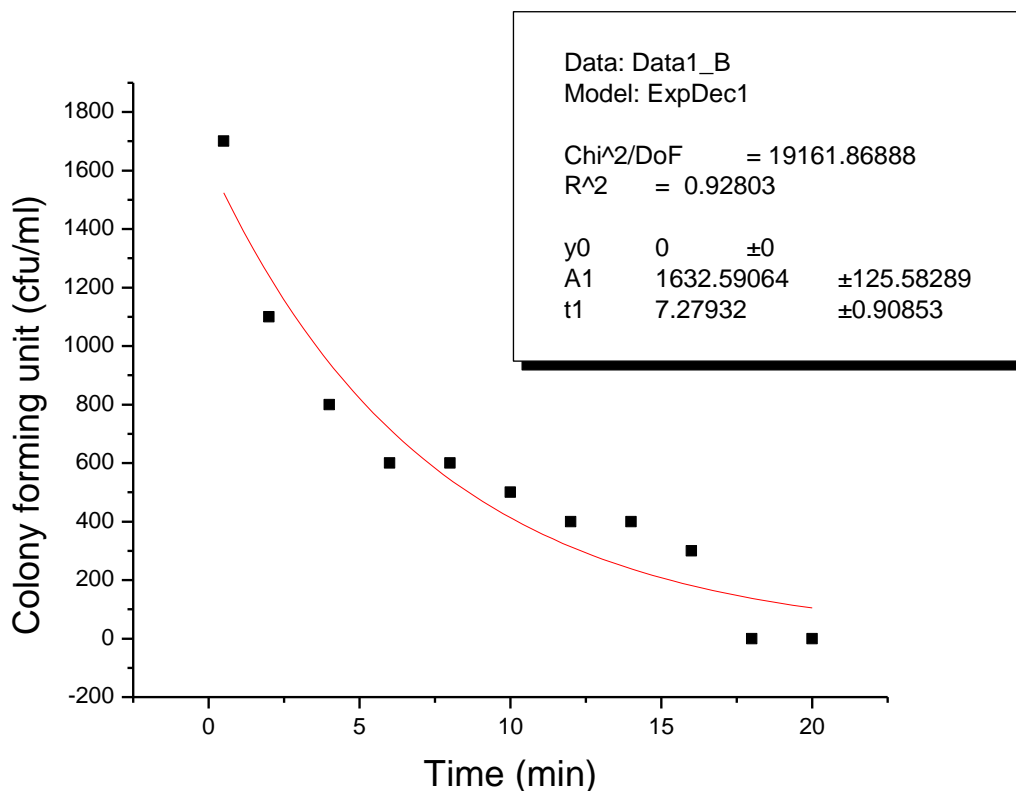


Figure 4.36: A first order analysis showing antibacterial effect of 32 wt. % Ag-MWCNTs at 20 °C.

4.7.2.4 First order analysis of the antibacterial activity of 32 wt. % Ag-MWCNTs nanocomposite material at 25 °C

Figure 4.37 shows the first order graph displaying results obtained after interaction of the Ag-MWCNTs nanocomposite material with *E. coli* bacteria at 25 °C. The hyperbolic graph obtained displayed the R-squared value of 0.94083 and the rate was calculated to be 0.121 min⁻¹. This shows that the rate at which the bacteria are inactivated is lower than that at 10, 15 and 20 °C.

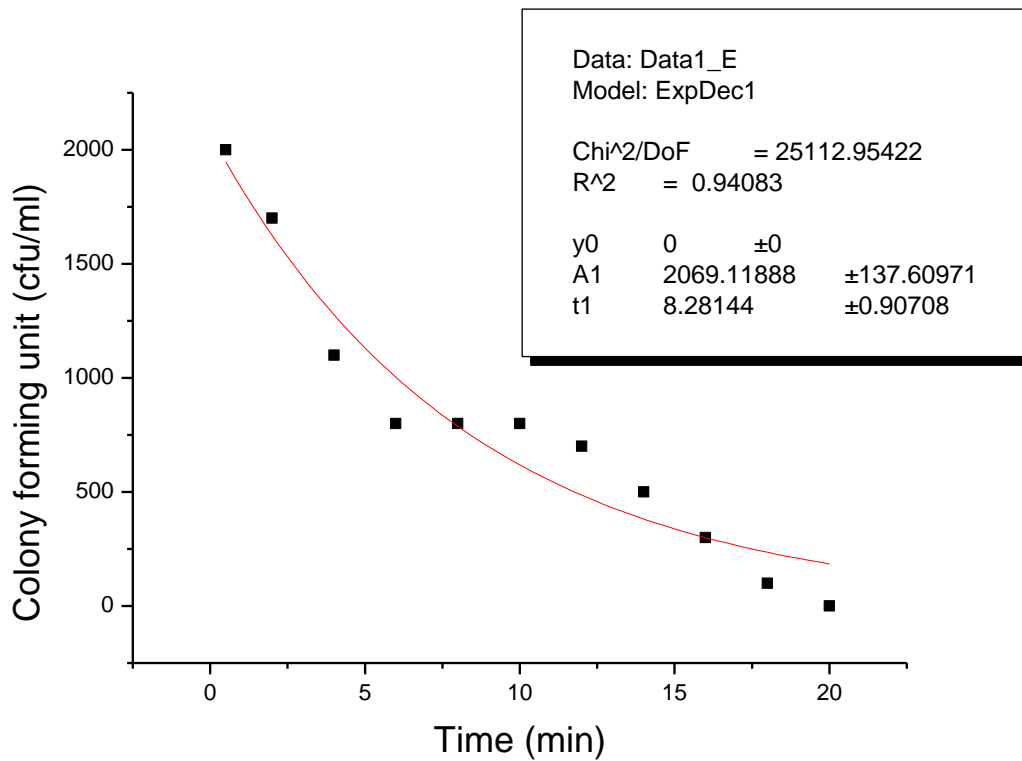


Figure 4.37: A first order analysis showing antibacterial effect of 32 wt. % Ag-MWCNTs at 25 °C.

4.7.2.5 First order analysis of the antibacterial activity of Ag-MWCNTs nanocomposite material at 30 °C

Figure 4.38 shows the first order graph displaying results obtained after interaction of the Ag-MWCNTs nanocomposite material with *E. coli* bacteria at 30 °C. The hyperbolic graph obtained displayed the R-squared value of 0.93089 and the rate was calculated to be 0.361 min⁻¹. This shows that the rate at which the bacteria are inactivated is lower than that at 20 and 25 °C.

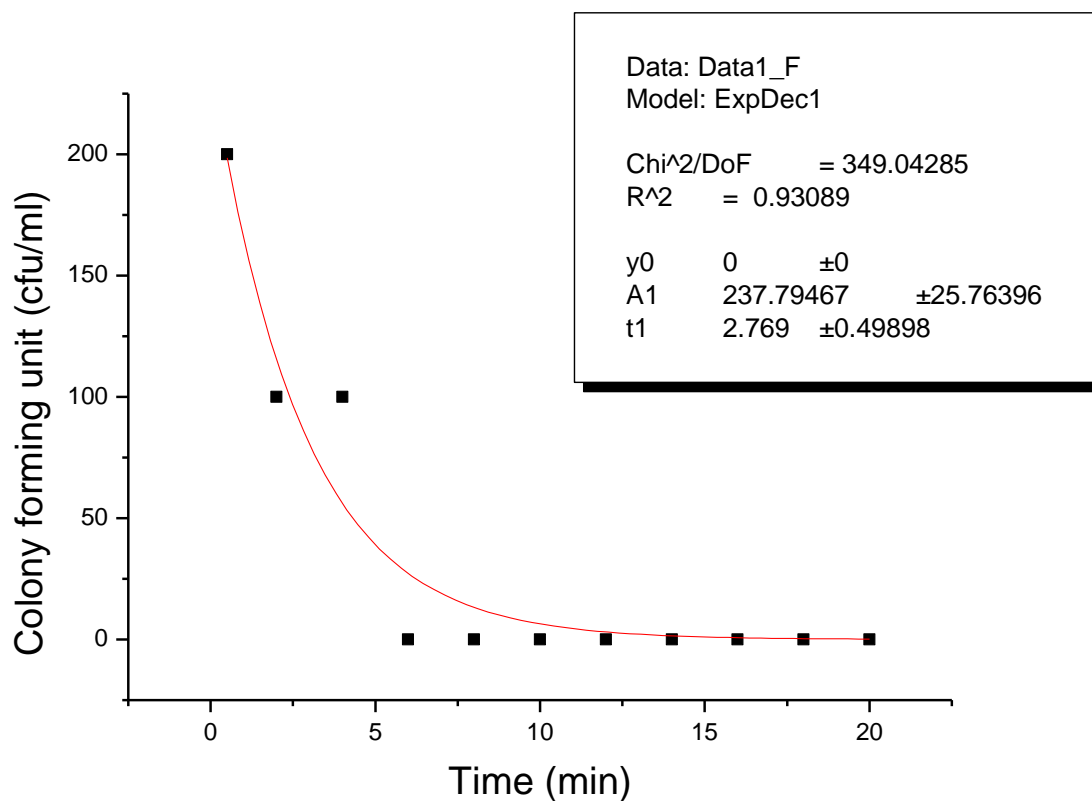


Figure 4.38: A first order analysis showing antibacterial effect of 32 wt. % Ag/MWCNTs at 30 °C.

4.7.2.6 Summary of the results obtained after determination of the kinetic order using first order analysis

Table 4.18 and Figure 4.39 show the activation energy determination of the *E. coli* bacterial reaction in the presence of Ag-MWCNTs. In this study, the rate of reaction decreased with increasing temperature except for the last reaction at 30 °C.

Table 4.18: First order rate constants for antibacterial effect of Ag-MWCNTs nanocomposites at different temperatures applied.

*Temperature °C	Temperature (K)	(1/T) (K ⁻¹)	t ₁ (min)	Rate (k)(min ⁻¹)	lnk
10	283	0.00353	2.61471	0.382	-0.962
15	288	0.00347	2.2038	0.454	-0.789
20	293	0.00341	7.27932	0.137	-1.988
25	298	0.00336	8.28144	0.121	-2.111
30	328	0.00305	2.769	0.361	-1.019

*All the reactions were undertaken within ± 3 °C temperatures.

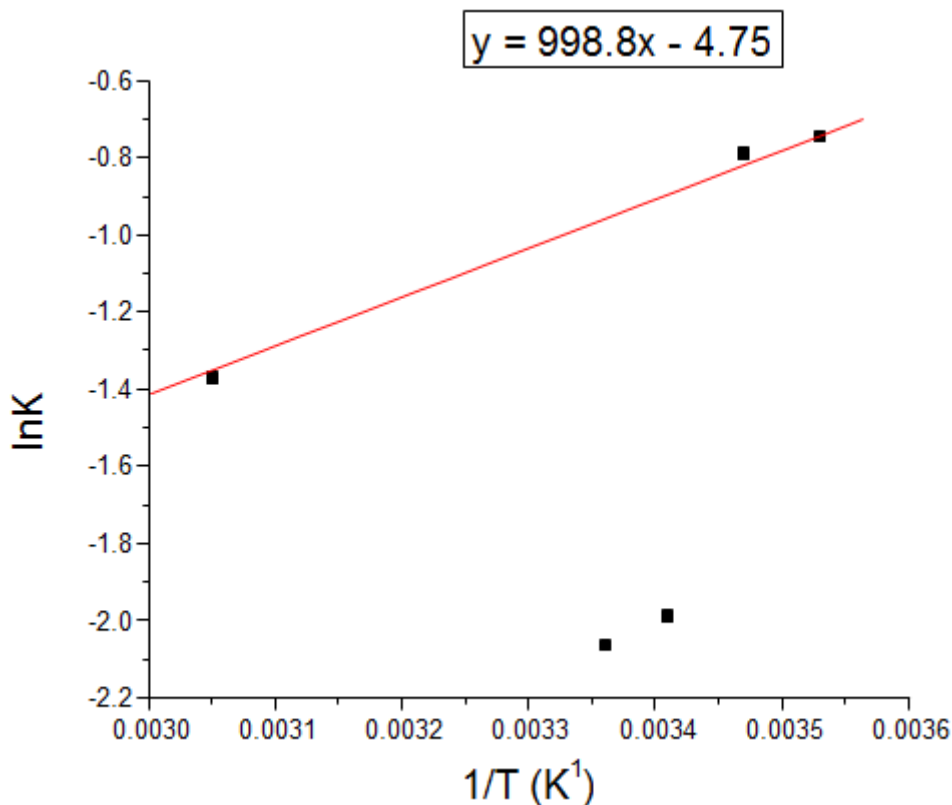


Figure 4.39: A plot of $\ln k$ vs. $1/T$ for determining the activation energy of the reaction.

The plot in Figure 4.739 was derived from the results obtained during different temperature monitoring of *E. coli* in the presence of Ag-MWCNTs nanocomposite material. The plot shows scattered points, which is due to different temperatures. The bacterial activity was not stable since its optimal activity is at 37 °C. This might have resulted in the bacteria's activity not being influenced by the temperature. The activation energy was calculated to be $-8.304 \text{ KJ.mol}^{-1}$ (see appendices for calculations). This means that the reverse reaction is sensitive to temperature and that its rate increases sharply as the temperature is raised [21].

If positive activation energy keeps a reaction from occurring until that amount of energy is provided from the environment, then negative activation energy would imply you could not stop the reaction from occurring. The bacteria already had sufficient energy for the reaction, so the only way to prevent the reaction would be to keep the reactants separate from each other [21]. In other words, it means that

whether in cold or hot conditions, the prepared nanocomposites are able to destroy the bacteria, even though it may effectively take place at different rates.

In a brief summary, different nanocomposites were synthesised and applied in the purification of water samples. The overall results suggest that the prepared nanocomposites could be of a potential use in water purification for municipalities and industries.

4.8 REFERENCES

1. Buang, N.A., Fadi, F., Majid, Z.A. and Shahir S. 2012. Characteristic of mild acid functionalized multiwalled carbon nanotubes towards high dispersion with low structural defects. *Digest journal of nanomaterials and biostructures*, 7 (1). 33 - 39.
2. Salipira, K.L., Mamba, B.B., Krause, R.W. and Durbach, S.H. 2006. *Polymerisation of cyclodextrin and multiwalled carbon nanotubes for use in water purification*. JHB, SA. 66 - 67, 78 - 80, 87 - 90, 95 - 100.
3. Mamba, E, Krause R.W.M., Malefetse, T.J. and Nxumalo, N. 2006 Monofunctionalized cyclodextrin polymers for the removal of organic pollutants from water. *Environmental Chemistry Letter*, 5. 79 - 84.
4. Rurille, B., Peeterbroeck, S., Gouttebaron, R., Godfroid, T., Monteverde, F., Dauchot, J., Alexandre, M., Hecq, M. and Dubois, P. 2007. Functionalization of carbon nanotubes by atomic nitrogen formed in a microwave plasma Ar +N₂ and subsequent poly grafting. *Journal of materials chemistry*, 17. 157 - 159.
5. Zhao, C., Ji, L., Liu, H., Hu, G., Zhang, S., Yang, M. and Yang, Z. 2004. Functionalized carbon nanotubes containing isocyanate groups. *Journal of solid state chemistry*, 177. 4394 - 4398.
6. Kim, Y.A., Hayashi, T., Endo, M., Kaburagi, Y., Tsukada, T., Shan, J., Osato, K. and Tsuruoka, S. 2005. Synthesis and structural characterization of thin multi-walled carbon nanotubes with a partially faceted cross section by a floating reactant method. *Carbon journal*, 43. 2243 - 2245.
7. Guzmán, M.G., Dille, J. and Godet, S. Synthesis of silver nanoparticles by chemical reduction method and their antibacterial activity. 2009. *International journal of chemical and biomolecular engineering*, 2. 105 - 106.
8. Puchalski, M., Dabrowski, P., Olesnicxa, W., Krukowski, P, Kowalczyk, P. and Polanski, K. 2007. The study of silver nanoparticles by scanning electron microscopy, energy dispersive X-ray analysis and scanning tunnelling microscopy. *Materials Science-Poland*, Vol. 25, No. 2. 1 - 6.

9. Jiang, H., Zhu, L., Moon, K. and Wong, C.P. 2007. The preparation of stable metal nanoparticles on carbon nanotubes whose surfaces were modified during production. *Carbon journal*, 45. 655 - 661.
10. Ma, P.C., Tang, B.Z. and Kima, J.K. 2008. Effect of CNT decoration with silver nanoparticles on electrical conductivity of CNT-polymer composites. *Carbon journal*, 46. 1497 - 1505.
11. Yamada, T., Hayashi, Y. and Takizawa, H. 2010. Synthesis of Carbon Nanotube/Silver Nanocomposites by Ultrasonication. *Materials transactions journal*, 51: 10. 1769 - 1772.
12. Wang, J., Li, H., Zhou, Zi, Li, X., Liu, J., and Yang, H. 2010. Tunable surface-plasmon-resonance wavelength of silver island films. *Chinese Journal of physics. B*, 19. 117310. 1 - 7.
13. Sing, K.S.W., in Fraissard, J.P. and Conner, C.W. 1997. Physical Adsorption: Experiment, Theory and Applications. Dordrecht, South Holland, the Netherlands: Kluwer Academic Publishers. 6 - 10.
14. Lukhele, L.P., Mamba, B.B., Momba M.N.B. and Krause, R.W.M. 2010. Water disinfection using novel cyclodextrin polyurethanes containing silver nanoparticles supported on carbon nanotubes. *Journal of applied sciences*, 10: 65 - 70.
15. Matlock, B.C., Beringer, R.W., Ash, D.L. and Page, A.F. 2011. Differences in bacterial optical density measurement between spectrophotometers. Thermo fisher, Wilmington, DE, USA. 1 - 4.
16. Sondi, I. and Salopek-Sondi, B. 2004. Silver nanoparticles as antimicrobial agent: a case study on *E. coli* as a model for Gram-negative bacteria. *Journal of colloid and interface science*, 275 (1). 176 - 177.
17. Baker, C., Pradhan, A., Pakstis, L., Pochan, D.J. and Shah, S.I. 2005. Synthesis and antimicrobial properties of silver nanoparticles. *Journal for nanoscience and nanotechnology*, 5 (2). 243 - 244.
18. Amro, N.A., Kotra, L.P., Wadu-Mesthrige, K., Bulychev, A., Mobashery, S. and Liu, G.Y. 2000. High-resolution atomic force microscopy studies of the *Escherichia coli* outer membrane: structural basis for permeability. *Langmuir journal*, 16. 2789 - 2790.

19. Spadaro, J.A., Berger, T.J., Barranco, S.D., Chapin, S.E. and Becker R.O. 1974. Antibacterial Effects of Silver Electrodes with Weak Direct Current. *Journal of antimicrobial agents and chemotherapy*, 6 (5). 636 - 638.
20. Lee, H.J., Yeo, S.Y. and Jeong, S.H. 2003. Antibacterial effect of nanosized silver colloidal solution on textile fabrics. *Journal of material science*, 38 (10). 2198 - 2199.
21. Benson, S.W. and Dobis, O.1998. Existence of negative activation energies in simple bimolecular metathesis reactions and some observations on too-fast reactions. *Journal of physical chemistry. A*, 102. 5175 - 5181.

CHAPTER 5

CONCLUSIONS AND RECOMMENDATIONS

5.1 CONCLUSIONS

β -cyclodextrin functionalised with allyl and benzoyl groups were successfully prepared. FE-SEM showed that the polymers had a spongy appearance and FT-IR confirmed the formation of both allyl and benzoyl β -CDs at 1596 cm^{-1} and 1646 cm^{-1} respectively. The nanocomposites demonstrated great capabilities in removing organic contaminants from water samples (i.e. 88% and 82% absorption efficiency of the contaminants by the mono-2-substituted benzoyl β -cyclodextrin polymer and mono-2-substituted allyl β -cyclodextrin polymer respectively). The benzoyl and allyl substituted β -CD polymers demonstrated approximately 100% antibacterial activity of *E. coli* bacteria after 90 minutes.

Silver nanoparticles were successfully synthesised by using sodium citrate as a reducing agent. Silver nanoparticles had particle sizes ranging from 50 to 100 nm with $0.994\text{ m}^2/\text{g}$ surface area. These nanoparticles were able to show 100% inactivity of the bacteria just after 30 seconds interactions at high loadings of Ag nanoparticles; the same percentage was achieved after 18 minutes at low loadings.

MWCNTs were successfully functionalised by a reduction method. FT-IR showed the presence of carboxylic acids and hydroxyl group on acid treated MWCNTs, with better dispersions observed under TEM. Approximately 32 wt. % Ag-MWCNTs nanocomposites were successfully incorporated onto the surface of MWCNTs. Silver attachment to MWCNTs was confirmed by FE-SEM, TEM, XRD and EDX. The crystallite size of Ag on Ag-MWCNTs was estimated to be 4.67 nm with $4.73\text{ m}^2/\text{g}$ surface area. These nanocomposites presented up to 100% inactivity of *E. coli* bacteria after 18 minutes. This nanocomposite also proved to be independent of temperature during water purification between $10\text{ }^\circ\text{C}$ and $30\text{ }^\circ\text{C}$.

Approximately 10 wt. % Ag/ β -CD nanocomposite were successfully synthesised by a reduction method. Silver attachment to β -CD was confirmed by FE-SEM, TEM and XRD. The crystallite size of Ag on β -CD was estimated to be 5.25 nm with 0.0391

m²/g surface area. These nanocomposites presented up to 100% inactivity of *E. coli* bacteria after 20 minutes.

Approximately 1 wt. %, 2 wt. % and 3 wt. % MWCNTs/β-CD were prepared. Their difference in MWCNTs loadings was studied by BET. The surface area decreased with an increase in carbon nanotubes loading (i.e. 3.65 m²/g, 2.23 m²/g and 1.76 m²/g for 1 wt. %, 2 wt. % and 3 wt. % MWCNTs/β-CD respectively). Similar results were also observed on the pore volume. These results suggests that a small amount of carbon nanotube addition in cyclodextrin polymers is generally required in order to achieve a high surface area of the nanocomposite materials. It was interesting to note that the high surface area of 1 wt. % MWCNTs correlated with the high performance observed on water purification studies (i.e. 97%, 96% and 95% absorption efficiencies for 1 wt. %, 2 wt. % and 3 wt. % MWCNTs/β-CD respectively).

1 wt. % Ag-MWCNTs/β-CD nanocomposites was successfully prepared. Silver doping was confirmed by TEM, EDX and XRD. The crystallite size of silver on 1 wt. % Ag-MWCNTs/β-CD was estimated to be 2.93 nm. It can be suggested that the particle size of Ag nanoparticles of MWCNTs/β-CD, might have played an important role in enhancing bacterial destruction. These nanocomposites were able to inactivate the bacteria in water samples by up to 100% in just 10 minutes. After a long exposure of these nanocomposites to *E. coli*, pits were clearly visible on the external structure of the bacteria suggesting that the nanoparticles are effectively bactericidal.

5.2 RECOMMENDATIONS

Since the nanocomposites showed the ability to remove 4-hydroxynitrobenzene contaminant in water, future should focus on other organic and inorganic contaminants.

The antibacterial effect of the 1 wt. % Ag-MWCNTs/ β CD should also be tested against removing other bacteria and viruses in water.

The antibacterial effect of nanocomposites should further be tested against a mixture of bacteria and organic contaminants to see if they are selective or not.

The effect of leaching of Ag nanoparticles should be investigated.

Investigation of the stages at which the nanocomposites should be applied during water purification should be done, e.g. after disinfection, after/before chlorination etc.

Reproducibility and recyclability experiments of the nanocomposites during water treatment should be done.

Further studies should spearhead the future use of nanocomposites in successful implementation of cost-effective large scale treatment applications for purifying municipal water and waste water from industries.

APPENDICES

1. The Scherrer formula was used to determine the crystallite size:

$$t = k\lambda / B \cos\theta$$

where;

t is the crystallite size,

λ is the wavelength of the X-ray radiation ($\text{CuK}\alpha = 0.15406 \text{ nm}$),

k is a constant taken as 0.94,

θ is the diffraction angle and

B is the line width at half maximum height.

2. The Initial colony forming unit for 10^{-4} plate was calculated as follows:

Colony forming unit = Number of colonies x dilution factor / volume diluted

$$117 \times 10^4 / 0.1 = 117 \times 10^5 \text{ cfu/mL}$$

This calculation method was followed throughout the remainder of the studies, unless otherwise stated

The percentage reduction was calculated from this formula for all experiments:

$$\text{Percentage inactivation} = ((\text{initial cfu} - \text{final cfu}) / \text{initial cfu}) \times 100$$

The percentage reduction in Figure 4.24 was calculated to be 100% meaning that there was no bacterial contaminant left since there was no bacterial growth, even after 48 h.

3. Calculation of Activation energy

The equation from the graph was found to be $y = 998.8x - 4.75$, where the slope is equal to 998.8

From the Arrhenius equation: $\ln k = -E_a/RT + \ln A$

The slope = $-E_a/R$

$$998.8 = -E_a / (8.314 \text{ J.K}^{-1}.\text{mol}^{-1} \times 10^{-3} \text{ KJ} / \text{J})$$

$$E_a = -8.304 \text{ KJ.mol}^{-1}$$

4. Percentage weight calculations

Wt. % = $\text{mass of metal} / (\text{mass of metal} + \text{mass of other nanomaterials present}) \times 100$